FACULDADE DE ENGENHARIA DA UNIVERSIDADE DO PORTO

FEUP

Study of Real–Time Estimation Techniques Related to the Autonomy of an Electric Vehicle

Pedro Rodrigues Pacheco

PROVISIONAL VERSION

Master in Electrical and Computers Engineering

Supervisor: Rui Esteves Araújo (PhD)

June 2011

"Eles não sabem, nem sonham,
que o sonho comanda a vida,
que sempre que um homem sonha
o mundo pula e avança
como uma bola colorida
entre as mãos de uma criança"

António Gedeão

Abstract

As pointed by many, electric vehicles will be part of the planet's future. However, in order to be able to obtain an efficient, functional and general purpose vehicle relying only in electrical power sources, it is necessary that some fields of study are detailed.

During the dissertation, various topics regarding the supply of a vehicle with all electrical power sources were addressed.

The initial part of the work deals with a literature review of energy sources. In addition to cover the various types of power sources pertinent to electric vehicle applications, possibilities for hybrid power systems were reviewed also and developed. Then methods to characterize the type of energy source reported (batteries) were proposed.

Through this, it became possible to design a test platform that allowed measurements of variables related to the battery in a controlled manner. This platform delivered results for the models that characterize the batteries. A comparison with cases reported in the literature was performed.

After realizing how the measurable battery variables relate to each other and their relation to the battery's charge, it was possible to focus our attention on estimation methods for the battery's state of charge. New information was collected in the literature regarding the most interesting methods in applications such as electric vehicles. These methods have been described and some were also tested under laboratory conditions. Results for estimation methods are presented which also include a comparative assessment among them.

Finally, a short literature review on methods to manage and control the flow of energy in an electric vehicle set the basis for the requirements of the best power electronics structure under this application, when considering fully electric power source hybridization. Both the power structure and control structure were chosen, described and simulated. The obtained results show that the choice was right even if not unique.

Resumo

Os veiculos electricos serão, tudo indica, parte integrante do futuro do planeta. Porem, para que se consiga obter um veiculo com fontes de energia totalmente electricas, que seja eficiente, funcional e de uma aplicação generalista, é necessário que alguns campos de estudo sejam detalhados.

Durante a dissertação foram abordados os vários topicos que compõem a alimentação de um veiculo com fontes de energia totalmente electricas.

A parte inicial do trabalho prendeu-se com uma revisão da literatura referente a fontes de energia. Para alem de serem abordados os varios tipos de fonte de energia pertinentes em aplicações como um veiculo electrico, foram revistas e elaboradas possibilidades de sistemas híbridos de alimentação. Seguidamente foram propostas formas de caracterizar um dos tipos de fonte de energia relatada, as baterias.

Tornou-se então possivel desenhar uma plataforma de testes em que podessem ser feitas medições à bateria de forma controlada de maneira a chegar a resultados relativos aos modelos descritos que caracterizam as baterias, comparando-os com casos descritos na literatura.

Depois de perceber como as variaveis mensuraveis das baterias se relacionam entre si e como se relacionam com a carga nela existente, foi possivel concentrar as atenções em metodos de estimação do seu estado de carga. De novo foram recolhidas informações na literatura relativamente aos metodos mais interessantes em aplicações como os veiculos electricos. Esses metodos foram descritos e alguns tambem testados em condições laboratoriais. São apresentados resultados e elaborada uma avaliação comparativa entre eles.

Apos uma pequena revisão de alguns metodos de gestão e controlo de energia presentes na literatura, foi possivel perceber qual a estrutura de potência que se aplica melhor aos requisitos de um veiculo electrico com fontes de energia totalmente electricas e hibridas. A junção de estrutura de potência com estrutura de controlo foi descrita e simulada, obtendo-se resultados que comprovam que a escolha foi acertada mesmo podendo não ser unica.

Agradecimentos

Felizmente tenho a sorte de poder agradecer a muita gente, pessoas que me ajudaram a percorrer o caminho que me trouxe ao final desta etapa.

As etapas da vida, por vezes duras, são mais fáceis de ultrapassar quando se tem amigos com quem se pode contar sempre. Agradeço principalmente a dois grupos de amigos, sem os quais nunca conseguirira chegar onde cheguei. Obrigado Bessa, Cris, hugo e teresa por me acompanharem durante os últimos 6 anos, por maus, mas principalmente bons momentos. Com um agradecimento especial para ti Teresa, por teres partilhadao comigo muito mais que os teus conselhos, bom humor e seriedade, por teres partilhado uma amizade que espero que fique para sempre.
Não menos impostante é o segundo grupo a quem quero agradecer. Obrigado Beto, Cátia, Lopes e Miguel Nuno por estarem presentes sempre e por, mesmo quando a saúde não ajudou, me elevarem o ânimo mesmo sem repararem. Que esta amizade que já dura há tanto tempo continue por muito mais.
Um muito obrigado também a duas pessoas muito importantes. Obrigado Mariana pela paciência e pelo carinho que me ajudaram muito neste último ano e obrigado Mortagua por teres sido um porto seguro sempre que precisei se sempre sem pedir nada em troca.
Obrigado ao pessoal dos laboratório I105, I101 e I002 pela companhia em noitadas de trabalho e noutras que de trabalho tiveram pouco.

Não posso também deixar de agradecer ao meu orientador prof. Dr. Rui Esteves Araújo pelas palavras sábias que me guiaram ao longo deste trabalho.

A minha família tem, obviamente, direito a uma palavra especial. Aos meus tios e primas, muito obrigado por todo o apoio e boa disposição. Um enorme obrigado aos meus 4 avós que, apesar de todas as dificuldades que passaram, continuam a ter uma força e dedicação aos seus que me inspiram todos os dias que passam.
um obrigado sem fim aos meus pais, aqueles que sao e sempre serã os meus maiores e melhores exemplos. Exmplos de dedicação, força, compreensão e paciência que sempre me guiarão.
Mas o maior obrigado vai para os dois Zés que, mesmo já não estando entre nós, me guiam, dão força e acalentam o espírito todos os dias da minha vida.

A todos, muito obrigado.

Contents

List of Figures

List of Tables

Abbreviations and Symbols

AC	Alternating Current
ANN	Artificial Neural Network
BF	Bandwidth Frequency
CER	Capacity Efficiency Ratio
DC	Direct Current
EBP	Error Backpropagation
EMCS	Energy Management Control System
EV	Electric Vehicles
FEUP	Faculty of Engineering, University of Porto
HEV	Hybrid Electric Vehicle
MLP	Multilayer Perceptron
MI	Multiple Input
MISO	Multiple-Input Single-Output
PEC	Power Electronic Converter
PHEV	Plug-In Hybrid Electric Vehicle
PI	Proportional - Integral Controller
SC	Supercapacitor
SLI	Starting - Lighting - Ignition Battery
SoC	State of Charge
SPC	Switching Power Converter
VEIL	Veículo Eléctrico Isento de Licença
VRLA	Valve-Regulated Lead-Acid Battery

Chapter 1

Introduction

The reality of the electric vehicle has been changing in the past few years throughout the world. Many companies historically related to internal combustion means of transportation, predicting that the electric vehicle will appear as a viable alternative to usual locomotion systems, are approaching their technology to fully electric vehicles.

In the last few years a great effort to maximize the autonomy of those electric vehicles, aimed as one of the main obstacles to their generalized adoption in general population. Battery technology is not fully developed, hence to use state of the art batteries, the ones with higher energy density, the price is high, thus raising the final value of the car. As a result of that recent effort some big automotive brands made big advances in their vehicles autonomy, thus are finally able to commercialize their fully electric means of transport. Other companies are now in the concept car step.

Focusing our attention on light vehicles, we can see that some major brands are leading the way to a high penetration of electric vehicles worldwide. Brands like Nissan, Renault and Fiat, already came up with fully functional plug-in electric vehicles commercializing them in some countries, Portugal is one of them.

The European Car of 2011 award winner (for the Car of the Year web site) is the Nissan LEAF has an AC synchronous motor that produces 80kW (109hp) from 2730 to 9800 rpm. This Nissan state of the art vehicle, as stated in [52], gets his power from a "new-generation"[52] battery that brings the Nissan Leaf autonomy to values from 75Km (worst case scenario), passing through around 160Km (US LA mode), to 220Km (best case scenario)[41].

But for now, the state of art electric vehicle is Tesla Roadster, from Tesla Motors, with an AC induction motor producing 288hp at 4400-6000 rpm [64]. The range is specified in [64] as 245 miles, around 392 Km (combined city/highway EPA cycle).

Paradigmatic changes happen in people's mean of transportation since the beginning of times. The invention of the wheel, the first horse tamed, the usage of chariots and the internal combustion engine were historical modifications that brought the world close to the probable next step, the electric vehicle. This section approaches various topics that ultimately lead to motivations on a

pursuit for new technologies and ideas related with the EV thematic. Some pertinent impacts that a high penetration of EVs in the society can provoke are therefore discussed.

1.1 Environmental Impact

Mostly since the later part of the 18th century, with the United Kingdom's industrial revolution, mankind became more and more dependent of fossil fuel. Those dependencies brought environmental, social and political issues that have wormed deeply in modern society. Human activities are affecting the global eco-system. Among all the factors that increase CO2 emissions, like population pressure or land usage, the most influential is without doubt combustion of fossil-fuel [61].

For the first time CO2 emissions from Annex I countries1 were surpassed by those from non-Annex I countries2. That change happened in 2008, that was also the year that Annex I countries first fell below 1990 CO2 emissions threshold. This trend can be explained by the recent financial crisis, economic slowdown and "price signal received by consumers after the high energy prices observed in 2008" [3].

Non-Annex I trends of CO2 emissions are in a continuous growth, on the other direction are Annex I countries that are consistently reducing CO2 emissions [3]. Figure 1.1 shows the global change of CO2 emissions worldwide.

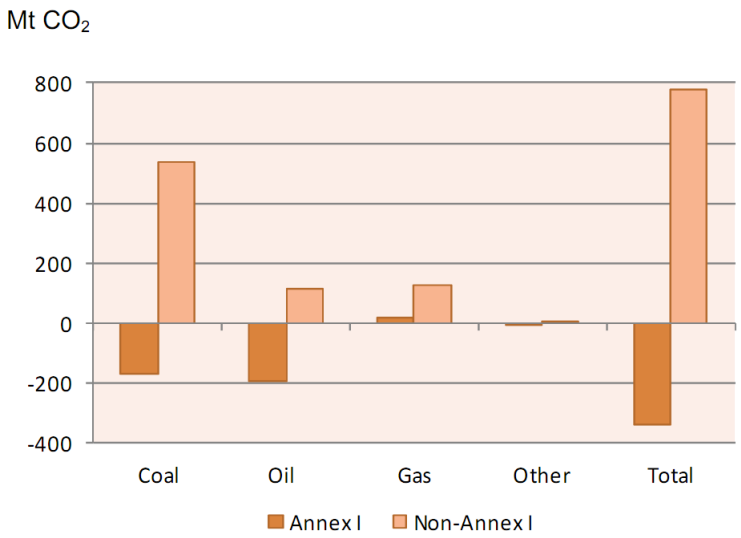

Figure 1.1: Global Change in CO2 Emissions (2007-2008)

1.1.1 CO2 Emissions by Fuel

Having 2008 as a reference we can see in "CO2 Emissions from Fuel Combustion Highlights" [3] that 43% of CO2 emissions were due to coal combustion, 37% from oil and 20% from gas. The next figure, 1.2, illustrates those numbers and shows trends since 1971 to 2008.

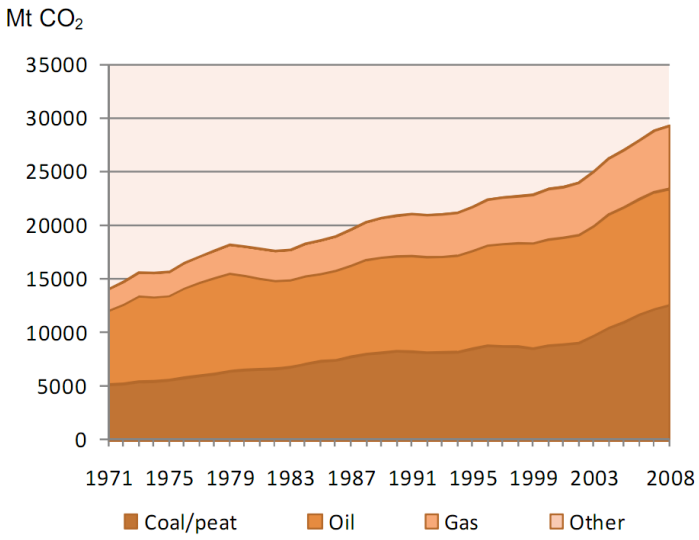

Figure 1.2: Trends in CO2 Emissions from Fuel Combustion

Now we can turn our attention to CO2 emission by sector, analyzing data from [3] it is possible to conclude that "the combined share of electricity and heat generation and transport represented two-thirds of global emissions in 2008". The next chart, inserted in figure 1.3 expresses those values visually.

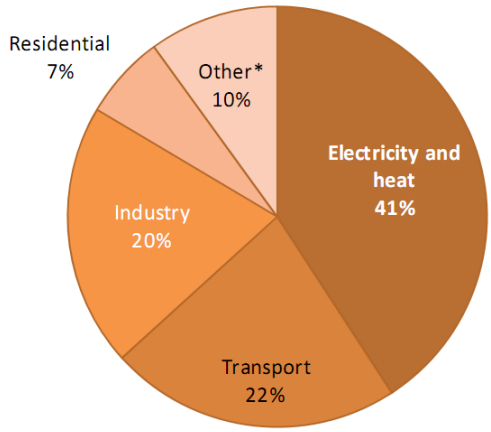

Figure 1.3: CO2 Emissions by Sector

Some conclusions can be achieved, the most important one is that the generalized entry in the market of the EV tends to reduce directly a great slice of CO2 emissions, the one named in the pie chart as "Transport" since most of the emissions are directly related to road transportation, the main target of the EV as seen in figure 1.3. Furthermore, global demand for transportation is, as WEO 2009 predicts, likely to increase by 45% until 2030 [3].

There are obviously some setbacks in the entry of the EV in the international scene. Looking

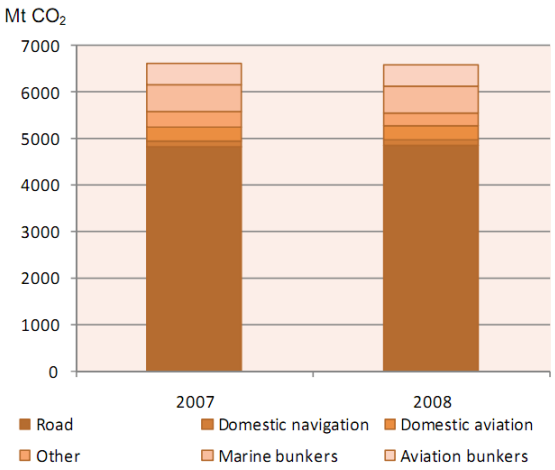

Figure 1.4: CO2 Emissions in the Transport Sector in 2007 and 2008

at the figure 1.4 a major problem is identifiable, an increase in emissions due to energy generation would happen.

A solution to that problem is needed. Policies can encourage a shift to new low-carbon emitting energies. With those policies came the increase in the last decade of renewable energy production [3]. As an example, there is an European Directive released in 2009 that sets ambitious targets for all countries in the EU, those targets will make the share of energy consumed from renewable sources to reach 20% of all the energy consumed, those values are set to achieve by 2020 [18].

1.1.2 Emission Trading Schemes

Giving the time needed for CO2 to disperse in the atmosphere, stabilizing the concentrations of greenhouse gases at a given level would require either a great reduction in emissions or an as soon as possible decrease of emission.

Some protocols were enabled complementing various national and community measures in order to achieve a recommended level to greenhouse gases concentrations. The Kyoto Protocol of the UNFCCC is by far the most evident multinational effort to mitigate climate change. "Having entered into force in February 2005, the Protocol commits industrialized countries (as a group) to curb domestic emissions by about 5% relative to 1990 by the 2008-12 first commitment period."[3] With this "as a group" clause economic transactions of emission allowances started among Protocol country members. "The Kyoto Protocol implies action on less than one-third of global CO2 emissions as measured in 2008."[3].

Some of non-participant countries in the Kyoto Protocol elaborated a protocol of their own. An example of those initiatives is the Western Climate Initiative, a collective emission system composed by 11 US states and Canadian provinces. "A number of other trading schemes are also under consideration."[3]

1.2 Socio-Economic Impact

A paradigmatic change such as EV worldwide dissemination must have a major impact on both economic and social structure. A great number of studies were done so we can have some perspective over the future changes in the world socio-economic structure.

1.2.1 Commercial and Industrial Changes

The scenario of world fossil-fuel combustions free is almost a utopia, but the EV proliferation gets us closer to that objective and brings up some problems related to companies that make a living either selling or producing products for ICE vehicles. In spite of those problems, some benefits are obvious, like the emergence of companies specialized in products needed for a functional EV.

To analyze the EV market entry impact, USA can be used as an example, because, being a country with a high fossil-fuel dependency, the industrial structure around petroleum and petroleum products is deeply cemented.

We can conclude from the data available in figure x that battery manufacturing companies tend to grow significantly in order to attend EV products demand. On the other hand, the petroleum and petroleum products are industries with a major setback in revenue. Those abrupt changes have obvious implications in human resources e.g. employment and import policies [44].

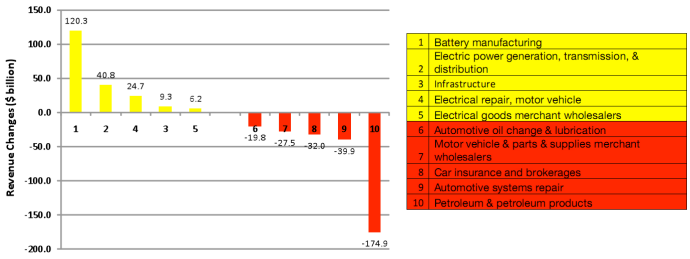

Figure 1.5: Top 10 Industries Direct Gains and Losses [44](edited)

1.2.2 EV and PHEV Market Penetration

A high EV market penetration would be a threat to electric power systems stability, so a good judgment about the share of EV and PHEV being used at the time is crucial. According to [2], EV and PHEV are going to grow in the next few years, bringing a huge new load to power generating and distribution systems. The worst case scenario to the electric power system is a high penetration rate of the EV and PHEV. Two market penetration scenarios were presented in [2], sales based on national announcements in figure 1.6 and sales targets if national targets growth rates extend to 2020 in figure 1.7.

According to an interview to Joao* Dias, an economic adviser in the Prime Minister's office, at 20 October 2010 to Reuters, Portugal has an aim of 750000 EV and PHEV on the road, around 10% of all road vehicles, by 2020.

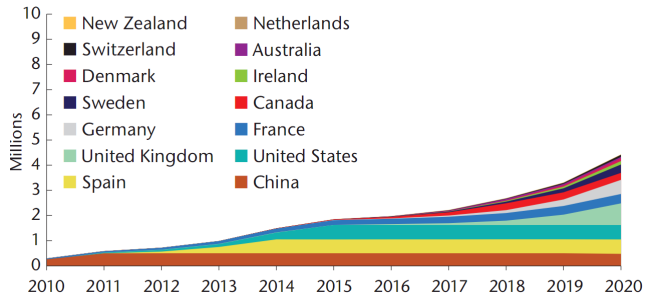

Figure 1.6: National EV/PHEV Sales Targets Based on National Announcements 2010-2020

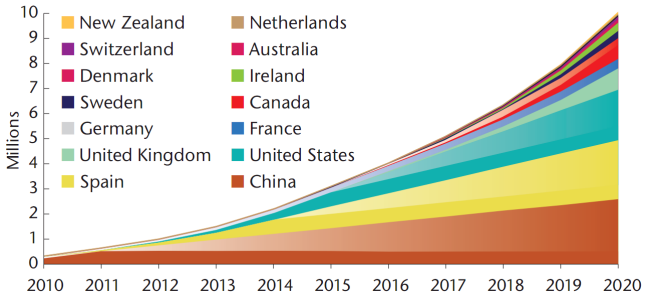

Figure 1.7: National EV/PHEV Sales Targets if National Target Year Growth Rates Extend to 2020

1.2.3 Energy Related Importation and Exportation Changes

Focusing the attention on Portuguese importation/exportation balance, we can see a continuous crescendo of energetic related importation, and worst, the commercial balance between exportation (assumed all FOB) and importation (assumed all CIF) is decreasing. The next figure 1.8 subtracts FOB to CIF and relates that value as that year GDP percentage [43].

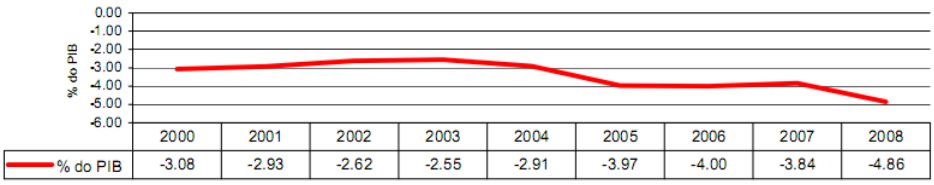

	2000	2001	2002	2003	2004	2005	2006	2007	2008
% do PIB	-3.08	-2.93	-2.62	-2.55	-2.91	-3.97	-4.00	-3.84	-4.86

Figure 1.8: (FOB - CIF) as percentage of GDP [43]

To have a good idea of how the EV dissemination nation-wide (in Portugal) would change Portuguese importation/exportation balance an energetic of importations and exportations characterization is needed. Figure 1.9 explicitly shows the relation between each product quantities with intra-EU estimated data for 2008. The figure was edited in order to translate it to English language.

Now is possible to understand the EV implication on the economy of a country such as Portugal knowing that 12.5% of all importation is to crude oil and refined petroleum [43] with a good

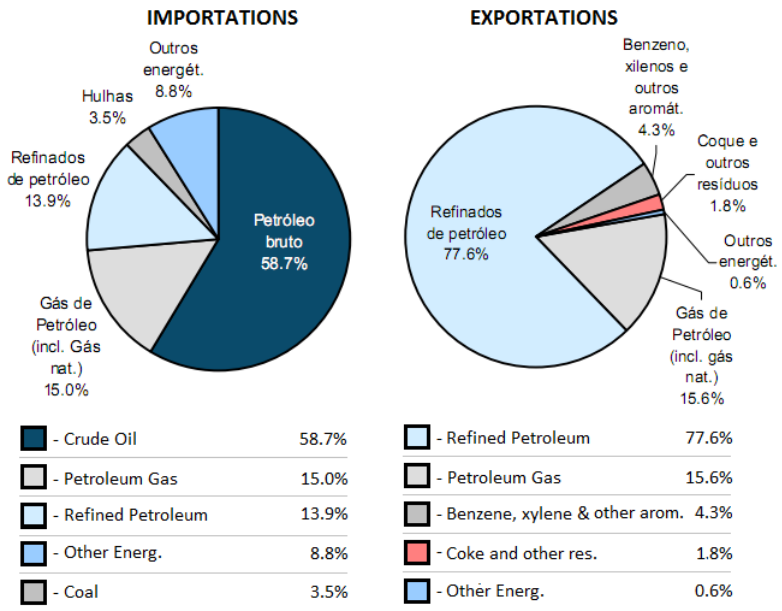

Figure 1.9: Energetic products transacted by Portugal in 2008 relative weight (edited) [43]

slice of that going directly to the transportation sector. That slice would definitely decrease, reducing substantially importation and opening doors to a widely use of emerging renewable sources of electricity. These exportations are only 6% of the total exportations of the country which is much less than the importations as viewed above in the document [43].

1.3 Technologic Impact

History tells us that most of technologic advances come from one reason, need. With the possibility of a high demand of products associated with the EV in the future it is only normal that a raise of some economic and academic interest happen. It is from that mutual interest that technology usually evolves.

1.3.1 Academic and Industrial Effort

The need for a versatile transportation sector with much less CO2 emissions brought the public attention to the EV.

A great number of universities all around the world are studying the electric vehicle and many times with companies or government support and funds.

A paradigmatic example of the visible EV technologic impact and attempt of being a magnet of innovative research, is ITS (Institute of Transportation Studies) UC Davis (University of California, Davis), with more than 60 affiliated faculty and researchers, 100 graduate students, and a $6 million annual budget, acquired by partnering with industry, government, and non-governmental organizations [55].

1.4 Impact on Electric Power Production and Distribution System

In this part, there is a need to focus in a single country that has a well-developed and economically healthy [50] electric power system in order to detain all the information needed to achieve pertinent conclusions. Portugal will be the country used for the study due to its electric power distribution system characteristics, renewable energy sources development state and extrapolation capability to most of the EU-25 member states with no nuclear power production.

1.4.1 Current Power Production Capability

To assess the Power System capability to accept a high market penetration of the EV is important to understand what the current power generation capability is. Figure 1.10 is based on values shown in reference [49] and shows the installed power by source in Portugal at the end of 2009.

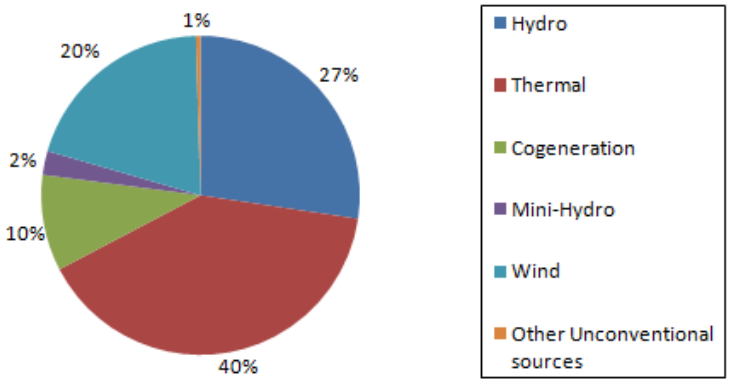

Figure 1.10: Portuguese installed capacity by source in 2009

In reference [49] we can see that the total of installed power is 16738 MW. In spite of that value, many of the sources are related to meteorological events. More than 40% of these capacities are not always available due to their time dependency.

1.4.2 Expected Power Production Capability by 2015

The installed power upgrade is nowadays underway in Portugal, many hydro plants are being constructed and are expected to be functional by the year 2015, like Alvito and Foz do Tua with a combined capacity of 476MW. Production reinforcements are being held at Venda Nova II upgrading it to Venda Nova III with an increase to 736MW installed power also expected to be functioning by 2015. Many wind turbines are being deployed as well. The next figure shows the expected Portuguese installed capacity by source in 2015.

Problems inherent to time constraining energy sources tend to grow. By 2015 the share of hydro and wind production is expected to break the 50% threshold.

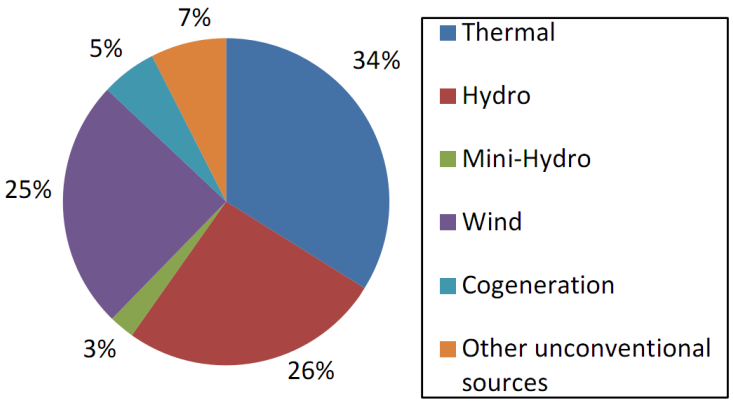

Figure 1.11: Expected Portuguese Installed Capacity by Source in 2015

1.4.3 Threats

Like every other technology entering the world market, it has some risks, in this section will be approached the challenges that companies responsible by production and distribution of energy will face during the EV dissemination (e.g. EDP and REN respectively).

1.4.3.1 Power Production System Stability

An unregulated entry of EV in the electric power system could get catastrophic very quickly. In [28] analytical approaches were made in order to assess the security of energy supply. Those studies came up with pertinent results for Portugal. The proposed methodology in [28] uses a modeled generation system and a monthly affectation of hydro systems. To combine those models with sources/loads which strongly depend on the time, like wind generation, unconventional sources and EV charging models, FFT was used. Two scenarios of EV battery charging were used. The first one is the dumb charging scenario, where the vehicle battery charging follows the natural behavior of Portuguese population, which is visible in the load diagrams showed in figures 1.12 and 1.13. No political or economic measures are used in this dumb charging scenario.

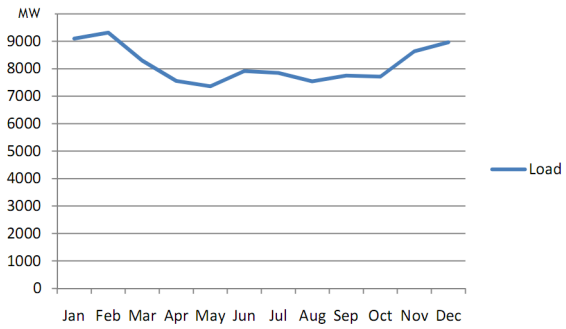

Figure 1.12: Portuguese System Mean Load Monthly Variation

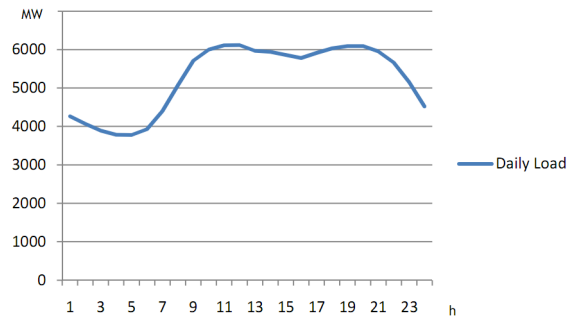

Figure 1.13: Portuguese System Mean Load Daily Variation

The next figure, 1.14 is merely illustrative of a dumb charge behavior and may not be representative of the Portuguese case.

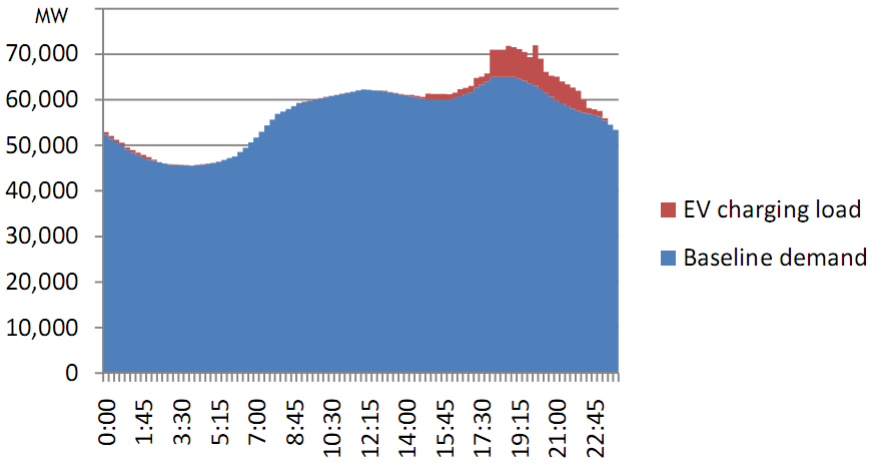

Figure 1.14: Dumb Charge Example [28]

The results of simulations were expressive in both LOLE and LOLF assessments.

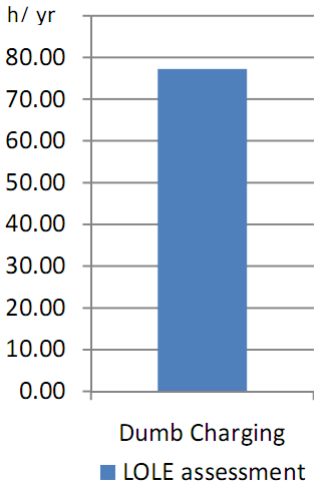

Figure 1.15: LOLE assessment for Portuguese System (edited) [28]

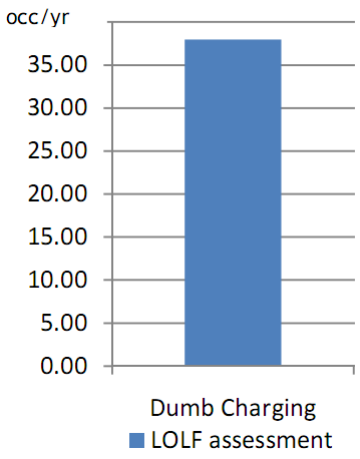

Figure 1.16: LOLF assessment for Portuguese System (edited) [28]

In a dumb charging scenario is expected that the system cannot supply the total demand for 77h in a year, this scenario affects in a drastic way Portuguese security of supply. Figures 1.15 and 1.16 shows the high influence of the dumb charging in the reliability indices with system failures occurring more than 35 times in a year.

These assessments prove that an unregulated EV entry in the electric network can be translated as a major threat to the system stability.

1.4.3.2 Challenges with Transmission and Distribution

"The transmission and distribution grid today serves a critical role in delivering electricity from generation sites to population centers"[51]

Usually the place where energy is consumed is not the same where it is generated, hence there is a necessity of a transmission and distribution grid. Thus the state of that grid will influence directly the quality and reliability of delivered power.

The Portuguese company responsible for energy distribution and transport is REN (Rede Electrica Nacional). This company has high quality of service standards, thus has a continuous improvement policies [49]. The main challenges of this kind of companies worldwide will be to keep the quality of service high, developing ways to predict congestions in some branches of the grid.

1.4.3.3 In Short

All these threats to the electric power system come from the peaks of energy needed to charge batteries. The energy usage efficiency of those batteries is then crucial. Managing the energy and power flow inside the EV can directly affect the electric power system positively.

1.4.4 Opportunities

The need for a "green" possibility for medium distance locomotion brought the spot light to the electric vehicle, with those lights investment is often a consequence, leading to revenue and intellectual knowledge.

1.4.4.1 Electricity Selling Revenue

It is clear that electric vehicle usage will increase electric consumption, thus more selling opportunities. According to "Impact of Widespread Electric Utility Business - Threats and Opportunities" [51], having an EV driving 33 miles per day at 0.35kWh per mile and average retail price of 11.36 cents/kWh it translates into an additional revenue of $480 per annum for every EV in service.

A similar approach can be used to Portugal. Assuming that the battery charging of every vehicles are made in the valley zone of the load diagram with bi-hourly contract, a wage of $0.0850/kWh$ can be achieved, this means an additional revenue of 358 per annum per EV. Assuming Portuguese perspectives of 750000 EV by 2020 are correct it implies a gross revenue rounding $260M$ per year.

1.4.4.2 Increase of Installed Capacity Usage - Valley Filling

The concept of Valley Filling is the assumption that some loads can be programmed to absorb power in periods of non-peak demand.

Many policies can be done to achieve this load profile, one of the most compelling is wage reduction in non-peak demand. Since is predictable that most of recharges of EVs will occur

during late evening and overnight, an increase of wage from 16:00 to 18:00 and a low wage from 20:00 to 6:00 could shift loads to a better period for the electric power system.

A question must be answered now, “Why do the Valley Filling concept increase the installed capacity usage?”.

Looking at figure 1.13 we can see a lack of demand 23:00 to 7:00. Some power sources are continuously active due to time needed to be deployed. Sources with time dependencies, in order to have efficiency must be active for periods when energy generation is possible, those time intervals can coincide with lack of demand periods. In short, during valley hours is possible that the power generated is more than the power dispatched. Nowadays excess of power is used to pump water backwards to the bayou in hydro plants, in order to transform electric energy in potential/kinetic energy. Even with pumping methods there is excess of power at occasions, thus that power is usually sold at very low prices or even given. With EV charging batteries in lack of demand periods installed power capacity would be used in a more efficient manner, minimizing investment in power upgrades and maximizing installed power use.

In [28] valley filling using EV battery charging is named “smart charging”, the next figure, 1.17 is illustrative that behavior.

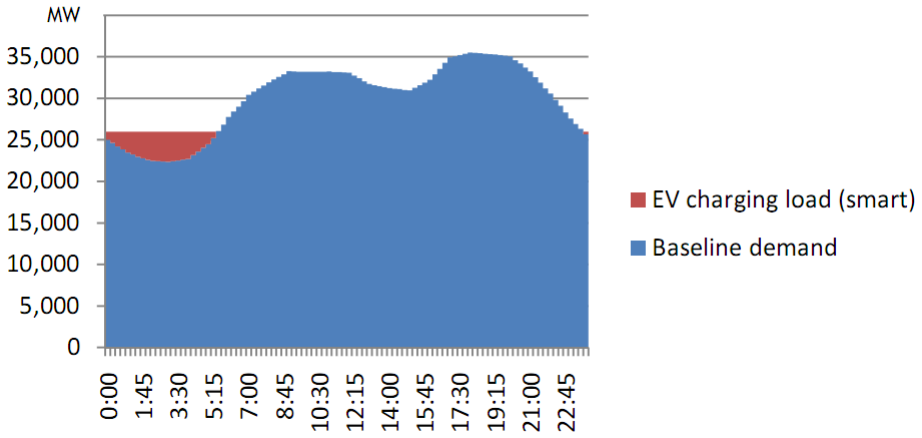

Figure 1.17: Illustrative representation of a valley filling with EV [28]

1.4.4.3 Vehicle to Grid (V2G)

“Vehicle-to-Grid (V2G) has been hyped as one of the most promising opportunities of the EV revolution.” [51]

The idea behind V2G technology is that utility firms will be able to manage plugged-in EV batteries to be used as distributed storage to serve as back-up capacity to help meet unusual demand spikes.

With dynamic pricing the EV owner could profit by plugging it in during the afternoon. These policies could encourage EV fleets in companies. Another possibility is the previously referred valley filling.

However, the authors believe that some issues may prevent V2G from becoming a reality in the next decade. Unproven economic justification for utilities and consumer, the complexity of knowing when to draw power from the vehicle, lack of support for smart grid technology and the need for development and wide scale installation of bi-directional power converters. But one of the most important issues brings batteries and battery management to the spot light. The early development stages of battery technology makes unlikely that either the car manufacturer or the utility will risk interconnections [51].

Contributions in battery technology and knowledge are crucial to a steady progression towards the, for now utopic, V2G reality.

1.4.4.4 In Short

Is noticeable that the EV entry brings many opportunities to the electric power system, but in order to achieve good results a good knowledge of battery and battery management is mandatory.

1.5 Master Thesis Structure

This master thesis will approach the energy sources in electric vehicles. The first chapter, 1 is an introduction and tries to show a general framework of the nowadays electric vehicle. The rest of the chapters, excluding chapter 6 which contains conclusions and future work, will be approached as the image shown in figure 1.18 illustrates. The structure shown can be viewed as a high level architecture of a hybrid energy system inside an electric vehicle.

With the image in figure 1.18 to help the description of the topics to be approached during this master thesis, one can understand that the second chapter, 2 will focus on the power sources pertinent in electric vehicles. A somehow detailed description about some pertinent power source technologies and the possibility of merging some of them into hybrid solutions will be done. Also in the second chapter, models to characterize one of the power sources technologies (in this case lithium based batteries) are detailed and discussed, but only in the third chapter, 3, after a first part spent designing a test bench setup, the results of the models collected in the second chapter are unveiled. The fourth chapter has a focus on state of charge estimations, discussing, detailing and testing some methods proposed in literature. The fifth chapter, 5, centres the studies on two major topics. An brief overview of energy management control systems present in literature is performed, followed by the second major theme, the power electronics needed to control the energy flowing from the primary energy source to the powertrain and other electric loads in an electric vehicle.

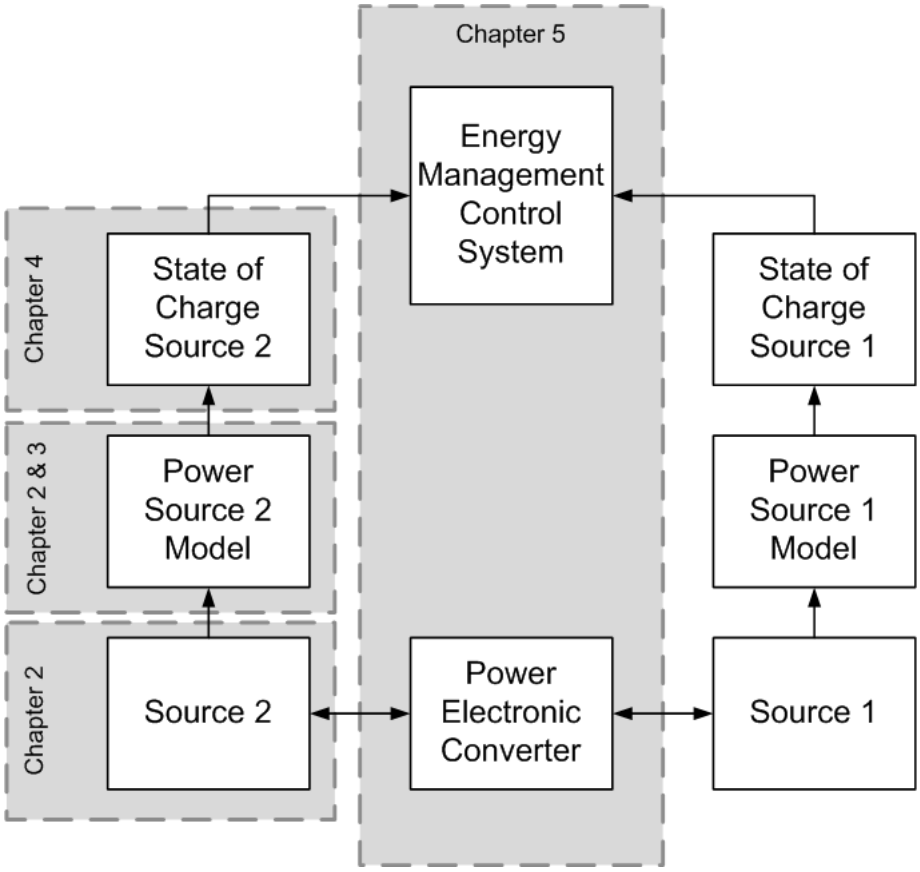

Figure 1.18: Thesis Structure

Chapter 2

Power Sources

Throughout the world, the increasing attention to the electric vehicle as a mean of transportation brought up scientific interest as well as government and industrial investments to the energy source sector inside the electric vehicle [31]. One can notice that attention by observing the join-ventures of well-known manufacturers all around the world. Some examples of those collaborations are AESC (2007), a Nissan, NEC and NEC Tokin association, SB LiMotive (2008), a Bosh and Samsung SDI team play [31].

Obviously the energy source requirements for an EV differ from others like HEV or PHEV. This section will discuss the energy sources of interest for the EV. An overview on energy sources technologies will be done before an introduction to the concept of sources hybridization. Several combinations of the power sources approached before will be reviewed in the subsection reserved for hybridization concepts. Afterwards, models and parameter estimation on two exemplificative energy sources will be described. Those energy sources will be li-ion battery and the supercapacitor.

2.1 Batteries

> "A battery is a device that provides a source of electrical energy to an external circuit by direct internal conversion of chemical energy."[31]

Many technologies of batteries are available or in development, all of them use the basic concept of electrochemical oxidation–reduction reaction of its active materials to generate electrical energy. For many different reasons some technologies are not suitable for electric vehicles applications, hence only the fully developed or assured technologies will be addressed in this part.

The big diffusion of the battery technology made standardization a necessary measure to take. Among many national institutes some international organizations like the International Electrotechnical Commission (IEC) and the International Standards Organization (ISO) defined with some battery standards.

In this subsection basic concepts about batteries will be written in order to the reader to get acquainted with some of the usually terminology and to have a general frame on the basic functioning of a generic battery. Secondary batteries will be detailed and primary batteries overviewed.

2.1.1 Basic Concepts

In order to understand the battery as a whole some basic concepts must be absorbed.

The output voltage of a single cell is, in theory, a function of the materials used in the cathode and anode, the composition of the electrolyte and the cell temperature. This voltage is similar to the open-circuit one. When connected to a load, internal polarization effects impose a voltage drop to the cell terminals.

The energy output is usually a low percentage of the theoretical one. This fact is mainly due to lack of stoichiometry balance in the active materials and to the non-null end-voltage (voltage of the cell when totally discharged) in a totally discharged battery. As stated in [31], the energy output can be from 16 to 37 per cent of the theoretical one. The actual energy output leads to an important concept named specific energy. It relates the total output energy with the weight of the cell or group of cells (measured in Watt-hour/kilogram).

Another important parameter that one should be acquainted with is the capacity of a battery. The capacity is the amount of electrical energy that a cell can deliver at a constant temperature when discharged at a constant rate, this is measured in Ampere hour (Ah). A high discharge rate imposes a low capacity. One can now use the battery capacity to extrapolate some performance parameters. The life cycle of a battery is the number of cycles that a battery can perform before its nominal capacity falls below 80% of its initial rated capacity" [31]. A high depth of discharge is a factor that can worsen the life cycle expected of a battery and that life cycle behaves, in almost all batteries, with a quasi-logarithmic function of the depth of discharge.

One of the main performance indexes is the specific power (measured in Watt/kilogram). This shows the power that can be used as work in a time instant.

2.1.2 Primary Batteries

> Primary " batteries are not capable of being easily or effectively recharged electrically and, hence, are discharged once and discarded." [39]

Usually, primary batteries have as their general advantages the commonly inexpensiveness and lightweight packaging.By having a good shelf-life, high energy density, moderate discharge rates, almost no maintenance and ease of use, primary batteries are used for a wide range of applications going from portable electronic and electric devices to toys and backup memory.

A particular case of a primary battery is a Reserve Battery, according to [39]. This sub-type of batteries are designed for a very particular objective: to meet extremely long or environmentally severe storage requirements that cannot be met with an active battery designed for the same purpose [39].

All these properties make this kind of battery a good emergency backup as a primary energy source, extending the electric vehicle autonomy. However they cannot be used as a primary energy source. In figure 2.1 some primary battery technologies are shown in terms of its specific energy and energy density, the main characteristics desired for a backup energy source.

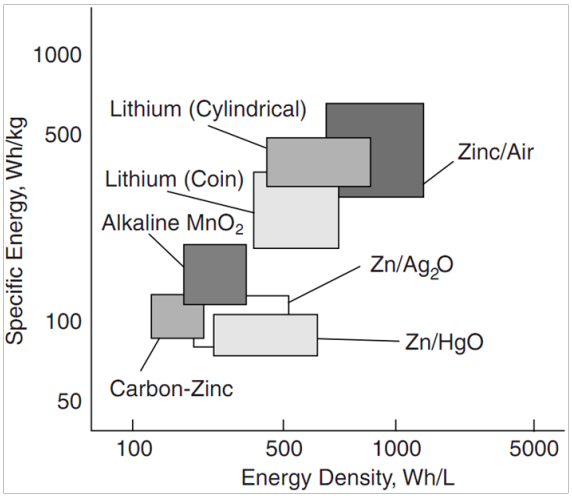

Figure 2.1: Primary Battery Technologies

2.1.3 Secondary Batteries

> Secondary " batteries can be recharged electrically, after discharge, to their original condition by passing current through them in the opposite direction to that of the discharge current. " [39]

In secondary batteries the energy density is lower than in the case of primary ones, the charge retention is rather poor and some capacity loss on standing occur. These factors make secondary batteries a bad choice if long term storage is needed. However this kind of battery is also characterized by a relatively high power density, high discharge rates, flat discharge curves and good low-temperature performance. These characteristics make secondary batteries a good choice in two major types of application, as an energy storage device (e.g. Uninterruptible Power Sources, Stationary Energy Storage, Electric Vehicles and Aircraft Systems) and just like a primary battery, only with the main attribute of being recharged instead of being disposed of [39].

According to [31], some types of secondary batteries are not suitable for electric vehicle applications. Between many secondary battery technologies only the fully developed and assured technologies will be treated in this part: Lead-acid, Ni-MH, Li-ion and Li-po. Due to cadmium toxicity Ni-Cd batteries will not be regarded in this part.

2.1.3.1 Lead–Acid

The lead-acid battery was invented in 1859 by Raymond Gaston Plantd continues to be the most deeply cemented technology for SLI (starting, lighting, ignition) applications with many suppliers worldwide. Its low internal impedance, high current delivery and tolerance to overcharging procedures make this kind of battery a good solution for automotive SLI applications. Due to its bulkiness, low energy density, specific energy, charge efficiency (70%), specific power and life cycle, this technology is not suitable for a primary energy source of an efficient electric vehicle. Moreover, when charged with a high current, the lead-acid battery overheats making it not appropriate for fast recharging.

With an enhancement of this type of battery in mind, some developments were made to improve some shortcomings of this classic technology.

One of the most known developments of lead-acid batteries are Valve Regulated Lead Acid (VRLA), introduced in 1970s, designed to prevent the electrolyte evaporation, spillage and gassing. These batteries are considered either as gel type VRLA or Absorbed Glass Mat (AGM) VRLA. These preventions impose some enhancements in robustness, with a higher resistance. No enhancements in specific power or energy density are described in [31].

A more recent development to lead-acid batteries, named Bipolar Lead-Acid, involve a stack of bipolar electrodes connected in series, improving the power level delivery, offering an increased energy density and quadrupling the power density, in relation to the classical lead-acid batteries.

The chart shown in 2.2 was drawn based on information present in [31] and [39] and roughly represents the positioning of the three lead–acid based technologies approached in a specific energy versus energy density chart.

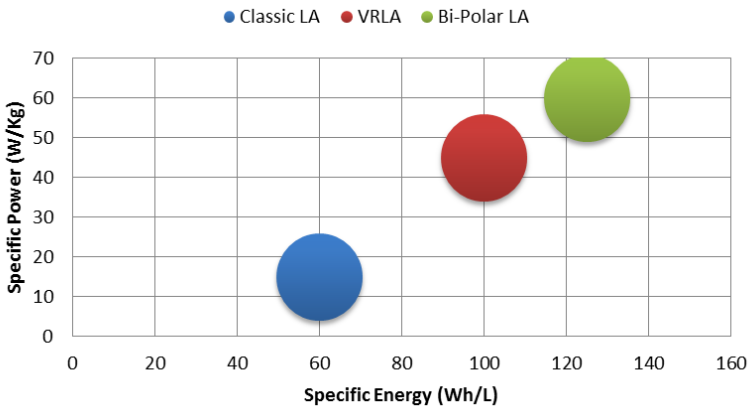

Figure 2.2: Lead–Acid Based Technologies

2.1.3.2 Nickel–Metal Hydride (Ni-MH)

Over 2 million hybrid cars use the Ni-MH batteries, a technology developed throughout the years with its origin in 1967 in the Battelle Geneva Research Centre, with a Ti-Ni alloy for the negative

electrode and a NiOOH for the positive electrode. The battery used nowadays in hybrid cars such as, Prius and Lexus Highlander from Toyota and Altima from Nissan, is an improved version of the one invented in Switzerland [22]. Ovonics altered and improved the Ti-Ni alloy and licensed the Ni-MH batteries in 1986.

Many advantages came with this type of battery: the high energy density and cycle life, the low internal impedance and the wide operating temperature made it an interesting solution. Some shortcomings still exist: the very high self-discharge rate, the coulomb efficiency with typical values of about 66% [31] and, depending on the application, the full power delivery that can go down to 50% DOD (depth of discharge), prevent this technology from a wider application window in electric vehicles.

In [22] some recent advances in NiMH batteries are shown. Ovonics driven by research of advanced materials for the electrodes of the NiMH battery, developed batteries with extended power through more cycles.

Figure 2.3, drawn with information present in [31] and [22], shows the targets for the specific energy and power of the next generation NiMH batteries when compared to the above described lead-acid batteries.

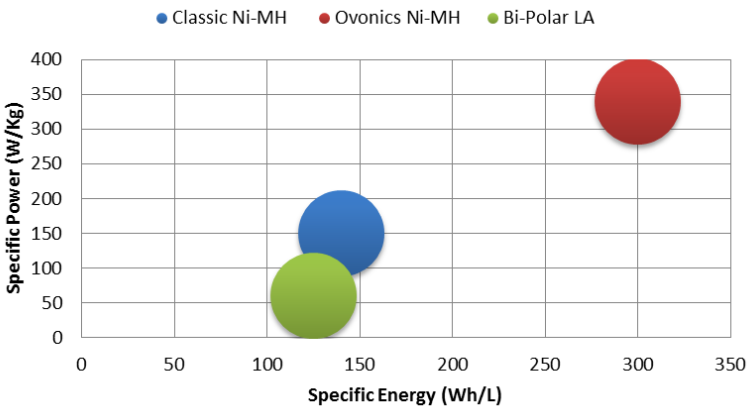

Figure 2.3: Nickel–Metal Hydride Based Technologies

2.1.3.3 Lithium Based Batteries

The typical lithium cell is composed by a carbon based anode and a lithium compound, such as Lithium Cobalt Dioxide or Lithium Manganese Dioxide cathode (other chemistries are possible). The electrolyte cannot be an aqueous material, since Lithium reacts violently with water. In this kind of battery the electric energy is generated when either the lithium ions inserted or extracted into the crystalline lattice of the host electrodes without changing their crystal structure [31, 39, 32]
.

The performance factors of Li-ion batteries make them an attractive solution for automotive applications. A high cell voltage (3.6V), a very high specific power and energy density, a low

weight, the possibility of faster charging without damaging the battery cells, a coulomb energy of almost 100% and a long cycle life, make this technology competitive even with some drawbacks: high initial costs, need for protective circuitry, degradation with high temperatures and high internal impedance when compared to other secondary battery technologies.

In the recent years, many companies and research institutions are directing their effort to create the next generation lithium based battery. The research is dealing not only with the electrodes, but with the electrolyte material as well. The variations to the classical Li-ion cell started with three variations of the materials used. The most mature of those first generation technologies is the Lithium Cobalt, this combination of materials made a battery with very high energy density, long cycle life and good typical cell voltage (3.7V) but, due to the toxicity of Cobalt, the application capability in the automotive industry is limited. The other two variations in materials are in the Lithium Manganese battery, with higher typical cell voltage (3.8V) but less energy density (about 20% less), and in the Lithium Nickel battery, with lower typical cell voltage (3.6V) when compared with Lithium Cobalt type but higher energy density (about 30% more when compared to Lithium Cobalt batteries). The research did not stop with these three types of Li-ion batteries and many variations of materials were tested. The tradeoff is shown in the next table, 2.1.

Table 2.1: Tradeoff between different types of Li-ion batteries[4]

Name	**Description**	**Automotive Status**	**Power**	**Energy**	**Safety**	**Life**	**Cost**
LCO	Lithium cobalt oxide	Limited auto applications (due to safety)	Good4	Good4	Low2,4 Mod.3	Low2,4	Poor2,3
NCA	Lithium nickel, cobalt and aluminum	Pilot1	Good1,3	Good1,3	Mod.1	Good1	Mod.1,3
LFP	Lithium iron phosphate	Pilot1	Good1	Mod.2,6	Mod.1,2,4	Good1,4	Mod.1 Good2,3
NCM	Lithium nickel, cobalt and manganese	Pilot3	Mod.3	Mod.3 Good7	Mod.3	Poor.3	Mod.3
LMS	Lithium manganese spinel	Devel.1	Mod.2	Poor.1,2,3	Excel.1 Good2	Excel.1 Mod.6	Mod.2
LTO	Lithium titanium	Devel.3	Poor.3 Mod.7	Poor.3	Good3	Good3	Poor.3
MNS	Manganese titanium	Research1	Good1	Mod.1	Excel.1	Unkwn.	Mod.1
MN	Manganese titanium	Research1	Excel.1	Excel.1	Excel.1	Unkwn.	Mod.1

For an electric vehicle standard application, using a secondary battery is an obvious choice. Other batteries could be used to supply emergency systems or range extenders, however in this thesis only the usual application will be studied, so the focus will be intensified on secondary type batteries.

In figure 2.4, a comparison is performed between the latest NiMh batteries and Lithium secondary batteries with values compiled from [31, 22, 4].

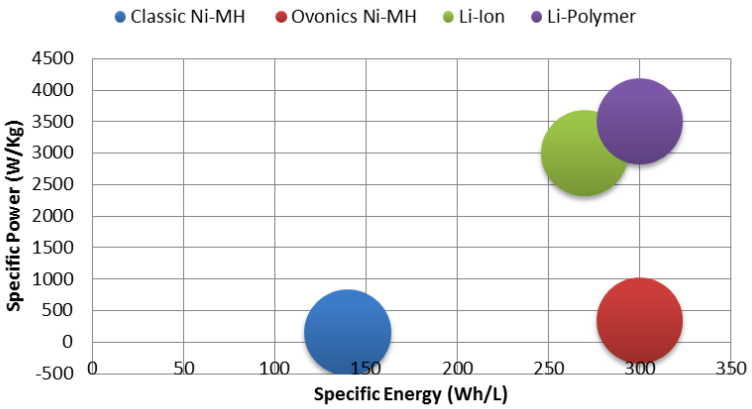

Figure 2.4: Lithium Based Technologies

2.2 Supercapacitors

When compared to normal capacitors (i.e. electrolytic), the supercapacitors have much more capacitance, hence a higher energy storage capability.

Contrary to common thinking, the supercapacitor is constructed much like a battery, being a basic cell composed with two electrodes, a separator and an electrolyte, working to separate positive and negative charges on to two separate plates separated, the afore mentioned electrolytes. Since no chemical change happen in the electrodes during the storage process, in most SC technologies, they tend to have a very high lifespan [35].

The decomposition voltage of the electrolyte determines the working voltage of the supercapacitor that depends greatly on the environment temperature, current intensity and lifetime required. There are three main supercapacitor technologies using two types of electrolytic material: one organic, with high working voltage, high energy density, wide temperature range and good compactness, and one aqueous, with low decomposition voltage and a narrow temperature range [31].

1. double-layer – This kind of technology is based on an electric double layer phenomenon [31]. The main convenience of this form of supercapacitor is its possible high capacitance (several thousands of Farad), that is mostly dependent of the active surface of the electrodes. Since those electrodes are usually made of porous carbon, the active area is greatly increased, imposing a very high capacitance to the supercapacitor. The research of materials is already open [31] and the main difficulty is in the finding of cheaper materials with the same or almost the same performance characteristics [8].

2. pseudo-capacitance – In an ideal double-layer the capacitance is not dependable of the applied voltage, but in the supercapacitor utilizing the pseudo-capacitance technology, there are an interaction between the solid material and the electrolyte, imposing a voltage-dependent charge transferring behaviour to the supercapacitor. This phenomena in which the charge transferred is voltage-dependent is the main basis for the name, pseudo-capacitance supercapacitor [8].

3. hybrid capacitors – Also known as asymmetric supercapacitors, the hybrid capacitors are composed by one electrode of a double-layer carbon material, much like in the double-layer supercapacitor technology, and the other electrode of a pseudo-capacitance material (e.g. Nickel), used in the pseudo-capacitance technology. The devices using this hybrid technology have significantly higher energy density when compared to the double-layer one, but as a shortcoming, the charger/discharger characteristics are highly non-linear [31].

In the next table, 2.2, some performance indexes for some types of supercapacitors are shown. In table 2.3 , some supercapacitors performance indexes by manufacturer are compiled.

Table 2.2: Performance Indexes for Types of Supercacitors [4]

Technlology Type	Electrode Material	Energy Storage Mechanisms	Cell Voltages	Energy Density Wh/kg	Power Density KW/kg
Electric Double Layer	Activated Carbon	Charge Separation	2.5 - 3	5 - 7.	1 - 3.
Advanced Carbon	Graphite Carbon	Charge Transfer or Intercalation	3 - 3.5	8. - 12	1. - 2
Pseudo-Capacitive	Metal Oxides	Redox Charge Transfer	2 - 3.5	10. - 15	1. - 2
Hybrid	Carbon/Metal Oxide	Double-Layer/ Charge Transfer	2 - 3.3	10. - 15	1. - 2
Hybrid	Carbon/Lead Oxide	Double-Layer/ Faradaic	1.5 - 2.2	10. - 12	1. - 2

Table 2.3: Performance Indexes for Supercapacitors By Manufacturers [31]

Manufacturer	V	F	Wh/kg	W/kg
Maxwell	2.7	3000	5.52	13800
NessCap	2.7	5000	5.44	13000
BatScap	2.7	2600	5.3	18000
Vina Tech	2.7	600	5	4000
ApowerCap	2.7	450	5.89	24600
JSR Micro	3.8	2000	12.1	9000

2.3 Flywheels

The flywheel energy storage system is a rotational mechanical system that recurring to its high moment of inertia stores kinetic energy. This kind of device has often a power electronics inter-

face to control the massive rotating cylinder supported by magnetic levitation in a low vacuum environment. The vacuum and the support by magnetic levitation tend to reduce rotational losses, hence preserving the stored kinetic energy.

$$E = \frac{1}{2} I_r \omega^2 \tag{2.1}$$

As we can see in equation (2.1), the moment of inertia and rotational speed are the key variables in this kind of system, thus a high speed and high moment of inertia is preferred. In 2.4 some materials that can be used to construct the flywheel are shown and related to their specific energy.

Table 2.4: Materials to Construct the Flywheel and respective energy

Material	Specific Energy
High Strenght Aluminium	41.5 Wh/kg
High Strenght Steel	54.7 Wh/kg
Glass/Epoxy	144.4 Wh/kg
High Strenght Aramid/Epoxy	193.7 Wh/kg
High Strenght Glass/Epoxy	213.3 Wh/kg
High Strenght Carbon/Epoxy	356.5 Wh/kg

Some literature consider this kind of technology to immature to be applied to EV [68], pointing as major drawback the necessity to find inexpensive materials capable to withstand the forces exerted with high rotational velocities and the extra forces applied to the vehicle causing loss of manoeuvrability to the vehicle [31].

2.4 Fuel Cells

The fuel cell technology started with Sir William Grove in 1839, but mostly because electricity was not well known, this first attempt was not successful. This technology had its first success in 1932 by Francis Bacon and was used in the Apollo space program in 1950s. Subsequently to this application many manufacturers, including some of the major auto makers and government agencies, made effort for an on-going research and development of the fuel cell technology [11].

The electricity generation method of a fuel cell involves fuel in the anode, an oxidant on the cathode and a reaction in the electrolyte. The fuel cell is able to produce electricity as long as the flow of fuel is maintained [35]. The main advantages of this technology are in the quiet operation, durability, reliability, zero or low emissions and high conversion efficiency of fuel to electric energy.

There are some shortcomings to this technology, due to the relatively low energy density of hydrogen (2.6kWh/L) when compared to a fossil fuel like petrol (6kWh/L) big fuel tanks are needed [35]. Moreover, this technology has a relatively low response time and is very expensive at the moment. The research and development nowadays is focused on hydrocarbon membranes to replace the current per fluorinated membranes [10].

In table 2.5 some fuel cell types are compared using the most significant parameters.

Table 2.5: Comparison Between Fuel Cell Types

	Phosphoric Acid	Molten Carbonate	Alkaline	Solid Oxide	Direct Methanol	Solid Polymer
Temperature	150 - 210	600 - 700	60 - 100	900 - 1000	50 - 100	50 - 100
Density (W/cm2)	0.2 - 0.25	0.1 - 0.2	0.2 - 0.3	0.24 - 0.3	0.04 - 0.23	0.35 - 0.6
Life (kh)	40	40	10	40	10	40
Cost ($/kW)	1000	1000	200	1500	200	200

2.5 Sources Hybridization

The energy storage system of the electric vehicle is one its major drawbacks.

Nowadays and in the near future, the most viable energy sources to apply to electric vehicles are batteries, fuel cells, supercapacitors and flywheels. Batteries, in spite of being the most mature energy source, are bulky, heavy, and expensive and cannot deliver either the needed specific energy or specific power. Fuel cells are a proven technology but not a mature one, they offer a good specific energy, but are incapable of accepting regenerative energy. Supercapacitors, as primary energy source in a standalone application, are unable to deliver the required specific energy, but they have very good specific power characteristics. Flywheels are a technologically immature resource to be used as an energy storage system in an electric vehicle [68].

The main objective of the researchers around the world studying sources hybridization is to take into use the best characteristics of the chosen energy storing devices, improving both vehicle driving range and cycle life of those devices.

No single power source technology is perfect in both energy density and power density. Some can be acceptable in those two parameters, but the possibility to arrange various types of power source technology to achieve one that is capable of delivering and accepting a high power and high energy drives industrial and academic institutions to power source hybridization studies.

With the energy storing elements described above, there are six possible types of hybridizations [12]. The most common are the conjunction between fuel cells and supercapacitors, and batteries and supercapacitors. Other combinations are possible and will be approached in this subsection. The energetic flow assumptions that will be done next assume power electronics structures that support those combinations and that an effective power converter control and correct energy flow control.

1. Battery-Battery Hybrid

   One of the hybridization options is to combine two batteries, one of each type. In section 2.1, various battery technologies were described. Some technologies are better in some aspects. Energy density is the main feature in some batteries while others are safe or have higher power density. The objective is always to achieve a power source that can be efficient in a wide spectrum of operations. With that thought in mind, one of the most important aspects in a power source in EV is to provide both peaks of power and plenty of energy, therefore a possibility is that one type of battery provides high specific power, and the other provides

high specific energy. This obviously is viewed as a starting point to choose a solution with much wider convergence to a very good hybrid power source.

Some data withdrawn from [42] about the most popular battery types are shown in figure 2.5, and is possible to gather sufficient pertinent information to choose a good hybrid power source system.

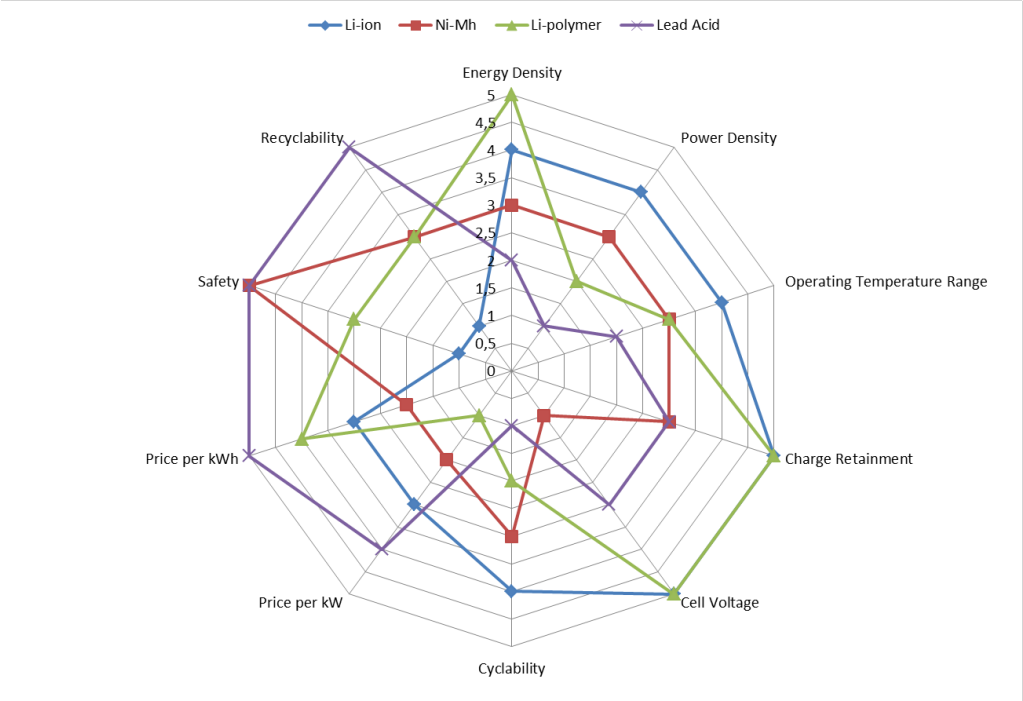

Figure 2.5: Battery-Battery Hybrid - data comparison from different battery types

When merging two or more power sources, one must use common sense to know how the characteristics of the hybrid power source will get. Using the properties described in 2.5, a system using a very safe technology and an unsafe one does not get any safer, hence, the minimum of the values of that characteristic is used, same thought can be applied to recyclability. In the price per energy and energy density characteristics will be considered the assessment of the technology used to provide the specific energy. Equal treatment is used to the battery type that would be used to provide power, when relating to the price per power and power density characteristics. In properties like charge retainment the value to be acknowledged to the hybrid solution is the one of the technology used to provide the specific energy, because that is the component that needs to hold the charge for a longer period. Cell voltage affects mostly the power electronics structure, but can be overcome with cell arrangement, thus the best assessment of the battery types composing the hybrid solution will be used. A weighted mean will be performed to temperature since both technologies are exposed to the same temperature. Cyclability value will be from the technology which provides specific power, since is the more likely to discharge completely more often.

After an empirical analysis, two battery-battery configurations prevailed. Those options are represented in 2.6.

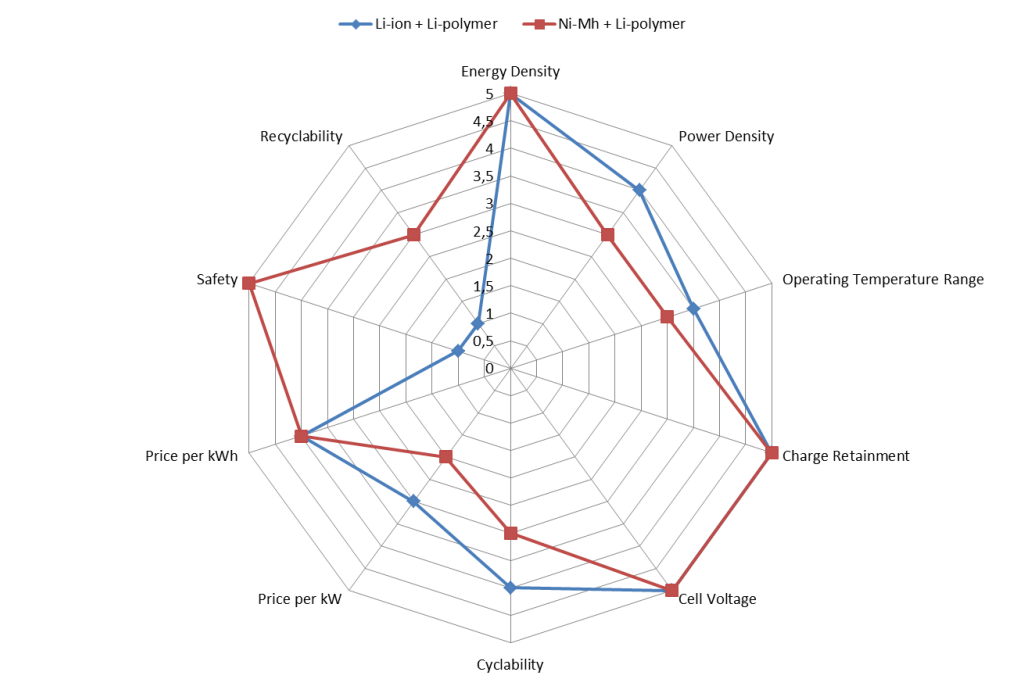

Figure 2.6: Battery-Battery Hybrid - configurations that prevailed

Hybrid configurations with the two lithium based technologies, Li-polymer to provide specific energy and Li-ion to provide specific power emerge with the best functional performance, but safety and recyclability are a great handicap in EV applications.

A much more balanced spectrum of operation can be attained with Li-polymer batteries to provide, once again, mostly specific energy and Ni-MH batteries to provide mostly specific power. A down side to use Ni-MH technology to provide specific power is due to its low voltage characteristics, this imposes many cells in a serial configuration to achieve an acceptable voltage and parallel configuration to be capable of providing the demanded peak current, hence many cells would have to be used.

2. Fuel Cell and Battery

   Fuel cells and batteries combination is a good collaboration. In spite of not having the possibility for a regenerative braking system, Fuel cells have inherently a very high specific energy, thus a very high driving range is possible. To bridge the regenerative shortcoming of the fuel cells, a battery constructed to deliver a high specific power can be used. By using figure 2.5 again, we can arrive at the conclusion that a Li-ion battery is a good choice when it comes to a high specific power, useful to either to absorb the downhill energy regeneration or regenerative braking and to provide instantaneous power to hill climbing or sudden

acceleration. The same drawbacks as to use Li-ion appear, safety and recyclability are poor. FC is a dangerous technology due to the usage of hydrogen, a highly flammable element.

3. Battery/Fuel Cell and Flywheel

   Once again, the batteries or fuel cells are used to provide the energy needed to obtain a high driving range and the flywheel technology provides the possibility of energy regeneration. Since flywheels are in their early stages of development is immature to take into account these combinations (Battery and Flywheel, and Fuel Cell and Flywheel) of power sources [68].

4. Fuel Cell and Supercapacitor

   Using both fuel cell and supercapacitor technology, the system is able to provide permanent and transient power as it is demanded by the load (i.e. the powertrain) [5]. This power sources interconnection is a reliable one in terms of energy and power deliverance. It has a very high driving range, due to the inherently good specific energy characteristics of the fuel cell technology and a very good power delivery and energy regeneration ratio, imposed by the very good specific power properties of the supercapacitor technology. This is, with the battery and supercapacitor, the most studied hybrid combination nowadays.

5. Battery and Supercapacitor

   With these two technologies working to the same objective, the possibility to absorb and provide both energy and power to and from the load, effective power source hybridization is possible. The battery is used, mainly, to provide the energy needed to a high driving range and the supercapacitor, with its very good specific power characteristics, provides the power peaks needed in some situations in an electric vehicle. The next table, 2.6, taken from [31], shows power and energy characteristics of various types of both supercapacitors and batteries.

Table 2.6: Power and Energy Characteristics of Types of Supercapacitors and Batteries

Device techology	Nominal Cell Voltage	Wh/kg	W/kg 90%
Supercapacitors:			
Carbon/carbon	2.7	5	2500 - 5000
Hybrid Carbon	3.8	12	1635
Lithium-ion Batteries:			
Iron Phosphate	3.25	90 - 115	700 - 1200
Lithium Titanate	2.4	35 - 70	700 - 2260
NiCoMnO2	3.7	95	1700
Other Types of Battery:	1.2	46	400
Ni Mt Hydride HEV	2.0	26	150
Zn-Air	1.3	450	200-400

In order for the reader to understand the advantage of using a hybrid power source with SC, a radar type chart is shown in 2.7, which compiles the information of single battery solutions, battery-battery hybrid solutions and the best solution so far, the battery-SC solution.

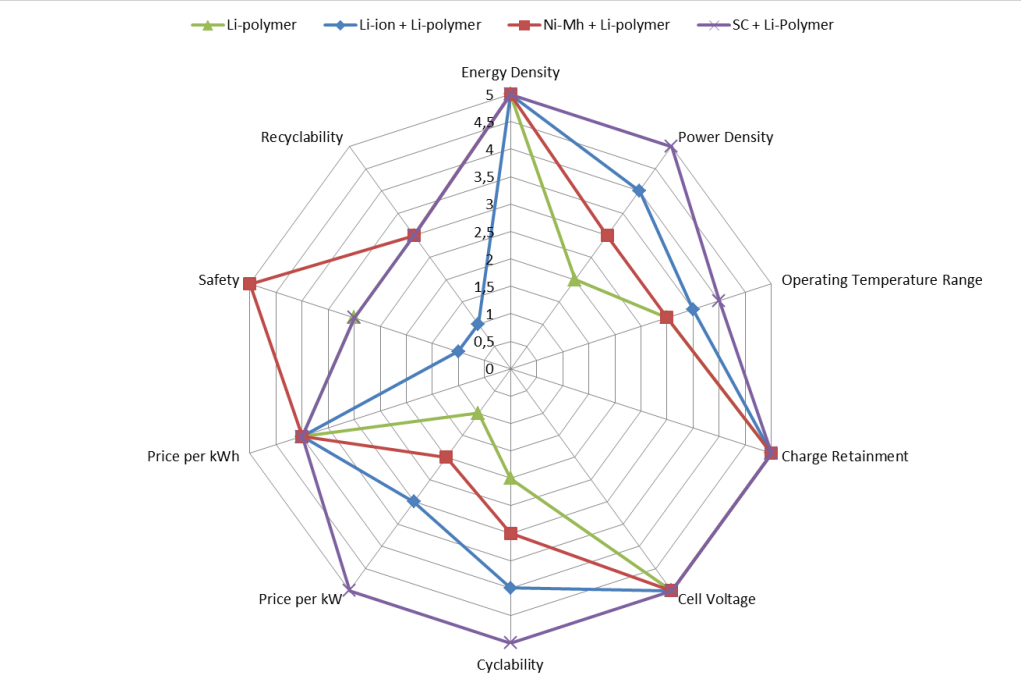

Figure 2.7: Comparison between Single Battery Solution, Battery-Battery hybrid Solution and Best Solution So Far

2.6 Models and Parameter Estimation

In this subsection some general concepts about model and parameter estimation will be described.

According to [37], which revised several literature on this topic, models can be divided as intuitive, graphical, mathematical and analogue. Intuitive models are based mostly in common sense. Resembling to when one needs to turn a vehicle, that person knows that the steering wheel must be moved. Graphical models are based on visual information, like a Bode plot or a system response to a step. Usually they are used to describe linear systems. This kind of models can be used afterwards to aid in the construction of mathematical models, which are mainly used to define more complex systems.

Mathematical models can be divided through various parameters, as in number of inputs and outputs, as modelling linear or non-linear systems, as being parametric or non-parametric, as to its time variance, as being on a time or frequency domain, as continuous or discrete and as being stochastic or deterministic. There are two possible ways to build a mathematical model, analytical or experimental. The first one is based on physics or economic laws and the second one in measured values from the system itself.

Analogue models are obtained through system analogy, a mechanical and an electronic oscillator can be described with the same linear and differential equation.

The more relevant of these concepts will be revisited throughout this subsection.

2.6.1 Modelling a Battery

In literature mostly two types of models are used to characterize a battery, from [13] to [27].

Some acknowledgements must be stated before the models description is shown. Two main decisions were made, only the discharge process will be modelled and temperature will be assumed to be in values around 23 and 60.

The first decision is due to time-spending procedures needed to achieve relevant data to be used to model the charging behaviour of a battery being basically the same as the ones for discharge models, hence not much more information would be attained and much time would be lost.

When temperatures are between the stated values, very low variations in the discharge behaviour appear, allowing for the temperature to be assumed as constant, not interfering directly to the measured values. This information is shown in 2.8 and was taken from [24], the datasheet of the used batteries.

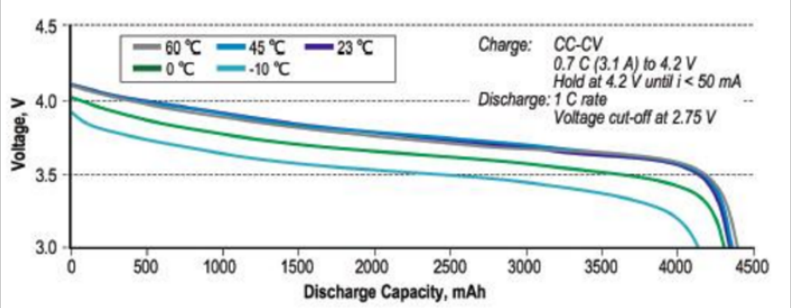

Figure 2.8: Discharging Curves of the Battery

1. Mathematical Model

   The objective in this part is to attain a mathematical curve that characterizes with low error the current, voltage behavior through time. This model must be achieved by measuring the given variables during discharge procedures.

   The idea behind this kind of model is simple. The battery is exposed to conditions that cover a spectrum of operation intended to be modeled. Measuring voltage, current and counting time during the discharge procedures a good dataset of samples can be obtained to fit those samples to a function.

   A good dataset should have scattered samples through the entire surface to be represented, this improves the fitting process, lowering the error of the final surface solution.

   Recurring to the nomenclature used in [37], the method that will be explained here has two inputs, time and current, voltage is considered a consequence of the discharge with a given current during a certain time and therefore is the output. Due to the premises stated this can be considered a multiple input - single output system (MISO). Not being possible to foreknow if this system is linear, a distinction is not performed. Since the final result is

expected to be a surface which models the behavior of the measured battery one can assume this model to be non-parametric in a time domain. The state of health (SoH) of a battery imposes a time variant model, but in this case SoH is assumed constant and therefore a time invariant system appears. The fitted surface may not state exactly the state of the battery, but an approximation, hence must be considered as a stochastic model.

A mathematical model such as the one presented have some limitations that must be known, its domain is limited to the functioning point in which the measures were made, no physical insight is given to the system since the factors calculated through fitting process do not hold any physical meaning by themselves [45]. Despite of being of a simple and relatively direct application, this kind of mathematical model is only interesting if the only requirement is to predict the output through the given inputs [37].

2. Electrical Model

   An electrical model of a battery can be viewed as analogue model, since the model is based in electrical equations that also define electrochemical behaviors. In other hand this model can be considered as a mathematical one followed by parameter identification based on samples measured in the system itself.

   Many electric models are proposed in literature, but the one of the first to be published was proposed by Shepherd in 1965 and the MATLAB/Simulink model is based in the equation by him proposed in 1960s [26, 65]. Nowadays, the most consensual electric model to a battery is composed by an ideal voltage source representing the open circuit voltage (V_{OC}) in series with a resistance, responsible for an almost instantaneous voltage drop every time current is demanded to the battery and a series of RC circuits, which are responsible for the dynamic response of the battery [45, 17]. The number of RC circuits were agreed upon the number two, since is the best tradeoff between accuracy and computational complexity [45, 26]. A schematic of the circuit is presented in figure 2.9 and in figure 2.10, taken from [45], a response to a current step of this kind of circuit is shown.

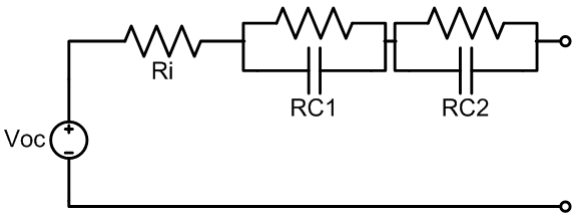

Figure 2.9: Electrical Circuit

By analysing figure 2.10 it is possible to describe the variables which we need to identify.

The response function is the sum of a step and two exponential decays. The sudden voltage drop is caused by the series resistance and the exponential decays caused by the two RC blocks in the schematic presented in 2.9, one with a higher time constant and other with a lower one. This leads to an expression to the output as shown in equation (2.2).

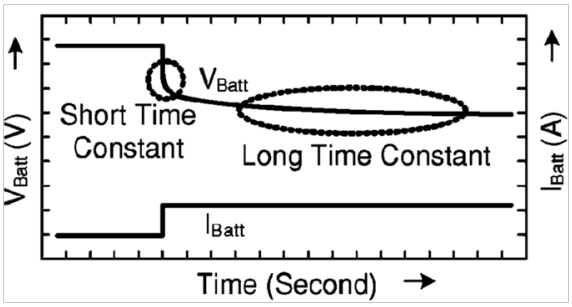

Figure 2.10: Circuit with a response to a current step

$$v_{batt}(t) = \begin{cases} V_{OC} & ,t \in [0, t_d] \\ \frac{V_1}{2} \times (e^{\frac{t-t_d}{R_1 C_1}} + e^{\frac{t-t_d}{R_2 C_2}}) & ,t \in [t_d, +\infty] \end{cases} \tag{2.2}$$

In equation 2.2, t_d is the time instant of a sudden current discharge, R_1,C_1, R_2 and C_2 are the resistances and capacitors from the *RC* blocks 1 and 2 represented in 2.9 respectively. Observing figure 2.10, one can find V_1 as being the voltage right aftert_d and V_{OC} being the initial voltage, when no current is being absorbed from the battery. Using Ohms law one can arrive at the relation between the variables composing (2.2) with the parameters to identify. Those relations are as stated in the next equations.

$$R_i = \frac{V_{OC} - V_1}{I_{batt}} \tag{2.3}$$

$$R_1 = \frac{V_1 - V_2}{I_{batt}} \tag{2.4}$$

$$C_1 = \frac{\tau_1}{R_1} \tag{2.5}$$

$$R_2 = \frac{V_2 - V_3}{I_{batt}} \tag{2.6}$$

$$C_2 = \frac{\tau_2}{R_2} \tag{2.7}$$

Some new variables are introduced in the formulation that led to the identification of the battery parameters. To calculate R_1 the voltage value in which is considered that the first exponential response has no longer significant effect, V_2, must be attained. That value is usually measured 60 milliseconds after the sudden current demand [62]. The variable τ_1 is the time constant of the exponential decay ruled by the first RC block, marked in 2.9 as RC1. The same approach can be used to find the second RC block characterization, but

since the second exponential decay tend to have a very high time constant , its effect in the output signal does not cease to have its influence for a long period of time, thus V_3 is usually measured as later as possible. the variable τ_2 is the exponential decay of RC2.

2.6.2 Modelling Other Power Sources

The same methods used to achieve battery models could be used to other power sources with special relevance to SC, where the application is almost exactly equal. All power sources approached in this master thesis are characterized as to their voltage and current. Therefore a mathematical model is possible to obtain measuring at least those variables throughout the discharge process, fuel consumption in the FC case or flywheel deceleration.

Much scientific effort is focused at obtaining equivalent electric circuits for power sources applicable in EVs. The ones stated in this master thesis have already electric equivalents [60, 20, 40, 66], thus with more or less ease the estimation of their parameters can be achieved through the voltage output signal, like in the battery parameter identification process.

Chapter 3

Test Setup Design and Battery Model Results

To acquire the data needed to construct the models described in 2.6, a design of a test setup was mandatory. This part of the work is one of the most important, because depending on the reliability of this setup are the measures needed to attain the models previously described. Obviously, errors in this part of the project would be propagated to other main subjects, like model estimation and state of charge analysis. The test bench was designed to meet the requirements desired to achieve good battery models. This design was executed with the premiss that the battery nominal features were known. The battery was of the Li-ion technology and with a nominal capacity of 4.4 Ampere hour [24].

In this section a test setup functional analysis will be performed followed by a requirement analysis and a component choosing process, which assures that all the aforementioned requirements are met. This finalizes the concept stage. After the concept stage is possible to show some detail on some of the component chosen, therefore the pertinent hardware will be scoped followed by the software solutions. The final part of this section will show the results of the model extraction procedures, which are also the results of the test setup.

3.1 Test Setup Design

3.1.1 Transportation and Operations Research

The main function of the test setup is to impose to a low-power battery, well-known discharge conditions and charge it according to the manufacturer's conditions, while its voltage and current are measured. Those operations must run in parallel, must be completely configurable and remotely controlled.

Based on those premises a centralized functional architecture was implemented and is represented in figure 3.1.

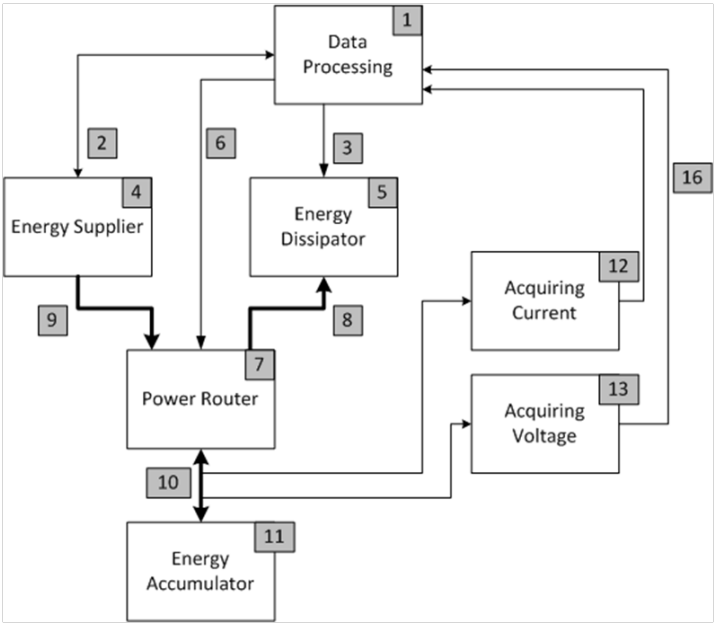

Figure 3.1: Functional Architecture

3.1.2 Requirements Analysis

Each pertinent block or interconnection of the figure 3.1 has a number associated, which is used in the left-hand side of table 3.1 to point the requirements for that block or interconnection. The right-hand side numbers are the number of each requirement to be used in the next subsection to choose the physical component that could perform that same requirement.

3.1.2.1 Important Requirements Discussion

In this part, only the requirements that are critical to achieve a low error model will be discussed. Obviously all requirements are important to meet, but the analytical ones are the only to be discussed, by coincidence, those requirements are related to voltage and current measurements.

1. The voltage accuracy requirement is based on the fact that, in a sudden discharge process with very low current, the voltage drop can by of only dozens of millivolt, therefore an accuracy of at least 5mV is recommended.

2. As mentioned in 2.6, the fastest phenomena to be measured is almost instantaneous and is not required to acquire that dynamic behaviour, hence the fastest measurements to be taken with detail are the ones occurring in the first exponential decay which has time constant of at least 60 milliseconds, hence according to [9] there must be at least two samples during that time, but an usual thumb-rule points to at least ten samples during that time period. Those values indicate a reference value of at least 6000 samples per second.

Table 3.1: Requirements for Blocks and Interconnection of Figure 3.1

1	Data processing capability at least 10x faster than the one of the with the higher frequency	1
	Must accept incoming and outgoing data to and from remote devices	2
	Compatibility with the programming language of the remote devices	3
2	Must be capable to interface 1 and 4	4
	Should not have EMI susceptibility	5
	Communication must be bidirectional	6
3	Must be capable to interface 1 and 5	7
	Should not have EMI susceptibility	8
4	Must be capable to supply the accumulator with compatible current and voltage levels	9
	Constant voltage and constant current modes of operation are mandatory	10
	Remotely command able	11
5	Must be able to dissipate the maximum power supplied by the accumulator	12
	Constant voltage and constant current modes of operation are mandatory	13
	Remotely command able	14
6	Should not have EMI susceptibility	15
	Compatibility between 1 and 7 must be assured	16
7	Decoupling between the current flowing from 5 to 11 and the one flowing from 4 to 11 must be assured	17
	Remotely command able	18
8,9	Unidirectionality must be assured	19
	Must be in conformity with the maximum current level supplied by 4 and 5 respectively	20
10	Must be in conformity with the maximum current level supplied by 4 and 11 respectively	21
11	Must be able to support to three energy accumulators	22
	The two terminals of each energy accumulator must be accessible through remote external commands	23
	Only one accumulator can be connected at each time	24
12	The current measure should not interrupt the energy flow	25
	Precision and resolution must be of at least 100A	26
	The transducer output must be a measurable voltage	27
13	Must have a high frequency rejection	28
14	An interface between the measured analog signals and 1 must be achieved	29
	Should not have EMI susceptibility	30

3. Current accuracy requirements have the same design parameters as the ones used in voltage. The minimum current variation is imposed to be of about 10 milliampere, that is the minimum variation to be measured.

4. Current sampling must keep up with the voltage measurements. Calculations between those two variables are needed, as an example, in the first serial resistance identification process. Contiguous voltage and current samples should have low time intervals for those calculations to have pertinent results, therefore a 6000 samples per second is a appropriate reference value to current acquisition speed.

3.1.3 A Possible Solution

In this subsection a possible solution is presented. All the requirements, in left-hand side with the same numbering as in the right-hand side of table 3.1, are met and shown in table 3.2. In posterior parts of this master thesis the chosen hardware will be detailed and their requirements convergence will be again approached.

In order for the reader to have a good understanding of the proposed system its architecture is unveiled in figure 3.2.

Table 3.2: Solution Requirements

1 2 3	LabVIEW? installed in a computer with at least a Processor Pentium III/Celeron 866 MHz or equivalent and with 256 MB of RAM
4 5 6	NI GPIB-USB-HS ? a National Instruments Cable + Board for GPIB communications
7 8	IT-E132, a USB to TTL Interface Cable
9 10 11	Fluke PM2832 Programmable DC Power Supply, a dual output, 60 Volt, 2 Amp Power Supply
12 13 14	BK Precision 8500 ,a 300W Programmable DC Electronic Load
15 16	DB25 Connector + LPT1 Cable + TBX-68 I/O Module + NI-18749C Cable + PCI ? 6024E I/O Board
17 18	G2R-14-DC12 Power Relay + BJT Transistor BD139 + External DC 15V DC Source + 2x Banana Plug 4mm (15A)
19	1N5401 Fast Recovery Diode
20	Wire with conductor area of at least 0.75mm2 (6A at 60C) + 2x Banana Plug 4mm (15A) + 2x Banana Jack
21	PCB Traces with a width of at least 5mm and thickness of 0.1mm
22	Acrylic Support
23	3xG2R-14-DC12 Power Relay + 3x BJT Transistor BD139 + External DC 15V DC Source and as in 15 and 16
25 26 27	LEM HY-5P
28	LabVIEW? Software
29 30	DB25 Connector + LPT1 Cable + TBX-68 I/O Module + NI-18749C Cable + PCI ? 6024E I/O Board

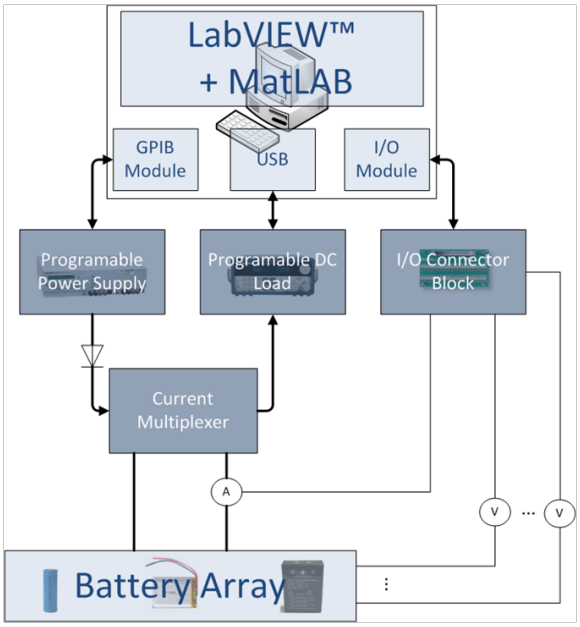

Figure 3.2: Solution Architecture

3.1.4 Hardware Description

In this part of the master thesis a detailed description of some of the most important components of the designed test setup.

3.1.4.1 DC Power Source

To charge the battery a DC power supply was needed. One of its major requirements was for it to be remotely programmable and controllable.

Fluke/Phillips PM2832 Programmable DC Power Supply gives a chance to remotely program two modes of operation through a communication protocol based on IEEE-488, also known as GPIB (General Purposed Interface Bus). Those two operation modes, constant current and constant voltage power supply, meet the previously mentioned requirements. As a device that was used mainly to charge at most three li-ion cells (the batteries with higher cell voltage) connected in a serial manner, only 12.6 Volt (4.2V x 3) of the possible 60 Volt is required. As to the maximum of 2 Ampere, will only impose a slower charge of the battery and have no prejudicial effects on the system. In table 3.3 the absolute maximum ratings to both current and voltage are shown [23].

Table 3.3: Absolute Maximum Ratings of the Power Supply

Voltage	60V
Current	2A

3.1.4.2 DC Electric Load

The chosen DC electric load is a BK-Precision 8500 manufactured by BK Precision. This DC load has two terminals to be connected with a DC source. Various modes of operation are possible in this device, constant current drawn from the power source, constant voltage applied to its terminal, constant power absorbed from the connected power supply and can even present itself has a (almost) perfect resistance to the power source. The remote programming requirement is met by a serial interface (RS-232 or USB).

When three low-power batteries, such as the ones used, are connected in a serial manner, if two times the nominal current demanded, instantaneous power can get to a value around 100 Watt (11.1 Volt with 8.8 Ampere). The programmable electronic load BK-Precision 8500 has operational specifications that meet the requirements, as shown in the table 3.4 [7].

Table 3.4: Operational Specifications of the DC Electric Load

Voltage	0 to 120V
Current	1mA to 30A
Power	300W

3.1.4.3 Current Router

A need to change remotely the current flow between load and supply determined that a current routing circuit should be designed. The solution encountered had, as central components, a DPDT power relay, to physically connect or disconnect the current conductors between load and supply

and a bipolar-junction transistor (BJT) with npn junction to receive the low-power commands and impose them to the relay.

The designed circuit is the one represented in figure 3.3 and implemented in PCB. That PCB is shown in figure 3.4.

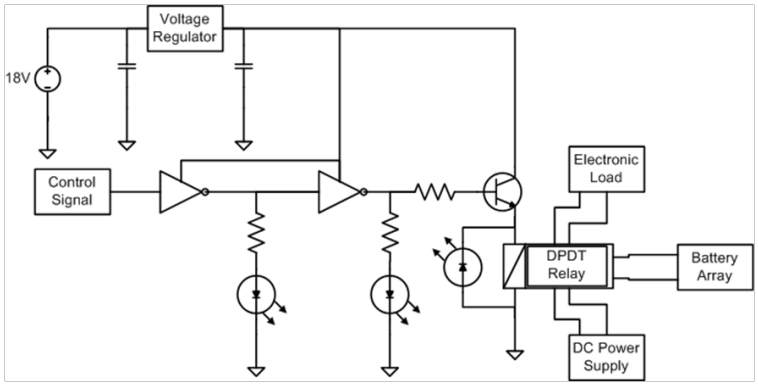

Figure 3.3: Current Routing Circuit Design

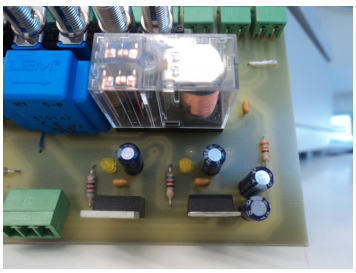

Figure 3.4: PCB with the Current Routing Circuit

Some informative components were added to the circuit. Two light emitting diodes (LED) provide the information of which instrument is connected to the battery. Those LEDs are connected to a NAND gate that performs both as a logic operator to the control signal and a current provider. A free-wheel diode is placed in parallel to the relay to dissipate the overvoltage energy once the BJT takes the inductive impedance of the relay out of conduction. For the BJT to switch must have a given current in the gate, so a resistance functions as a drive to a signal that also passes through the NAND gate to gain some power.

This circuit does not absorb any energy from the battery system, because is supplied by an external DC power supply through two voltage regulators, one for the negative and other for the positive voltage regulation. Both voltage regulators have a LED to indicate if the source is connected and with the desired voltage.

This circuit proved to be a good tool on interfacing the device responsible by operations control and the instruments which provide the energy flow.

3.1.4.4 Battery Connection Configurator

One of the requirements was to construct a way to allow for single cells of batteries to be connected in series with ease. Incorporated in the PCB where the current routing process was made, connectors were placed with manual switches like in the schematic presented in figure 3.5. The function of this circuit is to make the voltage of each battery accessible while a series connection can be performed sequentially. In figure 3.6 is possible to observe the circuit in the PCB.

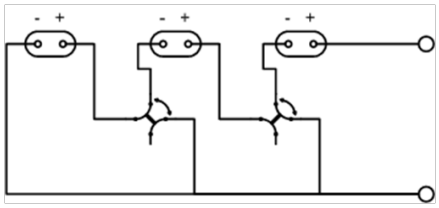

Figure 3.5: Battery Connections Scheme

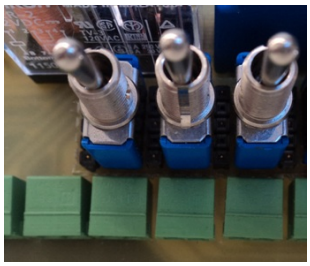

Figure 3.6: PCB with Battery Connections

3.1.4.5 Voltage Acquisition

The voltage acquisition is performed by a NI PCI-6024E Multifunction DAQ with the capability of acquiring up to eight differential analogue inputs with 12 bit resolution and a maximum sampling rate of 200K samples per second. The next table, 3.5 shows some of the most pertinent features of this multifunction DAQ [30].

Table 3.5: Features of the multifunction DAQ

Family	Analog inputs	Input Resolution	Max Sampling Rate	Input Range
NI 6024E	16 SE/8 DI	12 bits	200 kS/s	from -10V to 10V

Each NI PCI-6024E requires a cable, SH68-68-EP Cable, and a connector block, TBX-68 Unshielded, to be functional (besides the software that will be approached in the next subsection).

A requirement analysis can be performed to this equipment as to voltage accuracy and acquisition speed requirements:

The required voltage accuracy was determined to be 5 millivolt, according to the values present in table 3.5, the multifunction DAQ has an accuracy of about 1.5 millivolt when the voltage limits are between 0 and 5 Volt, the calculation of that value is presented in equation 3.1.

$$q = \frac{V_{max} - V_{min}}{2^{bits} - 1} \tag{3.1}$$

Acquisition speed requirements have to be met and at least one sample every 6 milliseconds have to be acquired, the same as 167 samples in one second. This voltage acquisition equipment has an integrated multiplexer which divides the maximum sampling rate for all the needed signals to be measured. If four signals are to be acquired (the signal related to current measurements is here considered as well), a sampling rate of about 50K samples per second can be achieved. This is possible to calculate using the equation 3.2.

$$\frac{SamplingRate}{signals} = \frac{200KS/s}{4} \tag{3.2}$$

This voltage measurement solution can perform well in the given parameters and meets all the above stated requirements. A picture of all the hardware used to perform the measurements is present in figure 3.7

Figure 3.7: Voltage Measurement Hardware

3.1.4.6 Current Acquisition

To acquire the current flowing through the battery a transducer had to be chosen. One of the requirements was that the transducer had to transform the current measured into a voltage. The instrument of choice was a LEM HY-5P. This current transducer has a voltage output going from -4 to 4 Volt that represent a current measured through the Hall Effect principle. Its transfer function, when transforming the current measured into voltage is stated in equation 3.3.

$$V_o = (\frac{5}{4} \times i) - 0.04 \tag{3.3}$$

The above equation is achieved by extracting linearity and offset of the output voltage as relevant parameters from the components datasheet [38]. Those and some other pertinent characteristics are shown in table 3.6.

For the current acquisition, the voltage output of the transducer must be acquired by the voltage acquisition component, the PCI-NI6024E. Therefore a resolution analysis must be performed to this measurement chain.

Table 3.6: Characteristics of the Current Transducer

Output Voltage	from -4V to 4V
Accuracy	<+- 1%
Electrical Offset Voltage	<-40mV

In the requirement listing, current has to be measurable at values variations of at least as 10 milliampere. This means that in order for that requirement to be met, the output voltage of the current transducer, when exposed to a current variation of 10 milliampere, must be higher than the least significant bit (LSB) of the ADC inside the voltage measurement equipment.

A current variation of 10 milliampere generates an output that varies 12.5 millivolt. Thus the resolution guaranteed by the 12bit of the ADC that enables a resolution of about 1.5 millivolt. The calculation of the values mentioned in this paragraph is based on the linear characteristic curve of the current transducer only.

3.1.5 Software Description

To control the hardware unit some software had to be implemented. The software in which the control program was developed was LabVIEW, a National Instruments creation based on a graphical programming environment. The huge variety of tools available to help on programming software to acquire and treat data and control instruments makes LabVIEW a good tool in applications such as the one in this master thesis. Even a potential drawback in calculus is bridged by the possibility to use software created by MathWorks, MatLab, as transfer functions with the block MatLab Script.

Therefore, two main development software were used, one to a higher level of detail, National Instruments LabVIEW and one to perform calculation, MatWorkss MatLab.

This development tool is specially indicated for signal processing, and instrumentation.

This subsection will describe the communication between LabVIEW and the instruments used in the hardware part, namely the DC power supply and the electronic load. After communication process is explained, both battery charging software and the implemented discharge software will be described. Ultimately that knowledge were used to create testbench software.

3.1.5.1 Communication with the instruments

As mentioned before, the devices responsible to both charge and sink the energy to and from the battery must have the capability to be controlled remotely.

1. Fluke/Phillips PM2832 and GPIB

   The DC power supply Fluke/Phillips PM2832 offers the possibility to be controlled through a GPIB interface. For this communication to take effect, hardware carrying information about the protocol used with GPIB, IEEE 488.1, is mandatory. National Instruments GPIB-USB-HS Cable has an integrated IEEE 488.1 controller for a full-functioning GPIB communication.

LabVIEW has complete support for GPIB communications. The blocks shown in figure 3.8, are responsible for the reading and writing in the bus. Those blocks allow the programmer to, at some level, ignore the protocol and focus only on the inputs and outputs, the messages to send, the messages received on when a query is done and its time-out. The GPIB address is mandatory. In the case of the instrument used the value of the GPIB address is a string named 28.

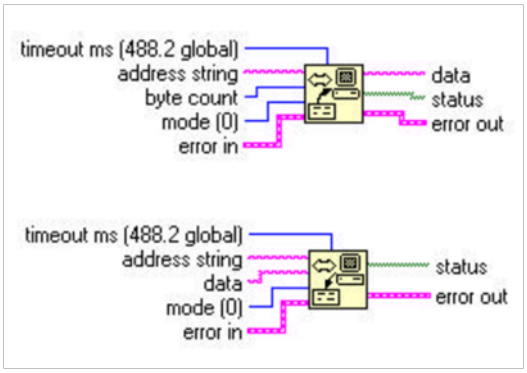

Figure 3.8: Reading and Writing Blocks of LabVIEW

Some remarks must be done to this part. Fluke PM2832 only accept, as a floating point separator, a .(dot) and not a ,(comma) , hence a search and replace block available in LabVIEW was used. That block search in the string containing the number with a comma as a floating point separator and replaces it with a dot.

The remote operation instructions are available in [23], the ones actually used are present in table 3.7.

Table 3.7: GPIB Commands

GPIB Command	Description
:INST:NSEL Channel	Selects the output channel to use
:INST:STAT Mode	Selects the operation mode (constant current or voltage)
:CURR Amplitude	Imposes the instrument to a contant current of a given Amplitude
:VOLT Amplitude	Imposes the instrument to a contant voltage of a given Amplitude
:MEAS:CURR?	Querry used to ask for the current measured at a given moment
:MEAS:VOLT?	Querry used to ask for the voltage measured at a given moment

2. BK-Precision 8500 and RS232

This hardware uses a serial communication protocol to send commands to the instrument. The instrument is capable to communicate with LabVIEW through drivers made available by BK Precision. The drivers are made recurring to LabVIEW functionalities related to serial communications using VISA. Basically these drivers are sub-programs controlling communications from LabVIEW to the instrument. In the next figure, 3.9, the drivers made available by BK Precision are shown.

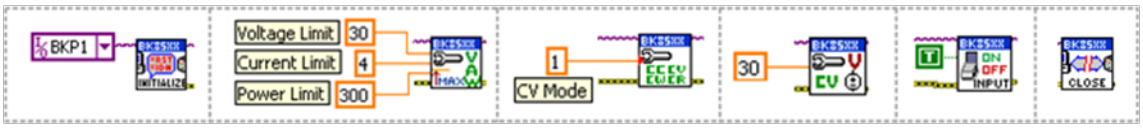

Figure 3.9: Drivers Available by BK Precision

From left-hand side to right-hand side:

- The first block implements an initialization of the communication between LabVIEW and the instrument. The input needed is the VISA source name which was named BKP1, referring to BK Precision instrument 1.
- In the second block is implemented a way to impose maximum values to voltage, current and power. These values prevail when the output would be higher in at least one of the variables.
- A mode of operation (0 constant current, 1 constant voltage, 2 constant power and 3 constant resistance) can be selected with the third block.
- The fourth block sends the instruction to impose a given constant voltage to the instrument. The other modes of operation have their own blocks to perform this operation and function in a similar way.
- By default the values sent to the instrument do not hold their values, acting as an impulse, to solve this setback a driver was made available the fifth block shown in 3.9 that, when it has an input of TRUE, the values sent before act as a step, holding the commanded values in the instrument.
- Ultimately, the connection should be closed by the sixth and last block. This blocks operation only disconnects the communication link between LabVIEW and the instrument and do not interfere with the values in the instrument.

3.1.5.2 Testbench Software Description

The testbench software was created based on some suppositions. The first one is that, to acquire pertinent data from the battery discharge process it must be completely charged respecting the manufacturers indications, conditions and restrains. After a complete charge, the discharge process can start. The battery is considered fully discharged when the voltage measured in its terminals is just below 3.00 Volt. After the battery is fully discharged, if more full discharges are to be done, the process is again performed until no more discharges are required. The acquisition is done in a parallel process and the data is stored in a .txt file.

An .xls file is used to schedule the discharge process, each sheet is referent to a full discharge process, thus if a .xls file has three sheets, three discharge processes will occur. The .xls file fields in which the user can edit to schedule the discharges are predetermined. The charging procedure is always the same and will be approached in part where the discharge software is detailed.

1. Charger

   Charging a Li-ion battery is a two-step process. The procedure stated in the battery manufacturers datasheet is based on first step with a constant current delivered to the battery until a voltage of 4.2 Volt is achieved, then the supply mode is shifted to a constant voltage one imposing those 4.2 Volt to the battery terminals, when the current is being drawn to the battery is below 0.01 Ampere the charging procedure is considered complete. The LabVIEW program responsible for the charging part is represented in figure 3.10.

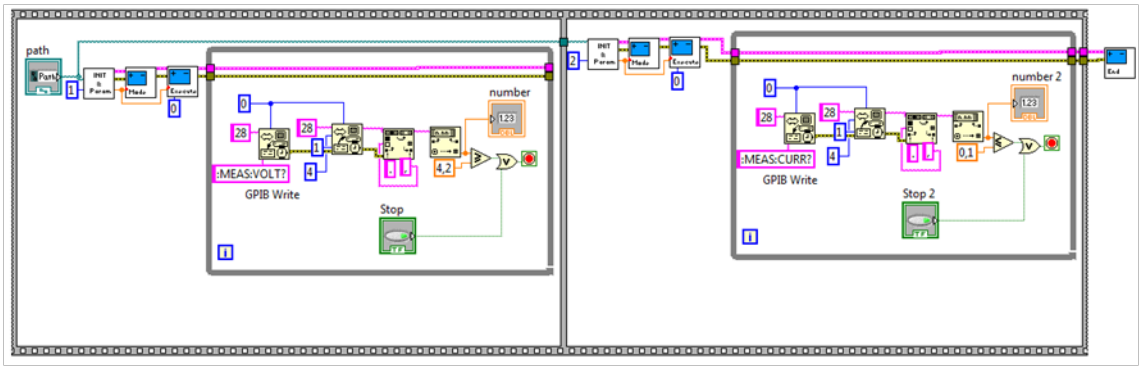

Figure 3.10: Battery Charger Labview Program

2. Discharger

   The discharging process has as many steps as the user wants. Through an .xls file the user can dictate the behaviour of the discharge process by choosing a mode to sink the energy (constant current, voltage, power or resistance), and the amplitude of the chosen mode variable. In figure 3.11 an example of a .xls that configures the system to sink the batterys energy through in a constant current mode beginning with a step of 1 Ampere of amplitude during 5 seconds and then a step of 2 Ampere for 5 seconds, and those values are repeated through time until the battery achieves a 3 Volt state.

   The LabVIEW program responsible for the discharging process is represented in figure 3.12.

   This part of the program starts by initializing the load with the limit values to voltage, current and power and the required mode of operation. After that a loop imposes determined amplitude to the load, waiting for the demanded time to expire, iterating the .xls file line. No mechanism is used impose that the load absorbs all the capacity of the battery exists, besides when the voltage gets to 3.00 Volt, thus the planning of the discharge process must be thoughtfully over-dimensioned in order to have guarantees to fully discharge the battery.

   The program jumps out of the loop only if the total time scheduled in the .xls file elapses, but once the voltage gets just below 3.00 Volt, a hardware protection (previously programmed in the Electronic Load) of sub-voltage triggers and forces the load into a no power absorption mode. This mode is not disconnected until another initialization of the instrument is performed, ignoring potential new commands.

J13

	A	B	C	D	E	F
1						
2		Combined Code	Hours		Topology Mode	
3		1	16,8		0	Load-0 Source-10
4						
5		Number of Lines	Time		Hardware Mode	
6		8065	60480		1	Constant Voltage - 0 Constant Current - 1 Constant Power - 2* Constant Load - 3*
7						* only available in Topology mode 0
8		Time(s)	Amplitude (SI)			
9	Timer Iniciator	0	0			
10		5	0,88			
11		10	0			
12		5	2,2			
13		10	0			
14		5	4,4			
15		10	0			
16		5	0,88			
17		10	0			
18		5	2,2			
19		10	0			

1

Figure 3.11: Discharge Configuration File

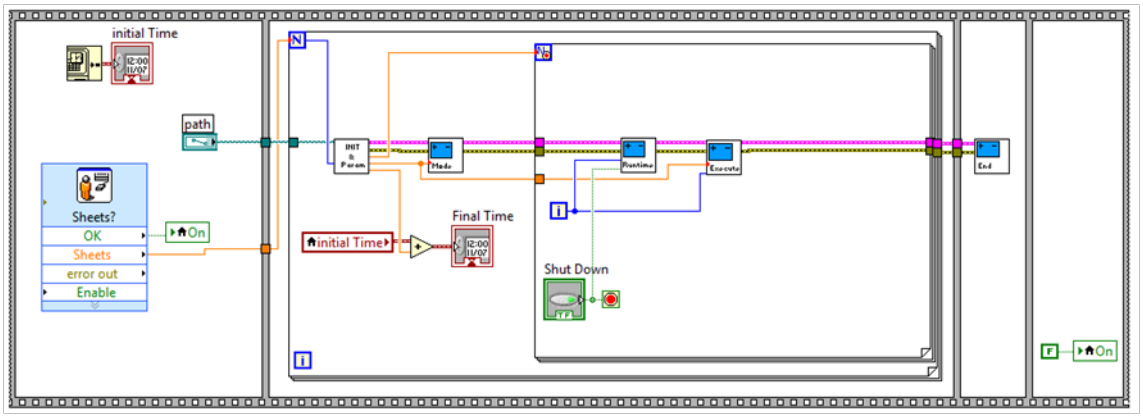

Figure 3.12: Battery Discharger Labview Program

3. Acquisition

Acquiring the dynamic data of the needed signals is a critical part of the test setup. Both the data existing in the sudden variations and the steady state values contain pertinent information, but acquiring the steady state information at the same rate as the sudden step response is an abusive memory usage, therefore a two-speed acquiring process was developed. The graphical programming of the acquiring process is represented in figure 3.13.

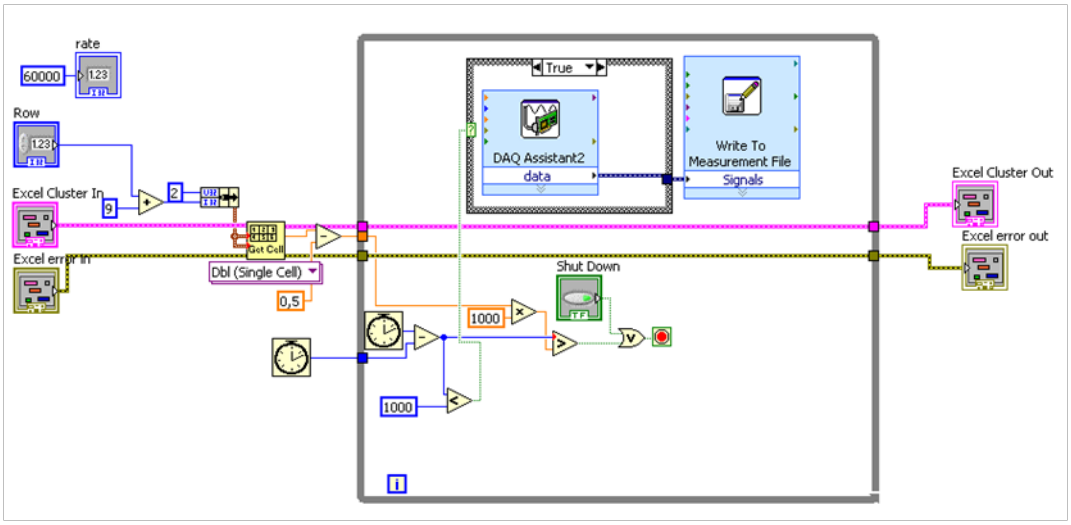

Figure 3.13: Acquisition Labview Program

Using the temporal knowledge given by the .xls file, since the amplitude management is previously scheduled, the program can act as if it has future knowledge, adapting itself to the incoming commands which generate dynamic chances in the signals to acquire. In practice, the algorithm counts the time left to the next change command, when that time is lower than 500 milliseconds a higher acquisition rate is imposed, after 1 second (500 milliseconds after the change command) a lower acquisition rate is again replenished.

The acquisition was performed in a separate machine. At first a program was implemented that had both the control and the acquisition processes in a parallel structure and pseudo-simultaneous loops, but due to a single processing core attribution to the LabVIEW software, only when the instrument control loop ended did the acquisition take place, loosing pertinent data. Since the objective of this project was not to optimize the number of devices used, another computer was used.

Right after the acquisition an existing Write to Measurement File block in LabVIEW was used, this block exports each sample to a .lvm file, which is exactly as a .txt only with an header in the beginning of the file. This .lvm file was used to posterior analysis in MatLab environment.

3.2 Modelling a Battery - Acquired Data and Results

Finally, with the test setup completed, was possible to gather data through experiments to compose the models mentioned in 2.6. This subsection will focus in the two aforementioned models. In each one of them some of the gathered data will be shown, followed by the resulting model and a comparison with the battery model of MathWorks MatLab for the mathematical model and a comparison with a reference paper results for the electric model.

3.2.1 Mathematical Model

As approached in 2.6, in order to compose a good dataset to be used as samples to a fitting procedure, well scattered samples must be acquired for both voltage and current. This premise leaded the way to various discharge tests. The first collection of samples was achieved by fully discharging the battery with constant current. For the current measurements to be well scattered, as mandatory to a good fitting process, various values of current were used. A complete discharge at 1.5C, 1C, 0.5C and 0.2C, being C the nominal current, was conducted extracting voltage, current and time data during those procedures. In order to have more samples two more types of discharge were implemented, constant power and constant resistance, the values used were, 1.5P, 1P, 0.5P and 0.2P and 0.9545 Ohm and 1.680 Ohm respectively. Where P is the nominal voltage (3.7 Volt) multiplied by the nominal current (4.4 Ampere).

The next chart present in figure 3.14 shows the characteristic curves of the constant current discharges.

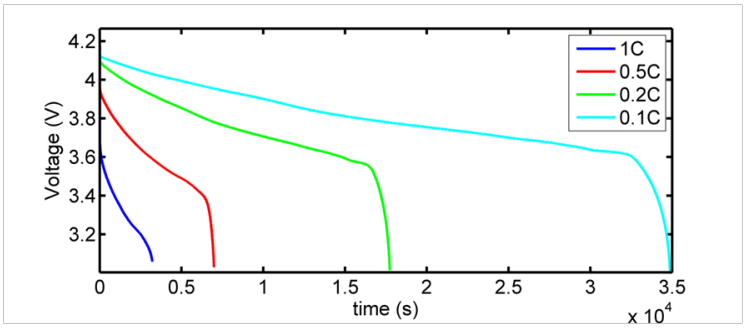

Figure 3.14: Characteristic Curves of the Constant Current Discharges

The fitting process of the samples gathered was done in the Mathworks MatLab environment. Some problems were faced at this point. The objective at that moment was to achieve a surface with current and time as inputs and voltage as output. As possible to observe in 3.14, the time variable has a highly non-linear behaviour. This kind of function, to be well approximated, needs an expression with very high order variables. A low-order polynomial function (fourth order) approximation was implemented to, at a first instance, validate the possibility to approximate such behaviour. The result is shown in figure 3.15.

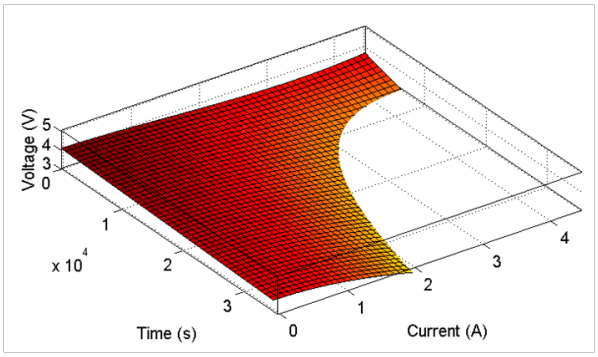

Figure 3.15: surface fitted with low-order polynom

The surface represented above proves the possibility to, given sufficient samples, to approximate a battery through a surface model, but does not represent at all the high-frequency characteristics observed as a knee in figure 3.14. The next step was to implement a higher order surface to represent the behaviour of the battery. With a tenth order approximation-function the result was rather poor in many zones of operation as visible in the resulting surface represented in figure 3.16.

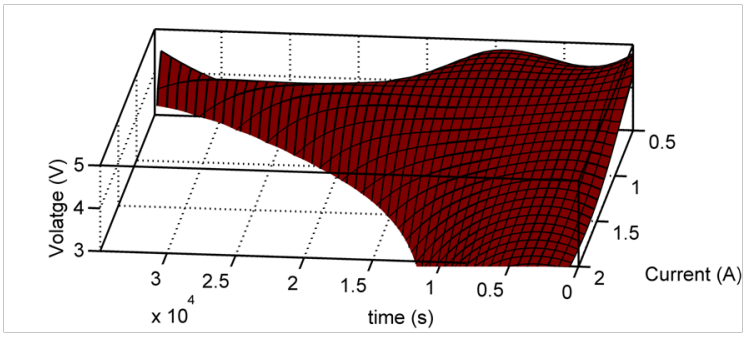

Figure 3.16: surface fitted with high-order polynomial equation

Is possible to observe in the picture above that great oscillations occur in very-low current zones, this is due to a low number of samples in that region, therefore fitting in that region is not constrained to those samples, diverging from the intended surface. That tend to happen with high order function approximations. No samples were collected for very low current regions due to time constrains. Samples with current rates near to null, the discharging procedure gets to time-consuming.

This model, as expected, is better to approximate abrupt changes, happening in the knee region, than a lower order surface. However, a comparison made in figure 3.17, shows that even with a fifth order (highest order possible in MatLab) variable representing the relationship between time and voltage, it is not able to approximate enough.

To conclude the analysis and to verify the validity of the model a comparison with the MatLab Model was performed, that comparison is possible to observe in figure 3.17.

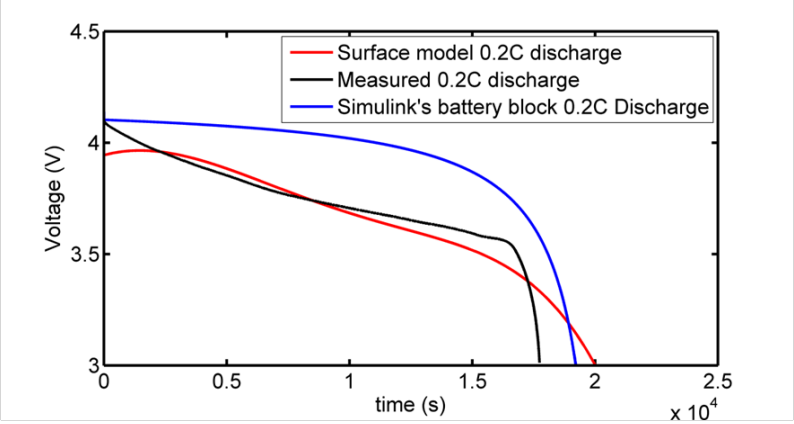

Figure 3.17: Comparison with MatLab Battery

Even knowing the actual discharge curve, using it to edit the battery parameters as purposed in [65] (the paper on which the battery block in SimPower Systems from MatLAb Simulink was based), the model is not at all accurate. Surface model, in the linear zone, has a decent behaviour implementing a fairly good approximation, providing that the current is high enough.

3.2.2 Electrical Model

This model is achieved through identification of some pertinent points in the output voltage when a sudden current is demanded to the battery, as described in 2.6. The carried discharge test was based on various steps with various current demands. The next flowchart, presented in figure 3.18 shows how the discharge procedure was done.

The last part of the pulsed discharge curve is shown in the following figure 3.19 as example of the acquired data.

Having pulsed discharges for a wide range of charges, various electric models can be calculated, enabling the possibility to achieve to a function that relates the identified electrical parameters of the battery to its charge. With the .txt file with the acquired data saved, it was possible to use once again the MatLab environment to previously calculate the charge left in the battery at every sample, using as the total charge the one state in the batterys manufactures datasheet and decrementing it as it was consumed. The vector with the actual charge is then concatenated with the loaded data from the .txt data.

Pertinent results were obtained with the identification process. Those results will be shown next, starting with the internal resistance in figure 3.20, followed by the first RC block represented in figure 3.21 and figure 3.22, with the results of the second and last RC circuit.

To validate the results obtained when it comes to its magnitude, they were compared to a similar test performed in [26]. Figure 3.23 shows that all parameters have coincident magnitude, somehow validating the model to its structure.

With a comparative analysis comes the idea that the results obtained in this master thesis are pertinent. In [45], for every 10% of SoC, measures would be taken by imposing to ten 850 mAh

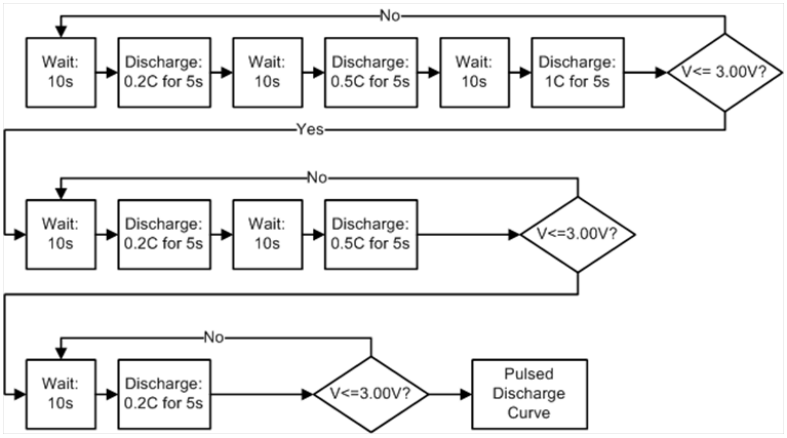

Figure 3.18: Discharge Procedure

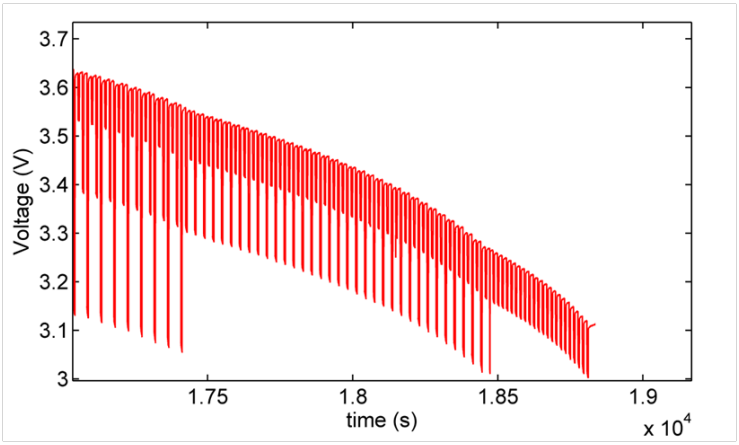

Figure 3.19: Pulsed Discharge Curve

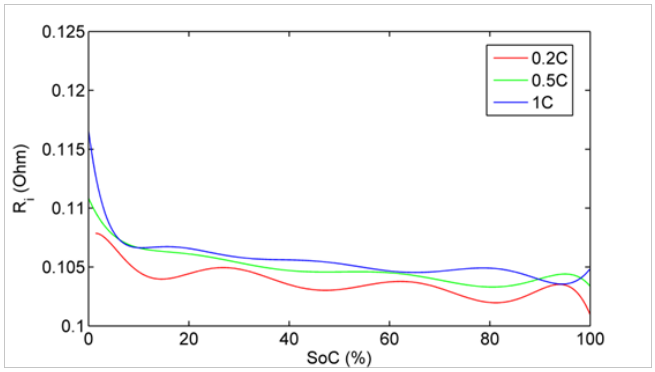

Figure 3.20: Internal Resistance

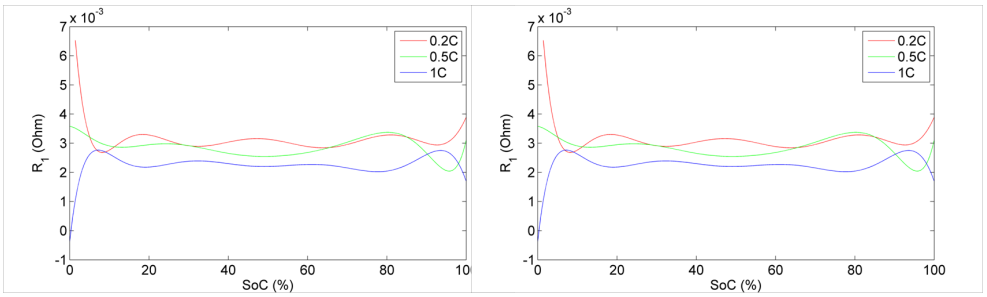

Figure 3.21: Results of the First RC Block

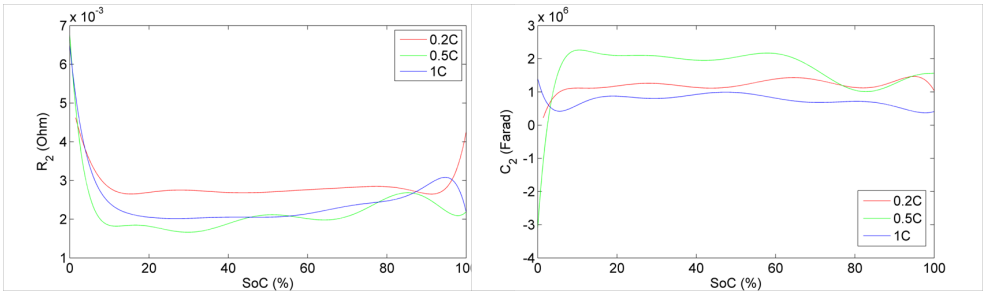

Figure 3.22: Results of the Second RC Block

(milliampere per hour) batteries a pulsed discharge and averaging the results. Being of a different technology (even if alike in some aspects), of different power range and measured with different methods, the results shown in figure 3.23 are merely informative and only with intent of having a critical glance at the results obtained in this part of the master thesis.

Resistive parameters identified with the proposed method are within the amplitude range of the ones that can be observed in figure 3.23. However, the capacitors values shown in figures 3.20, 3.21 and 3.22 have much higher values than the ones presented in figure 3.23, that can be explained by the difference of capacities (Ampere per hour) between the two power sources.

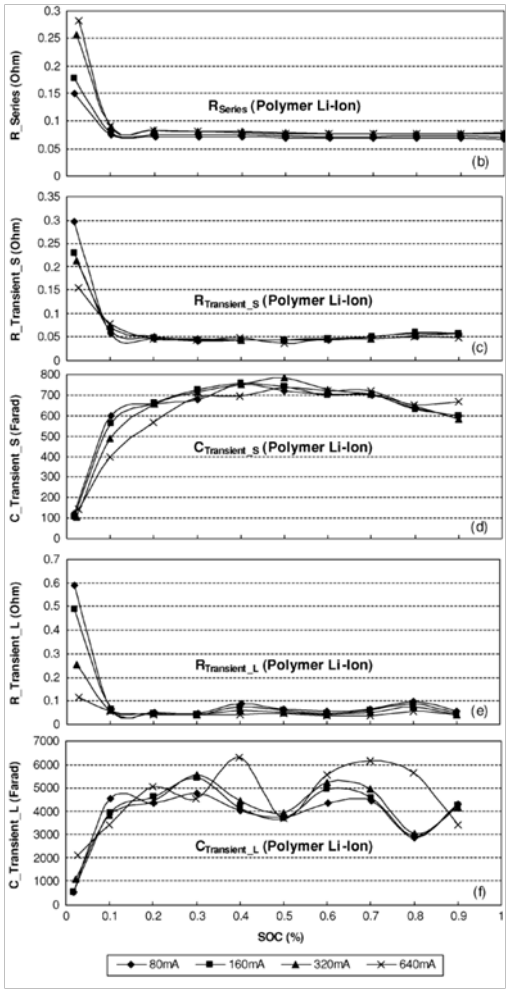

Figure 3.23: Validation of the Results in Magnitude

Chapter 4

State of Charge Estimation

> "SoC is the percentage of maximum possible charge that is present inside the battery" [57].

The state-of-charge of a battery helps to answer a meaningful question on the EV subject. Many devices used nowadays have a battery as their primary energy source, thus knowing how much energy is contained in that source, the objective of the SoC, helps to understand how long it takes until that device stops working. As interesting as it may seem to know exactly how much energy does a battery have, that estimation is not always easy and is even harder when that estimative is needed in real-time applications.

In electric vehicle applications a power source SoC is pertinent information to both the energy management system (i.e. ESS) and the electric vehicle passenger. The first due to energy control and the second to know what is the vehicle range. In both cases a real-time SoC estimation is important.

Many approaches to measure the SoC of a battery are proposed in literature. In this section, different techniques will be scoped and the most pertinent to this master thesis will be discussed and tested using the test-bench proposed in 3. Some SoC estimation methods are not suitable for real-time applications (e.g. Discharge Test [56]). However, they can be used to feed information to other methods (e.g. Artificial Neural Network [57]). Hence, even non-real-time estimation methods will be documented.

The methods that will be covered in this chapter are the Discharge Test, the Open Circuit Voltage, the Ampere Hour Counting and the Artificial Neural Network. A small overview is also included from other SoC estimation methods.

Every SoC estimation procedure was performed with a battery previously charged to its full charge according to the specifications instructed in the battery datasheet and using the software developed to that effect described in 3.1.5.2.

4.1 Discharge Test Method

The Discharge Test is a SoC estimation method which involves a battery spending a part of its charge under controlled conditions in order to compare measurements to a known scenario. According to [56], this method is the most reliable one.

4.1.1 Estimation Software Description

Interrupting the normal functioning of the circuit, the method imposes the battery to a constant current of 0.2C. During the time that the battery is delivering 0.2C to the load, the voltage to its terminals is measured and compared to a previously known characteristic curve (Voltage vs SoC).

The voltage versus SoC curve is attained through battery discharge with very low current. In this way, not only less energy is spent during the SoC estimation period, but also more accurate results are obtained because a very low current discharge is more accurate on the calculation of the total capacity of the battery.

The flow chart shown in 4.1 is indicative of the method used.

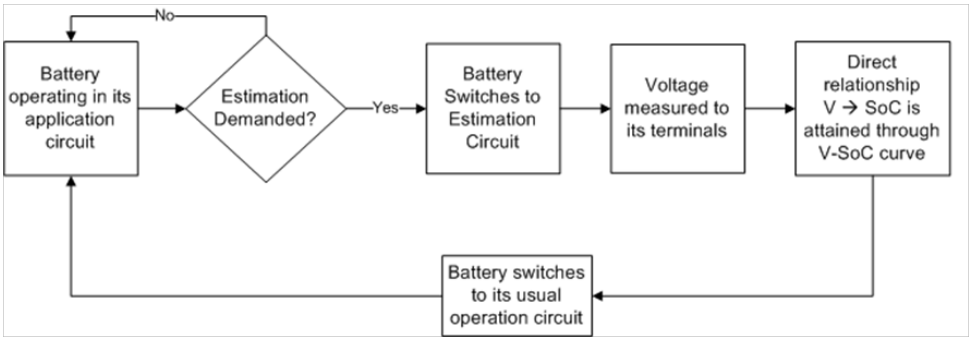

Figure 4.1: Discharge Test Software Description

To simplify the first and only decision branch, the estimation demand is represented by a current measure, every time a sample is measured with a current with values with very low variation to 0.2C, the system assumes an estimation demand and calculates the SoC.

The need to open the main circuit and perform both a time and energy consuming task to estimate the SoC appears as evident drawbacks of this method.

In 4.2 is presented the LabView program responsible for the calculation of the SoC and the store of the results for posterior analysis. Due to the possibility to feed information to other SoC estimation methods, the current flowing through the battery and actual time are also acquired even if not needed to the particular method in discussion.

The first part of the flat sequence imposes the initial conditions such as the calculation of the role model V-SoC curve to be used as a lookup-table. The second part acquires the relevant inputs. A loop is implemented in the third step of the flat sequence, which runs until the measured voltage indicates a SoC lesser than 0,5%. The fourth and last part is responsible to store the data acquired and calculated since 100% to 0,5% of SoC.

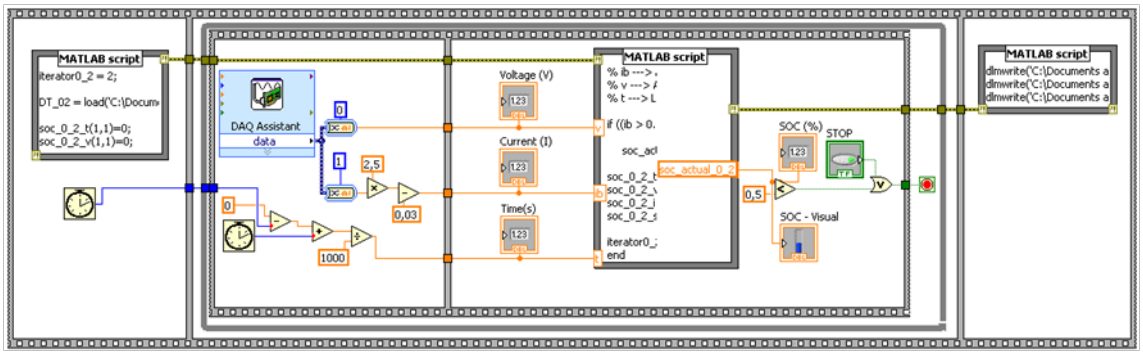

Figure 4.2: Discharge Test Labview Program

4.1.2 Inputs

In order to estimate the SoC at a given moment, only the voltage and the V-SoC curve are needed.

The voltage is acquired via DAQ-mx and the curve V-SoC is calculated as an initial condition for SoC estimation program. The state diagram shown in 4.3 allows a perception of how the V-SoC curve was constructed recurring to the 0.2C constant current discharge curve.

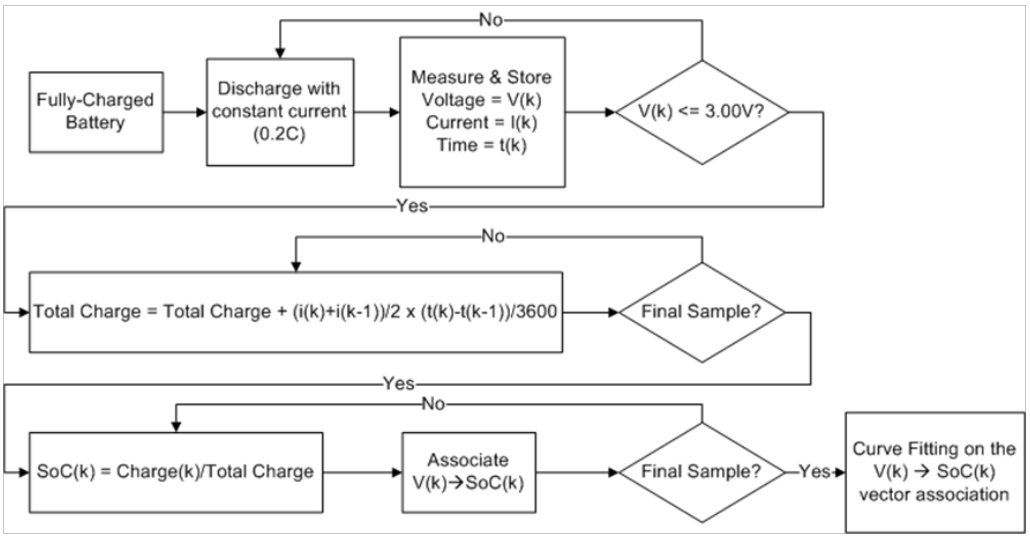

Figure 4.3: V-SoC curve determination in the Discharge Test

The resulting input curve is characterized in figure 4.4 through various fitting methods.

At this phase an evident task was in hands. A function which can approximate the sampled data with little error should be achieved. Some methods were tested with a the MatLabs fit function concluding that the region between 100% and around 10% of the SoC could easily be approximated by every tested methods, only the zone where almost all charge has already been consumed, from 10% to 0% of SoC represents a great threat to a small error function approximation. That phenomena can be observer with higher detail in figure 4.5 which represents a zoomed frame of 4.4.

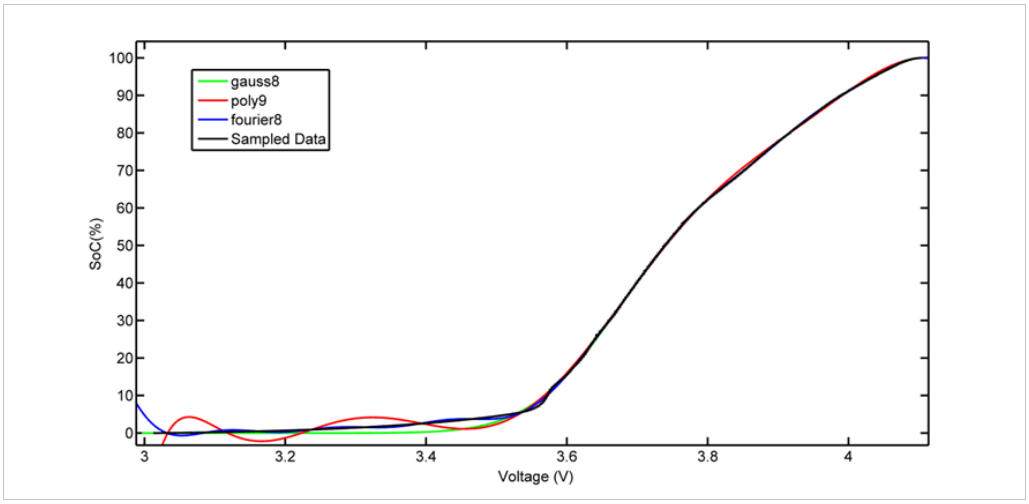

Figure 4.4: V-SoC curves obtained through various fitting methods

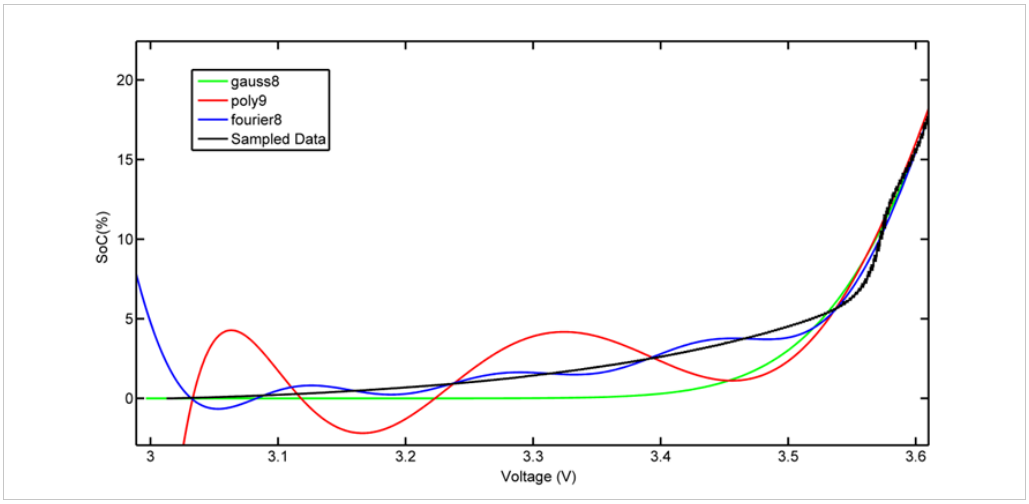

Figure 4.5: V-Soc curves in detail

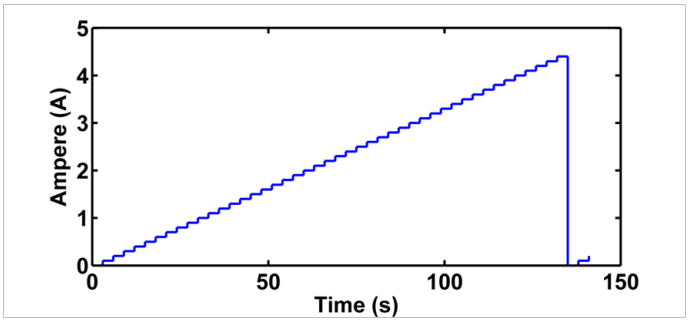

Figure 4.6: Discharge Current Behaviour

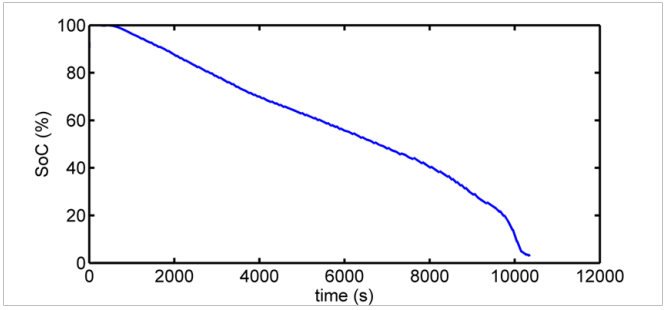

Figure 4.7: Discharge SoC

No very good solution to approximate by a function the sampled data was obtained. The method that showed the best performance was fourier8, representing a Fourier series with eight terms, the equation to this method is presented in equation 4.1.

$$SoC(v) = a0 + a1 \times cos(v \times p) + b1 \times sin(v \times p) + ... + b8 \times sin(8 \times v \times p), \qquad p = \frac{2 \times \pi}{(max(v) - min(v)} \quad (4.1)$$

A very high error in the final in the final 0.5% of SoC appear, although the discharge is imposed to stop when the SoC achieves the value of 0.5%, that error could be, for now ignored.

4.1.3 Results and Discussion

Finally the SoC estimator built was submitted to a discharge. The discharge, which would be used to obtain results in all the other methods of SoC estimation, is cyclic and each cycle has the behaviour represented in figure 4.6, a stair case going from 0 to 4.4 Ampere with a resolution of 0.1 Ampere and 3 seconds between each step change.

As expected, throughout the time, the SoC was estimated, represented in figure 4.7 whenever the current went to levels where the SoC characteristic curve was pre-known.

Although the estimation shown in figure 4.7 has a meaningful trend, the error inherent to the stated estimation exists and is mainly due to error in the approximation procedure. As expected, throughout the the region between 100% and 10% of the battery's charge, the decay was without major slope changes.

4.2 Open Circuit Voltage Method

This method can be seen as a particular case of the Discharge Test, stated in section 4.1. Once again, the technique compares the voltage measured when the SoC estimation circuit is connected (in this case simply open) with the voltage measured during another test assumed as accurate [47]. However, in this case, the current drawn from the SoC estimation circuit is just as high as the measurement instrument absorbs. Since the voltmeter used has very high impedance, the circuit is assumed to be in open.

This method is especially suitable for applications where no current is demanded from the battery for long periods or periodically [56]. Obviously, as it happens with the method discussed in 4.1, the Open Circuit Voltage technique cannot be used in online applications, despite the possibility of usage to feed information to other kind of methods.

4.2.1 Estimation Software Description

The flowchart represented in 4.8 is illustrative of the method applied in this part. Despite many similarities with the Discharge Test method represented in figure 4.1, some differences are evident. A circuit to withdrawn current in a controlled manner is not needed, instead a disconnection of the battery from the main circuit is done and the voltage to the its terminal measured. The main difference is in the V-SoC curve input.

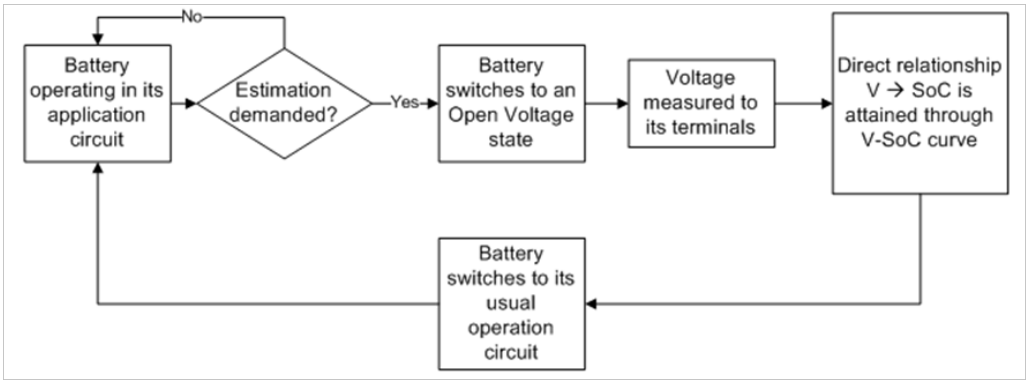

Figure 4.8: Open Circuit Voltage Software Description

As happened with the Discharge Test method, a LabVIEW program was developed to perform the operations required to estimate the SoC with the method discussed in this part. The architecture, design and mode of operation of the LabVIEW program are very similar to the one used in Discharge Test, thus this topic will not be further discussed for this specific SoC estimation method.

4.2.2 Inputs

As in the SoC estimation method Discharge Test, the only two inputs needed are the voltage measured when the battery is exposed to a known behaviour and the curve that characterizes that known behaviour (V-SoC curve).

The V-Soc curve is obtained by discharging the battery with a pulsed current signal. Whenever the current is null, the voltage at the battery terminals is measured and the SoC value is calculated and stored. The state diagram represented in 4.9, illustrates the acquisition and calculation of that V-SoC curve.

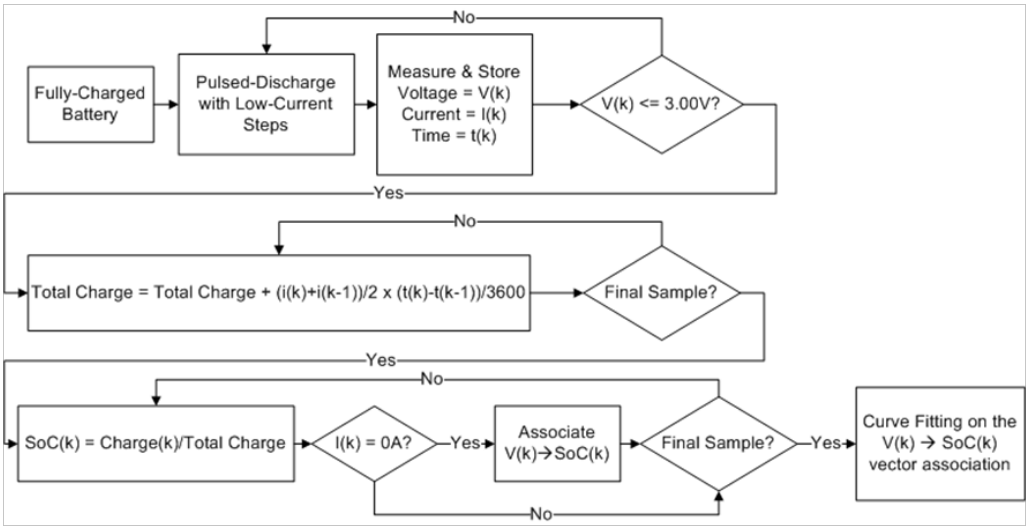

Figure 4.9: V-SoC curve determination in the Open Circuit Voltage Method

The resulting input is shown in 4.10. Once again a study in which would be the best fitting method to the given data samples was ellaborated and are present with more detail in 4.11. The V-SoC curve for this method is very similar to the Discharge Test V-SoC curve when shape characteristics are compared. Hence is predictable that the method which will better approximate a function to the data samples will be the same.

Once again fourier8 was the chosen fitting method. Again all methods converge almost perfectly to high SoC regions, with once more the problematic areas being the very low SoC, were, this time, among the methods tested, only the eight term Fourier series achieved good low error features, with an almost perfect approximation.

4.2.3 Results and Discussion

The estimator proposed in this part was put to a test. The results were stored in a .txt file so they could be analysed more thoroughly. Taking advantage of those datasets, the charts presented in figure 4.12 were obtained.

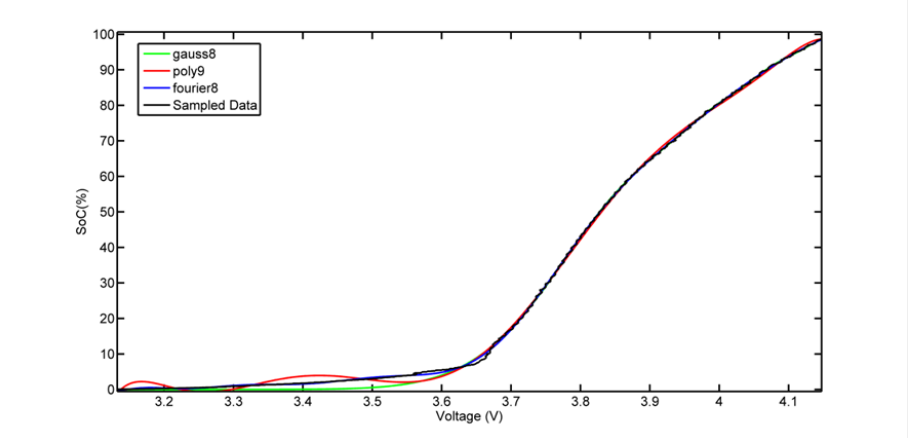

Figure 4.10: V-SoC curves obtained through various fitting methods

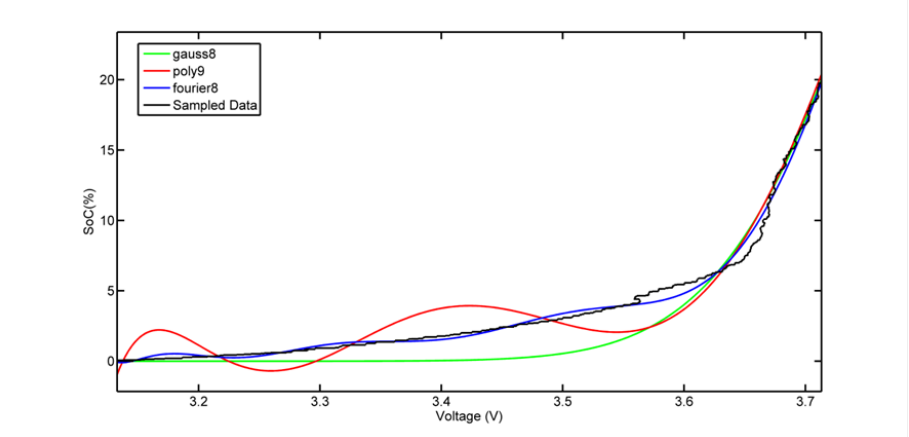

Figure 4.11: V-Soc curves in detail

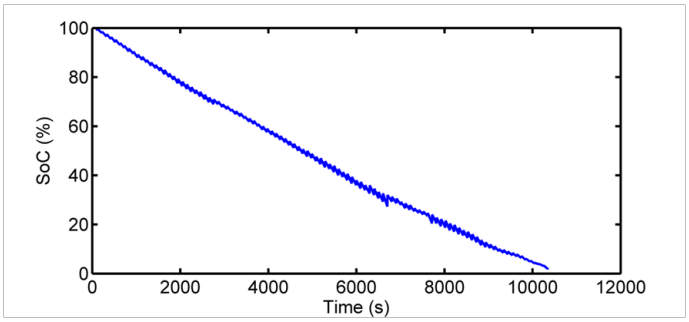

Figure 4.12: SoC obtained with the Open Circuit Voltage Method

4.3 Ampere Hour Counting Method

The Ampere Hour Counting Method is based on the supposition that equilibrium between charge and discharge exists. Therefore, if the initial battery charge is known, one can derive the existing charge inside that battery at any time by counting the inflow and the outflow of current. This count can be performed due to the direct relation between current and charge flowing through the battery. Therefore, if a starting point is given to battery charge, the value of the current integral directly indicates the actual SoC [56].

This method is considered in the literature to be one of the most common techniques to estimate the [56, 16]. However, this kind of SoC estimation procedure has two main drawbacks that, if not taken into account, can be viewed as flaws and can generate errors in the final estimation results. Incorrect current measurements impose errors that, due to the integral, can get summed to high values. This can be overcome by investing money on an accurate current measurement device. The second error bringer is the fact that not all the current drawn to the battery is used for charging and, during the charging phase (i.e. with negative current) losses must be taken into consideration. In the master thesis losses in the charging process will not be further discussed, since its focus is only in the discharging process, as explained before.

Unlike the SoC estimation methods presented before, the variable to be measured does not have a linear relationship with the capacity that a battery can deliver. The greater the current demanded by the load, the lower the capacity that the battery can provide without the risk of electrode degradation. In figure 4.13, one can see that, after calculating the total battery capacity based on the constant current discharge test, the capacity decreases as the current demanded by the load grows. In [71], this fact is approached under the name Capacity Efficiency Ratio (CER). After having the samples of current and correspondent capacity capability, a fitting procedure to achieve a curve for CER can be used. In figure 4.13, the samples and the fitted curve is shown.

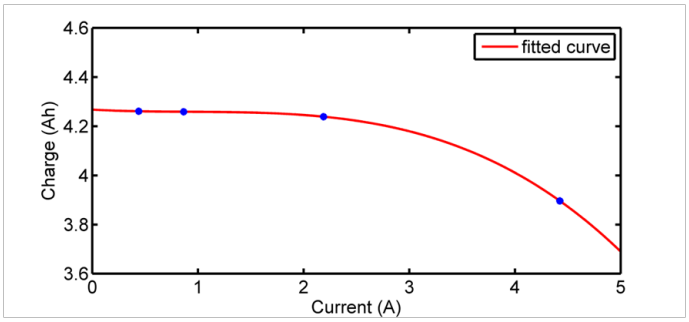

Figure 4.13: Non-linear Relation Between the Current Demanded by the Load and the Charge

The equation to be used as the SoC estimator can now be obtained by merging the information present in the equation 4.2 [71], which represents the coulomb counting procedure, with the polynomial function achieved to the CER phenomena, which is shown in equation 4.3.

$$SoC(t) = S(0) - \int_0^t \frac{i(t)}{C_n} \tag{4.2}$$

$$CER(i) = (-0.008209) \times i^3 + 0.02261 \times i^2 - 0.02329 \times i + 4.268 \tag{4.3}$$

The information given by equation 4.2 is rather useful and provides a visual insight of the battery behaviour. Just by looking at the equation one can understand that when high currents are demanded to the battery, some of the charge is lost. Eventhough, an almost flat CER is achieved when low-current applications are used, raising some of the major benefits of batteries. In applications where a well dimensioned battery is applied, a high efficiency can be obtained.

4.3.1 Estimation Software Description

The software developed to estimate the SoC through this method is based on the discrete form of equation 4.4, presented below:

$$SoC(k) = S(k-1) - CER \times \frac{i(k) + i(k-1)}{2} \times \frac{t(k) - t(k-1)}{3600} \tag{4.4}$$

Similarly to the previous estimation methods, a LabVIEW program was developed with MatLab Scripts to estimate the SoC of the battery. The program structure, presented in 4.14, is similar to the ones described in the other methods. In the first step, initial conditions are imposed, which correspond to the polynomial factors of the function that characterizes the capacity efficiency ratio and the initial SoC value, assumed to be 100% as a consequence of a previous CC-CV battery charge. The initial state of the estimator is also defined. Next, the while loop takes advantage of 4.4 to calculate the SoC at each moment. The final step occurs when a SoC of 0.5% or less is observed. This final step stores both input and output variables into a .txt file for further analysis.

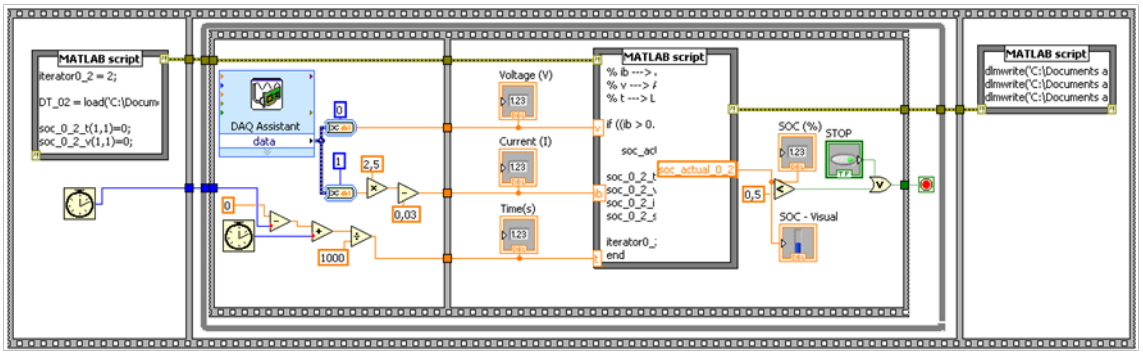

Figure 4.14: Ampere Hour Counting Labview Program

4.3.2 Inputs

This method has as inputs the current and the time from both the actual and the previous sample. In order to use the values of previous samples, they are stored in an array during the SoC estimation procedure, as happened in the method based on the fitted battery model. The Voltage of each sample is also stored.

Another input needed is the CER function relating the capacity with the current demanded to the battery. The data contained in 4.13 was used to generate Capacity versus Current points to be fitted recurring to the fit function in MatLab.

4.3.3 Results and Discussion

After exposing the estimator developed to current demands shown in figure 4.6, some interesting results were attained. In figure 4.15 the final result of the Ah SoC estimator.

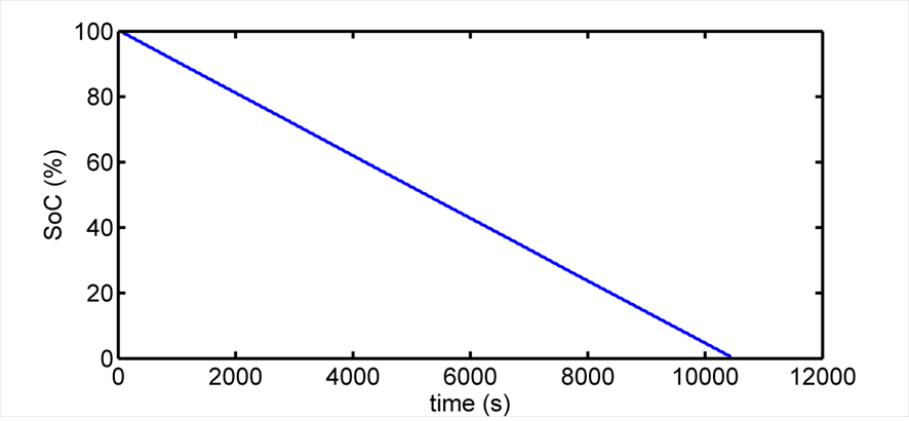

Figure 4.15: SoC Estimation Result of Pulsed Current Discharge Using the Ampere-hour Counting Method

Following the current demand, the SoC estimator output slope is very low when the current is low and high when the current is high, this proves that the coulomb counting process is working, but to understand if the CER function is improving the estimation of the batterys SoC one must compare the two estimators. The same LabVIEW program was used to achieve SoC estimation where the effect of CER function was ignored (by altering the estimation calculation in the main MatLab script). The comparison is shown in figure 4.16.

A zoomed image of the estimation curve shown in figure 4.16 is presented in figure 4.17. The zoomed image shows an error of about 100 seconds between the two estimation procedures, a relatively low error, but depending on the applications this factor can be very important.

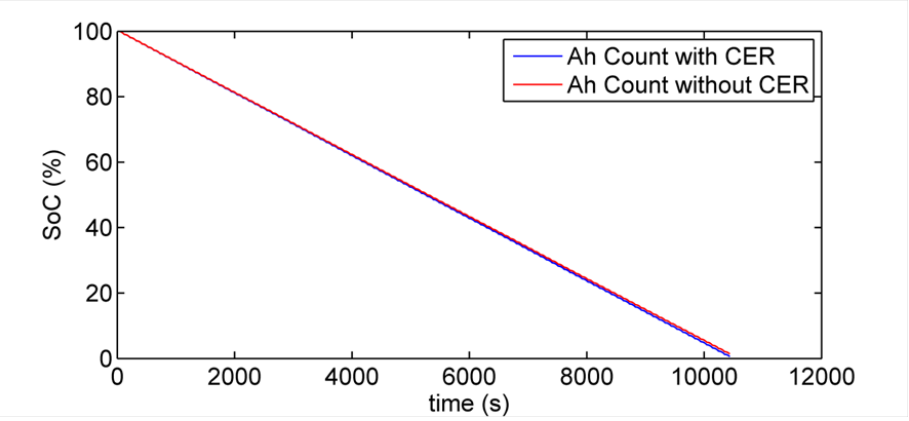

Figure 4.16: Comparison between Ampere Hour counting method with and without CER

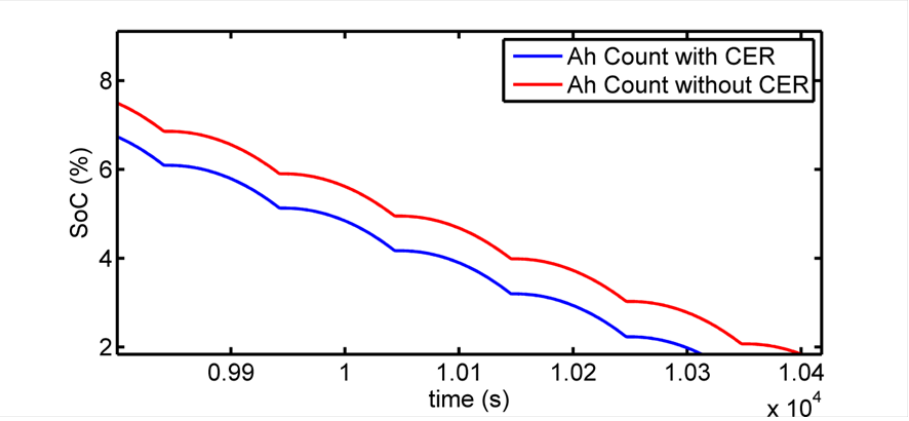

Figure 4.17: Comparison between Ampere Hour counting method with and without CER in detail

4.4 Artificial Neural network (ANN)

> Neural network learning methods provide a robust approach to approximating real-value, discrete-valued, and vector-valued target function [46].

Artificial neural networks are used in a huge variety of applications. In the SoC estimation, this method integrates heuristic interpretations of input data and achieves approximate rather than exact estimates for the SoC of a battery.

In [56], Piller made a literature review on existing methods to estimate SoC. In his discussion about the pertinence of each estimation method, he mentions computational intelligent methods as a promising approach in opposite to other exact estimation methods involving high costs and high computational power.

In figure 4.18, one can see the basic structure of an ANN, a perceptron. A perceptron takes a vector of real-valued inputs, calculates a linear combination of those inputs in a neuron, filters that result with an activation function and finally generates an output. In order to obtain more and more accurate values, the ANN needs to be trained. Training an ANN implies a weight attribution to input linear combination, which are also called synapses. In other words, the training procedure iteratively calculates the weight that implies how much an input affects the output.

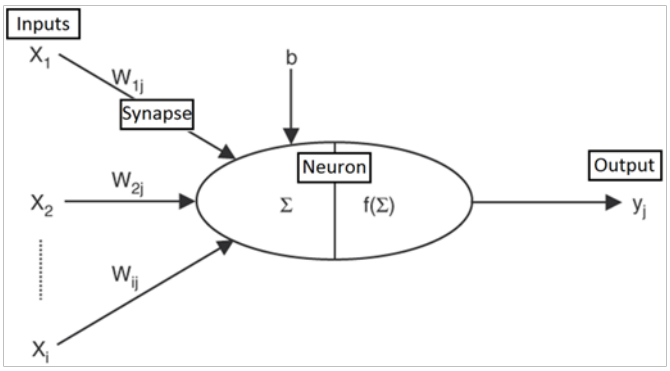

Figure 4.18: Basic Structure of an Artificial Neural Network

Different ANN structures exist, but even the more complex ones have as basic elements the perceptron. Despite some ANN training techniques proposed in literature, training complex ANN structures can be puzzling.

4.4.1 Choosing an ANN Architecture

In order to choose a pertinent neural network, some aspects must be covered.

Adaptive networks are classified into two different categories based on the direction of their connections. Those networks can be feedforward, when the output of each node propagates from the input side (left) to the output side (right) unanimously [34] or recurrent if a feedback link exists in the network. To application where only mapping inputs into outputs are needed, feedforward topologies are usually the most used.

In literature, the multi-layered perceptron, one of the most used feedforward ANN, is considered an effective tool due to their universal approximators characteristics, hence they are good solution to fit basic electric measurements to SoC outputs [1], as is the intention in this master thesis.

The general multilayer perceptron is composed by at least one input layer, one hidden layer and one output layer. Except for the input layer, all the others are composed by perceptrons, series of input signals wired by synapses to a neuron which contains an aggregation function and an activation function. The ANN represented in 4.19, the one used in this master thesis for SoC estimation, is a multilayer perceptron (MLP) with two input nodes, because two inputs are used (actual current and voltage), one hidden layer containing three perceptrons with an unbiased sum as linear combination and sigmoid activation function, followed by a single output perceptron equal to the ones used in the hidden layer, except for the activation function which is linear and not a sigmoid.

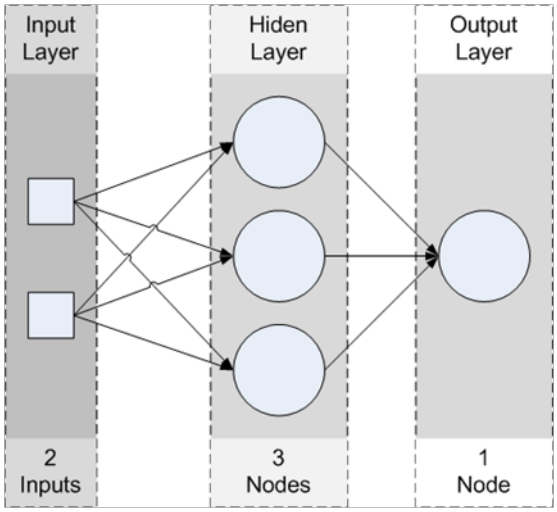

Figure 4.19: Multilater perceptron MLP

The activation functions afore mentioned, sigmoid and linear, are shown in table 4.1.

Table 4.1: Signmoid and Linear Activation Functions

Name	Expression
Linear	A(x)=x
Sigmoid	$A(x)=1/(1+e^{-x})$

This kind of ANN is considered as a general purpose function approximator [34, 19], hence appropriate for SoC estimation application.

It is known that both excessive and lacking of neurons in the hidden layer can lead the ANN not to achieving low output-to-target errors. Some rules-of-thumb were proposed in [54] to arrive at a value to the number of neurons in the hidden layer. The main purpose of these rules was to overcome problems such as: (1) overfitting, (2) lack of good training data and (3) exaggerated

training time. This MLP forms a multiple-input single-output function, usually named MISO systems.

4.4.2 Choosing an ANN Training Procedure

Usually, training methods to an ANN can be classified as either supervised or non-supervised. A supervised method, shown in figure 4.20, contrarily to unsupervised ones, takes advantage of complete training datasets with both inputs and target outputs [34]. The main goal of training an ANN is to arrive at synaptic weights that make the ANN to respond to inputs with outputs as similar as possible to the targets given as training datasets. As an example, a training dataset states that an input with the value 10 must respond with 20. A well trained ANN to that specific point of operation would, with the same input (10), respond with a value similar to the one used as target (20).

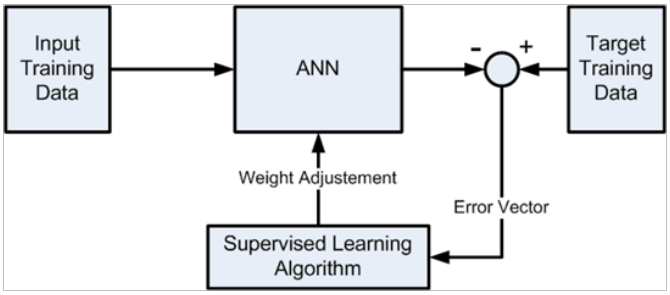

Figure 4.20: Supervised Training Method

When training an ANN, we want the ANN give the same outputs as seen in the training data. On the other hand, we do not want to make the ANN too specific, making it give precise results for the training data, but incorrect results for all other data. When this happens, we say that the ANN has been over-fitted. This problem has already been approached, happening also when excessive hidden layer neurons are used.

Many training procedures are available to the topology mentioned before. In the case of this master thesis, a supervised training algorithm is the most pertinent, mostly due to a large amount of available data from other algorithms. The ANN can, therefore, be fed with input-output reliable data from the other methods, making this a weighted junction of all the other estimated values. Note that outliers must be deleted from the dataset.

To select one supervised training algorithm among a few available was the task in hands. Different supervised training algorithms are now briefly reviewed:

1. Early forms of supervised machine learning applied to ANN were based on iterative methods where random weights were attributed to the network synapses. In each iteration, the weights are changed based on how further away the result is from the target-value. This occurs until a minimum error between output and target is achieved [46]. This method does

not guaranty a convergence to a low error even if the dataset used to train the ANN is perfect. Thus, it was not considered to be a good approach for this application.

2. The (1) perceptron training rule, (2) the gradient descent and (3) the delta rule are more deterministic approaches of training. All these methods try to consistently and iteratively arrive at a low output to target error.

3. Error backpropagation, EBP, is the algorithm that results from applying the descent training algorithm to a multilayer network with a fixed set of neurons and synapses. EBP was a significant breakthrough in machine learning applied to ANN, since is the base knowledge to most of the modern learning algorithms, but it has significant convergence rate problems [72]. Being so widely used, many variations to the EBP were proposed to attempt to speed up the algorithm. Heuristic approaches such as adding momentum to the learning process, or varying the learning rate variable, brought slight improvements. More visible progresses were obtained with the use of various second order approaches [72], where the Marquardt-Levenberg (LM) variation had specially good results. This approach is considered in [72, 25] as the most efficient method when applied to function-approximation applications such as the one in this master thesis. The chart presented in 4.21, taken from [25] (and edited to hold axis labels), shows the MSE (Mean Squared Error) between output and target on a 4-D function approximation, proofing that the MLBP algorithm has very good performance results in function-approximation function. In the chart, it is compared with the other backpropagation algorithm mentioned is the conjugate gradient (CGBP) one. (in [25] a sudden nomenclature change exist on naming the algorithm, they stop using the name Levenberg, but the method is the same, that is why, in 4.21 only MBP appear rather than MLBP).

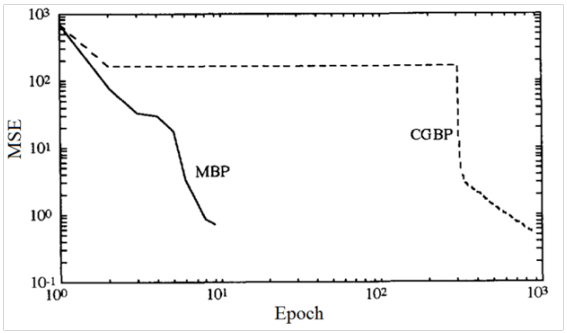

Figure 4.21: Mean Squared Error Between Output and Target on a 4-D Function Approximation with the MLBP algorithm

Explanation of the Levenberg-Marquardt backpropagation training routine goes out of the boundaries of this master thesis. In this project proof was gathered that MLBP training algorithm is a good solution to the application proposed and therefore it was used as a black box.

4.4.3 Estimation Software Description

The basic structure of the software developed to estimate the SoC of a battery with an ANN is similar to the structure of the other estimators described in previous sections. In figure 4.22, one can see the structure of the program which uses, once again, a MatLab script into a LabVIEW visual environment.

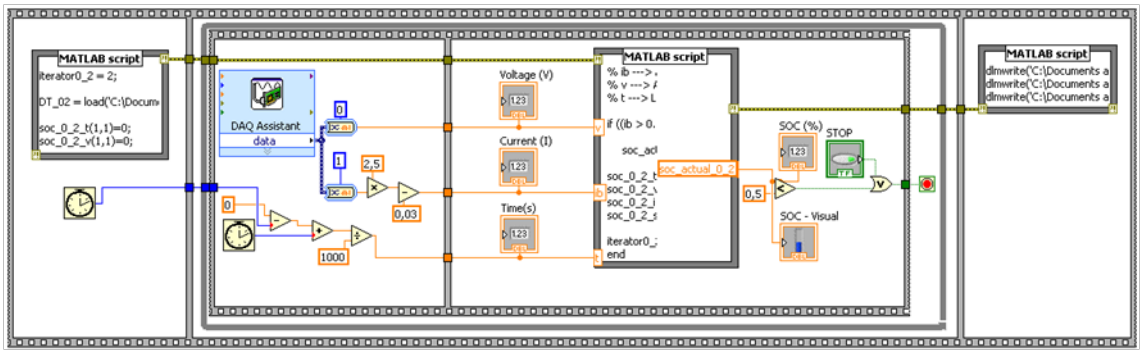

Figure 4.22: ANN Labview Program

After the establishment of the initial conditions and the acquisition of the input signals, the neural network trained is used in a MatLab script which has as single output, the SoC value. The acquisition followed by ANN usage is performed cyclically until the estimated SoC is lesser than 0.5%. When that event is observed by the LabView program, both input and output values saved during the whole process of discharge are stored in a .txt file to future analysis.

In this method, the initial conditions are computed as presented in the flowchart of figure 4.23:

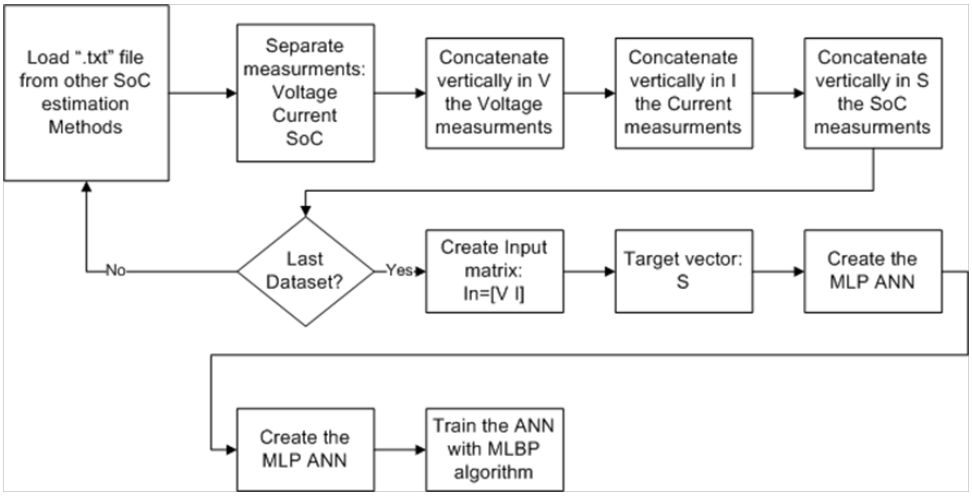

Figure 4.23: Initial Conditions for the ANN Method

The first step in the initial condition setting is to gather the information contained in .txt files,

the results obtained with the other algorithms. That information is to be provided as the training dataset. The training procedure needs a matrix containing the inputs to be used arranged in columns and a column vector with the targets, hence that operation is performed in the second step. Next, the ANN is defined with the topology described in section 4.4.1. Finally it is trained as detailed in section 4.4.2.

4.4.4 Inputs

As inputs, this SoC estimation system needs a pertinent dataset for the ANN training, and acquisition of signals referring to the ones present as inputs to the training dataset. The selection of a good dataset for training the ANN is a very important action in order to obtain good results from the trained ANN. In function-approximation applications, the inputs for the training dataset should be all independent variables that can characterize the output.

By empirical knowledge one can observe that, one value of measured battery voltage combined with one value of current provide one and only one SoC estimation, providing that temperature influence is not considered (as explained in section 2.6). Thus one can assume that actual current and voltage, measured from the battery, are independent variables on calculating the actual SoC and therefore those should be the input variables used in the training process. Those training input variables are taken with the correspondent SoC target from the other estimation methods.

The other inputs to the estimator are voltage and current measured at that moment at the battery.

4.4.5 Results and Discussion

After imposing the same current demand already imposed to the other SoC estimation methods, the ANN based estimator achieved some promising results, which are shown in figure **??**.

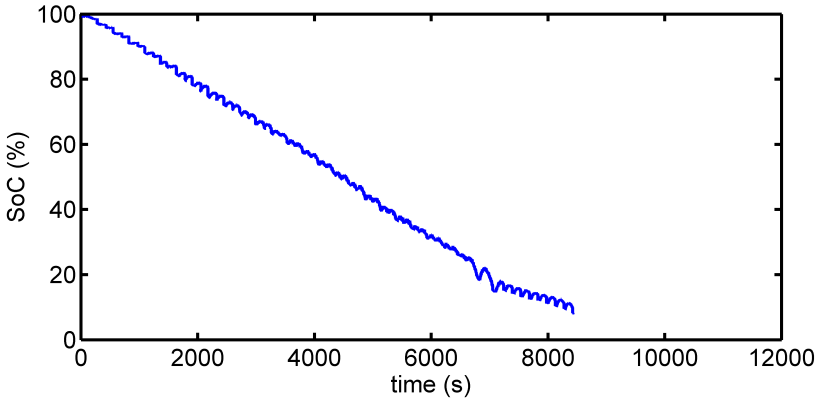

Figure 4.24: Results for the ANN Method

The estimator based on ANN showed a fairly good estimation process in the linear zone of the discharge behaviour, but as in some of the methods that were used as training, it struggles in the

non-linear zone (<10%) to attain an accurate estimation. Due to the high amount of data fed to training of the estimator, being sometimes inaccurate, an oscillatory behavior appears, mostly as predictable in the non-linear region. The results were promising showing that the ANN estimator is a technology to take into consideration in this type of application.

4.5 Other SoC Estimation Methods Overview

Many other SoC estimation strategies are proposed in literature and some of them will be overviewed in this section, although no tests were performed to them:

- Impedance spectroscopy is mostly used to investigate electrochemical processes, such as batteries. This technique imposes a small amplitude input to the battery and measures its AC impedance characterized by its dynamic behaviour. Those values are used to calculate the actual SoC. Despite many papers written on the subject, very few implement a practical SoC estimation based on this method due to the huge influence of temperature on the measurements which impose impracticable errors in the SoC estimation [29]. However, according to [58], this is a possible method for SoC estimation in lithium based batteries.
- Another possible method is by measuring the internal resistance of the battery. Is known that the internal resistance of a battery varies with its SoC, thus that fact can be taken into advantage. That resistance is measured when a sudden current is demanded to the battery, exactly as described in 2.6.
- The final method that will be approached in this master thesis is based on Kalman Filters. A Kalman filter is a powerful tool and is used mainly as an inner state estimator and can be applied to any dynamic system, such as a battery.

Although not described in this master thesis, more methods exist, such as heuristic tactics with linear models or measuring the physical properties of the electrolytes [56].

4.6 Comparative Table

Table 4.2: Comparative Table

Technique	Field Application	Advantages	Drawbacks
Discharge Test	All Battery systems Used for capacity determination in the begining of life	Easy and Accurate Independent of SOH	Offline Time intensive Modifies the battery state Loss of energy
Ah Balance	All Battery systems and most applications	Online, easy accurate if enough acllibration points are available and with good measurement	Needs a model for the losses Sensitive to parasite reactions Cost intensive for accurate current measurments Needs regular re-callibration points
Physical Properties of Electrolyte	Lead, possibly Zn/Br and Va	Online Gives information about SOH	Error if acid stratification Low Dynamic Problem of stability of sensors in electrolyte Sensitive to temperature and impurities
Open Circuit Voltage	Lead, Lithium, Zn/Br and Va	Online Cheap	Low dynamic Error if acid stratification Needs long rest times (current =0) for lead systems Problem of parasite reaction (e.g. Sb poisoning by lead)
Linear Model	Lead PV, possibility for other battery systems? (not tried yet)	Online Easy	Needs reference data for fitting parameters
Artificial Neural Network	All battery systems	Online	Needs training data of a similar battery
Impedance Spectroscopy	All systems	Gives information about SOH and quality Possibility of online measurement	Temperature sensitive Cost intensive
DC Internal Resistance	Lead, Ni/Cd	Gives information about SOH Cheap and Easy Possibility of online measurement	Good accuracy but only for low SoC
Kalman Filter	All battery systems Dynamic applications (e.g.HEV)	Online Dynamic	Needs large computing capacity Needs suitable battery model Problem determining initial parameters

0

Chapter 5

EMCS and the Associated Power Electronics

Providing that a dual-source (at least) is used to provide both energy and power to an EV, it is obvious that two ways to control the energy flow must exist, a high level one (Energy Management Control System) which gathers information and decides on the source to demand the power, quantifying it and a lower level one (Power Electronics control)that imposes the behaviour defined by the EMCS to the power source devices through a power electronic structure. This arrangement can be observed in figure 1.18, present in the first chapter.

5.1 EMCSs Overview

An interesting energy management control system general definition is proposed in [59], showing a power splitting scenario where two different storage units are used to deliver the demanded power to a load. That notion is shown in figure 5.1.

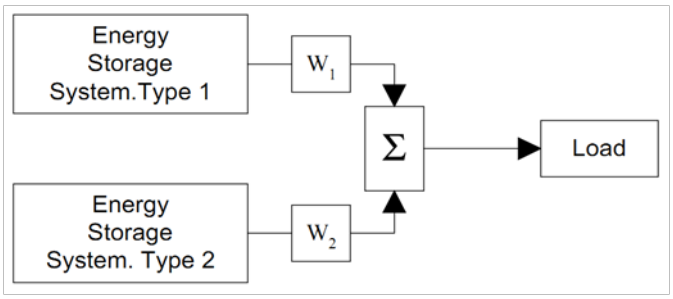

Figure 5.1: Energy Management Control System

This figure illustrates the job which the EMCS must execute, varying the weight factors (w1 and w2) to find a ratio between the two devices which contribute to both their lifespan and to a

maximized range of the vehicle. This weight control is necessary due to both dynamic variations of the power/energy needed to supply the load and difference in power to energy ratios of the storage devices.

To achieve the goal stated above, some strategies were studied and proposed throughout the world. A main drawback in the search for information about EMCSs procedure was identified. This control process is not well documented to fully electric vehicles. Much of the endeavour was related to hybrid vehicles using some kind of fuel engine. Some of that knowledge can be applied to the fully electric hybrid-source vehicle, but with caution.

Usually the methods that will be discussed next are assessed based on its performance with data gathered from standard driving cycles, international standards that characterize various driving scenarios.

Some high-level strategies are presented to control the energy flowing between hybrid energy source and load. Some of them are rule-based [33], using the vehicle speed and acceleration to directly control the power and energy split between the two power sources. The decision is based in rules which are based in the macroscopic energy and instantaneous power needs of the vehicle. As an example, when an EV is going uphill and needs to pick up pace, the acceleration will demand a high instantaneous power to feed the needed positive variation of torque, in this case the device with higher energy density would provide the mean power while the unit with higher power density would provide the instantaneous power peaks.

The rule-based methodology is one of the many strategies based on computer intelligence that seem to offer some promising results [59]. Statistical data of aforementioned driving cycles can be used to achieve an optimal control of the energy existing stored in an electric vehicle [63].

The usage of previously known driving cycles informs every method of future events, allowing the system to be prepared to react to those, sometimes sudden changes. That prior knowledge lead to Fuzzy-Logic based EMCSs, allowing the system to have some predictive awareness, relying on predictions rather than future events [36]. That prediction thought leads to frameworks based on ANN with supervised training, such as the one approached and proposed in [48].

The EMCS is mostly a way to indicate the energy which is drawn from each power/energy supply. Through measurements of physical behaviours such as pace, acceleration and weight, give relevant information to empirically or analytically calculate or estimate the reference values of power/energy to the low level structure, based on power electronics and its control.

5.2 Power Electronics Converters Applied to EV

Throughout the last decade vehicular technology moved toward replacing mechanical, hydraulic and pneumatic systems by electrical ones. This crescendo in electric devices absorbing energy has reached a maximum in the last few years with the uprising interest in electrically propelled vehicles. A way to interface the primary energy system (e.g. batteries) was therefore needed and power electronic circuits (PEC) offer that possibility.

The PECs used in EVs (and in any other application) are always designed based on the power supply to be controlled and the load to be fed. The power electronic structures usually existent in an electric vehicle depend of both designed power sources and powertrain specifications.

Throughout this subsection the general categories of PECs will be overviewed to have some insight about the topic when multiple-input DC/DC topologies are introduced, allowing the finding of a possible topology for the case addressed in this master thesis. A small-signal model will be derived to ultimately achieve a transfer function for the switching power converter (SPC) allowing the calculation of linear controller constants. Finally some simulations of the chosen SPC are presented.

5.2.1 DC/DC PEC General Categories

The most common power sources in an electric vehicle are direct current ones, imposing a DC voltage in the converter input and since the output, usually is a DC bus, a DC/DC power converter is the logical choice to interface the power source with the DC bus.

A DC/DC converter is a switching device that converts a certain unregulated input voltage to a regulated one. Various DC/DC topologies are available. Many classifications can be achieved to DC/DC converters, being the one presented is a possible one.

1. Hard-Switching

   Hard-switching power converters are not concerned with either voltage or current across the semiconductor. This usually degrades the power converter energetic efficiency, but typically simplifies the control strategies.

   Most of the classic basic converter topologies are non-isolated. Boost (step-up), buck (step-down), buck-boost, SEPIC (single ended primary inductor converter), dual-SEPIC (zeta), and Cuk converters are examples of non-isolated topologies. Isolated topologies for basic power structures, such as the already mentioned boost, buck or buck-boost, are available and when the intended application is in electric vehicles, those are preferred mostly to provide safety for the loading devices [6]. Obviously the isolation parameter imposes some issues. It increases electro-magnetic interference, area, volume, weight and cost. Since a transformer is mandatory, leakage inductance appears, reducing even more the power converter efficiency.

   Current directionality must be analysed in each case due to the many extensions available to the aforementioned classic topologies.

2. Soft-Switching

   The converters designed to switch their semiconductors at an instant in which their power is null are labelled as soft-switching converters. This name arises due to a theoretically loss free switching technique. Most modern day DC/DC converters are soft-switched converters

[6]. The soft-switching are generally classified as the resonant converter (RC), quasi-square-wave converter (QSC), quasi-resonant converter (QRC), multi-resonant converter (MRC) and zero-transition converter (ZTC)[14].

There is a common feature of all soft-switching converters. The existence of a resonant bank is mandatory to shape the current or voltage waveforms of the power converter in order to achieve the final objective of having a waveform (either voltage or current) passing through zero at time of the switch. According to [14], the zero voltage switching (ZVS) is usually preferred to zero current switching because it can eliminate the major switching losses due to the discharging of its inherent junction capacitance [14].

In electric vehicles applications the isolated topologies are preferential and bi-directional topologies (for some power sources) are mandatory. The isolation parameter implies the use of a transformer and the current bi-directionality imposes the use of a topology that provides a way for the current to flow either to the load or to the source [6].

5.2.2 Multiple-input DC/DC Topologies for Hybridization Purposes

Recently, the multiple-input (MI) DC/DC converters were developed to interface more than one power source with a single load. This concept fits in the hybridization profile, which is the diversification of the input power sources.

Several MI converters were in recent times proposed with the objective of combining various power sources. In the topologies compiled in [15], each one has its own advantages and issues, leading to a difficulty in a choice for an appropriate topology for a specific application.

In the next figure, 5.2, combination strategies are shown. From left to right, a sharing output filter capacitor combination, switches, energy transfer inductor and capacitor combination, and a magnetic-core sharing combination are presented.

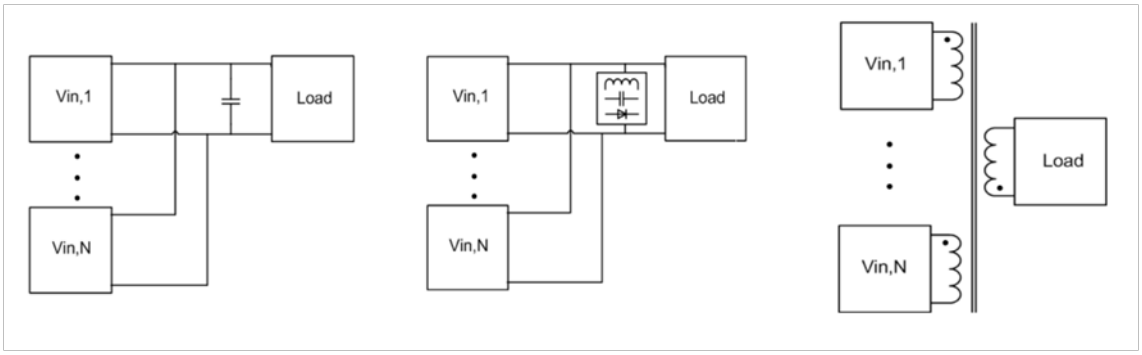

Figure 5.2: Types of Multiple-Input Combination Strategies

These three main topologies have their benefits and shortcomings, which will be approached in this part.

1. Output Capacitor Sharing

This MI technique must use a DC bus voltage control. It has the possibility to append the power source directly to the DC bus or use a power converter to match the voltage level required in the DC BUS, allowing the power source to have a different voltage level when compared to the DC bus one. Providing that the bus capacitor is capable of maintaining a constant voltage (recurring to the DC BUS voltage control), there are no limits for the number of power sources that one can append to the DC BUS. The next figure, 5.3, is an example of this type of MI converter, in this case with a hybridization with fuel cells and SC, which is approached in [5]. Increasing the number of power sources means an increase of control complexity.

Example of a MI Converter

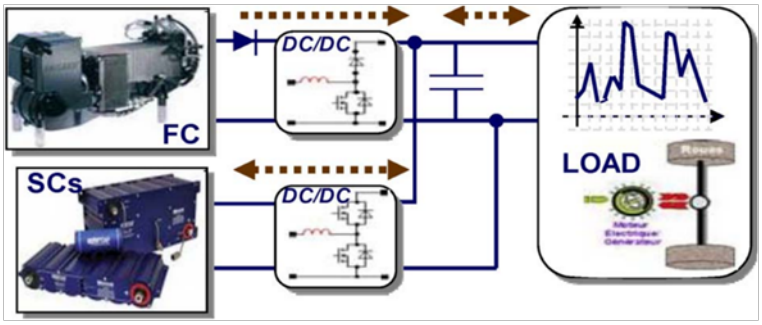

Figure 5.3: Example of a Multiple-Input Converter

2. Switching Device Sharing

   Multiple inputs aggregated to the same switches or energy transfer elements such as inductors or capacitors implement this kind of MI technique. Usually the shared components are used to interface the power source with the DC BUS while filtering or conditioning some waveforms. In [15], a MI-Cuk and a MI-SEPIC topologies are proposed. These switching devices can be considered to be output capacitor sharing devices, since they rely on an output filter capacitor to create a DC BUS.

3. Magnetic Core Sharing

   Unlike the aforementioned MI techniques, this introduces a galvanic isolation, imposing the energy to be exchanged through the magnetic fields of a transformer. In spite of copper usage in transformers, bulking and increasing the weight of the converter, input to output galvanic isolation is a very good attribute in electric vehicle applications. Modularity is extremely reduced, the number of inputs must be accounted in the first design of the converter, since appending another power source after the converter is produced implies a reconfiguration of the transformer, hence a new one.

In [15] a compilation of output capacitor and switching device sharing multiple-input DC/DC converters are shown and classified in a table, which is represented in, 5.1. Magnetic core sharing

devices are, for now, discarded due to complexity, cost, bulkiness and loss increase. The assessment of the converters is qualitative and goes from —- to ++++ passing through 0, where —- is the worst comparative classification and ++++ is the best.

Table 5.1: Multiple-Input DC/DC converters qualitative assessment

Topology	Expected Cost	Modularity Potential	Reliablility	Flexibility
Buck	+	0	+	-
Boost	0	+	++	+
Buck-Boost	+	0	+	0
Cuk	0	0	0	++
SEPIC	0	0	0	++
G1(1)	0	0	-	+
Boost/Buck-Boost	0	-	+	+++
Flyback	+	0	0	0

Reliability is one of the main requirements when a switching power converter is applied to EV and because the other attributes are above average as well, the MI Boost converter is the chosen topology. In figure 5.4 the chosen Power Electronic Converter (PEC) is shown.

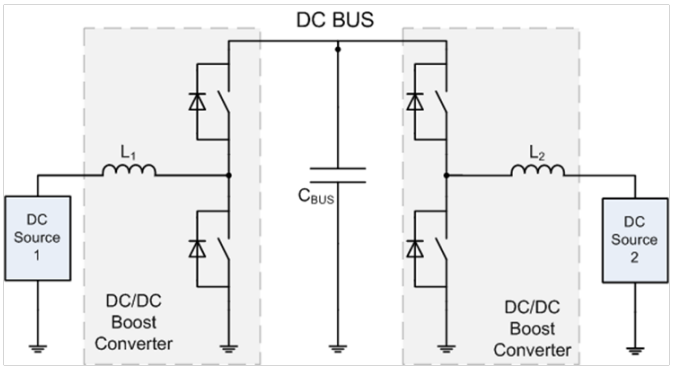

Figure 5.4: MI Boost Power Electronic Converter

5.2.3 Modelling the Chosen PEC

To achieve a model of the chosen PEC only one of the legs will be considered, e.g. the DC/DC power converter responsible for the power flow control of DC source 1, relating to figure 5.4. By attaining the behaviour of one of the legs coupled with the power supply with lower response time (SC) one can assume that both the SPC topology and its control will work in every power sources with higher response times (e.g. battery). The same analysis done in this part can be applied to another leg. The figure representing the DC/DC boost converter is 5.5.

The objective of this part is to achieve a small-signal equivalent to the SPC. To achieve that goal one needs to do a converter state analysis and an averaging and linearizing step.

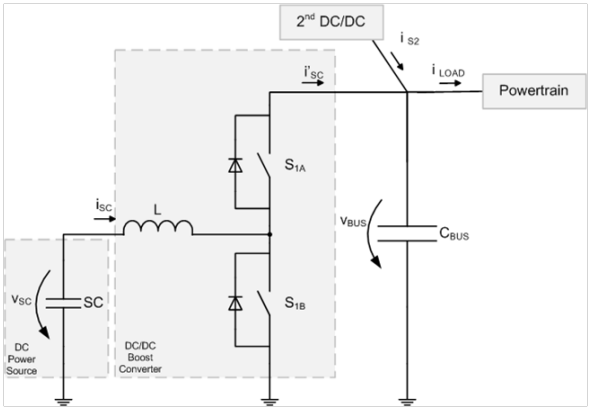

Figure 5.5: DC/DC Boost Converter

In order to design the control laws, which will be discussed further in this master thesis, a set of mathematical differential equations describing the power converter needs to be established according to circuit laws (Kirchhoffs Circuit Laws).

5.2.3.1 Converter State Analysis

Typically, the state variables of the power converter are the energy storage elements, (such as the inductor current), the capacitor voltages and the control input variable, which is the modulation gate signal. The state variables that can be found in this kind of converter are the DC bus voltage, the power supply voltage and the inductor current. Based on the functionality of the semiconductor switch, the solid-state switches can be represented as ideal where losses and the interior structure are ignored. The switching function can be deduced in accordance with the converter operation principle.

$$Vconv = f \times v_{BUS}, where f = [0,1] \tag{5.1}$$

The switching model is determined based on the power stage topology and Kirchhoff's circuit laws. Following the steps suggested on [21] to obtain the averaged equations to any PWM switching power converter, the next step is to attain all the possible states for the converter and characterize them recurring to the Kirchhoff laws of circuits mentioned above. Assuming a bipolar control for the converter, we can achieve the two states that govern its function. The equations 5.2, 5.3 and 5.4 refer to a state where S_{1A} at its on and S_{1B} to its off state is shown and followed by the equations that describe its behaviour.

$$C_{BUS} \times \frac{dv_{BUS}(t)}{dt} = i_{SC}(t) + i_{FC}(t) + i_{load}(t) \tag{5.2}$$

$$C_{SC} \times \frac{dv_{SC}(t)}{dt} = -i_{SC}(t) \tag{5.3}$$

$$L \times \frac{di_{SC}(t)}{dt} = v_{SC}(t) - v_{BUS}(t) \tag{5.4}$$

Equations 5.5, 5.6 and 5.7 extends the same analysis made to the previous system state, only with the solid state semiconductors S_{1A} at its on and S_{1B} to its off state.

$$C_{BUS} \times \frac{dv_{BUS}(t)}{dt} = i_{FC}(t) + i_{load}(t) \tag{5.5}$$

$$C_{SC} \times \frac{dv_{SC}(t)}{dt} = -i_{SC}(t) \tag{5.6}$$

$$L \times \frac{di_{SC}(t)}{dt} = v_{SC}(t) \tag{5.7}$$

5.2.3.2 Averaging and Linearizing Step

The small-ripple approximation allows the finding of equivalence between the mean value of the state variable and the sum of the mean values of the plots.

By applying the moving average operator $\frac{1}{T}\int_t^{t+T} x(t).dt$ to the switching model, one can obtain the averaged model:

$$C_{BUS} \times \frac{d\overline{v_{BUS}}(t)}{dt} = f(t) \times \overline{i_{SC}}(t) + \overline{i_{FC}}(t) + \overline{i_{load}}(t) \tag{5.8}$$

$$C_{SC} \times \frac{d\overline{v_{SC}}(t)}{dt} = -\overline{i_{SC}}(t) \tag{5.9}$$

$$L \times \frac{d\overline{i_{SC}}(t)}{dt} = \overline{v_{SC}}(t) - (1 - f(t)) \times \overline{v_{BUS}}(t) \tag{5.10}$$

After rearrangement, the state-space representation is expressed below.

$$\begin{bmatrix} \dot{\overline{v_{BUS}}}(t) \\ \dot{\overline{v_{SC}}}(t) \\ \dot{\overline{i_{SC}}}(t) \end{bmatrix} = \begin{bmatrix} 0 & 0 & \frac{1-f(t)}{C_{BUS}} \\ 0 & 0 & -\frac{1}{C_{SC}} \\ \frac{1-f(t)}{L_1} & \frac{1}{L_1} & 0 \end{bmatrix} \times \begin{bmatrix} \overline{v_{BUS}}(t) \\ \overline{v_{SC}}(t) \\ \overline{i_{SC}}(t) \end{bmatrix} + \begin{bmatrix} \frac{1}{C_{BUS}} & \frac{1}{C_{BUS}} & 0 \\ 0 & 0 & 0 \\ 0 & 0 & 0 \end{bmatrix} \times \begin{bmatrix} \overline{i_{FC}}(t) \\ \overline{i_{load}}(t) \\ 0 \end{bmatrix} \tag{5.11}$$

5.2.3.3 Small-Signal Equivalent

Although the operating point for duty-cycle is not constant because of the nature of the electrical variable variations, the coefficients of the state space are constant values. Therefore, at every operating point, the small-signal model is always the same and independent of the varying operating

point. So, we can deduce the small-signal model of the power converter.

Having the averaged equations of the converter, we can now impose them an operation point and linearize its behaviour around that quiescent point. Thus a steady state analysis with low variations inputs can be obtained. The quiescent point analysis impose the proceedings mentioned in the equations below, from 5.12 to 5.17. The linearization below shows that an averaged value has a small-signal AC component and a DC component.

$$\overline{v_{BUS}}(t) = \widetilde{v_{Bus}}(t) + V_{BUS} \tag{5.12}$$

$$\overline{v_{SC}}(t) = \widetilde{v_{SC}}(t) + V_{SC} \tag{5.13}$$

$$\overline{i_{SC}}(t) = \widetilde{i_{SC}}(t) + I_{SC} \tag{5.14}$$

$$\overline{i_{FC}} = \widetilde{i_{FC}}(t) + I_{FC} \tag{5.15}$$

$$\overline{v_{Load}}(t) = \widetilde{i_{Load}}(t) + I_{Load} \tag{5.16}$$

$$f(t) = \tilde{d}(t) + d \tag{5.17}$$

The equations obtained around the chosen operation point are shown below. Notice that those formulations have both linear and non-linear components.

$$C_{BUS} \times \frac{d(\widetilde{v_{BUS}}(t) + V_{BUS})}{dt} = (1 - (\tilde{d}(t) + d)) \times (\widetilde{i_{SC}}(t) + I_{SC}) + \widetilde{i_F C}(t) + I_{FC} + \widetilde{i_{Load}}(t) + I_{Load} \tag{5.18}$$

$$C_{SC} \times \frac{d(\widetilde{v_{SC}}(t) + V_{SC})}{dt} = -(\widetilde{i_{SC}}(t) + I_{SC}) \tag{5.19}$$

$$L \times \frac{d(\widetilde{i_{SC}}(t) + I_{SC})}{dt} = (\widetilde{v_{SC}}(t) + V_{SC}) - (1 - (\tilde{d}(t) + d)) \times (\widetilde{v_{BUS}}(t) + V_{BUS}) \tag{5.20}$$

Considering the concept obtained in the equations

$$\begin{bmatrix} \dot{\widetilde{v_{BUS}}} \\ \dot{\widetilde{v_{SC}}} \\ \dot{\widetilde{i_{SC}}} \end{bmatrix} = \begin{bmatrix} 0 & 0 & \frac{1-d}{C_{BUS}} \\ 0 & 0 & -\frac{1}{C_{SC}} \\ \frac{1-d}{L_1} & \frac{1}{L_1} & 0 \end{bmatrix} \times \begin{bmatrix} \widetilde{v_{BUS}} \\ \widetilde{v_{SC}} \\ \widetilde{i_{SC}} \end{bmatrix} + \begin{bmatrix} \frac{1}{C_{BUS}} & \frac{1}{C_{BUS}} & 0 \\ 0 & 0 & 0 \\ 0 & 0 & 0 \end{bmatrix} \times \begin{bmatrix} \widetilde{i_{FC}}(t) \\ \widetilde{i_{load}}(t) \\ 0 \end{bmatrix} + \begin{bmatrix} \frac{I_{SC}}{C_{BUS}} \\ 0 \\ \frac{V_{BUS}}{L_1} \end{bmatrix} \times \tilde{d}(t) \tag{5.21}$$

Based on the small-signal model, we can design the controller for the power converter. From this point forward, i'_{SC} will be used to express $d \times i_{SC}$.

5.2.4 System Control, Transfer Function and Controller Constants

The two main objectives of this part are the presentation of a control strategy and a transfer function that will enable us to design a controller for the current and voltage loops.

5.2.4.1 Current Control (Inner Loop)

To obtain a current control, a feedback must be done and a controller must be tuned to drive the current flowing through the inductor (i_{SC}). Some considerations are essential to linearize this block, so a linear controller can be used for an inductor current regulation. Usually the dynamics associated with current are much faster than the ones related to voltage, hence as the DC bus capacitor is design to cut-off higher frequencies, it is possible to assume that $V_{BUS}(t)$ stays constant during $i_{SC}(t)$ regulation. The same idea can be applied to the SC Bank. With that though in mind, we can obtain a model to be used in the inner loop control. Using Laplace transform on equation 5.4 and arranging it we arrive at the equation shown in 5.22.

$$i_{SC}(s) = \frac{V_{SC}(s)}{L_S} - (1 - d(s)) \times \frac{V_{BUS}}{L_S} \tag{5.22}$$

Since the model obtained is a linear one, a PI controller can be used. The next figure, 5.6, exemplifies a possible control topology of that closed loop control.

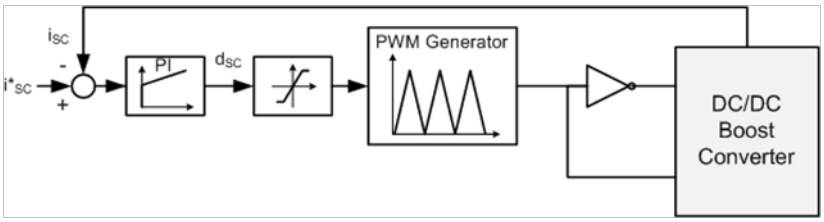

Figure 5.6: Closed loop current control topology

5.2.4.2 Current Control Closed-Loop Transfer Function

After having a closed loop control topology it is possible to achieve a transfer function that serves as low frequency model for the whole block. The block diagram for this control method is in figure 5.6 and the equation 5.23 is the generalization of a closed loop gain, such as the one presented in figure 5.7.

Figure 5.7: Closed loop current control Block Diagram

$$H_{closed-loop}(s) = \frac{C(s) \times P(s)}{1 + C(s) \times P(s)} \tag{5.23}$$

The process to be controlled is presented in the equation 5.22, but in order to be used in the closed-loop derivation it needs to be with the input and output as shown in figure 5, hence $P(s) =$

$\frac{i_{SC}(s)}{d(s)}$. The equation 5.22 rearrangement is expressed in equation 5.24, in those rearrangements, oscillations given by both Bus and supercapacitor voltage are treated as perturbations and therefore neglected.

$$P(s) = \frac{V_{BUS}}{L_S} \tag{5.24}$$

Some simplifications still can be made to $P(s)$, since $\frac{v_{SC}(s)}{i_{SC}(s)}$ can be viewed as the impedance of the power supply (i.e. the SC), we can conclude its impedance when exited with a relatively high frequency, the bandwidth one. The equation 5.24 leads to the bandwidth transfer function 5.26 and does not include perturbation plots and therefore derived from the conjunction of 5.23 , 5.24 and 5.25 , the Laplace domain equation for the controller C(s).

$$C(s) = K_{p1} + \frac{\omega_{I1}}{S} \tag{5.25}$$

The proportionality gain K_{p1} and the integral gain regulator ω_{I1} are the variables present in 5.25. The close loop transfer function for the current regulation is given by:

$$H_{BF}(s) = \frac{\frac{V_{BUS}}{LS} \times (K_{p1} + \frac{\omega_{I1}}{S})}{1 + \frac{V_{BUS}}{LS} \times (K_{p1} + \frac{\omega_{I1}}{S})} \tag{5.26}$$

5.2.4.3 PI Controller Constants

Many methods are available to derive PI controller parameters, one of them is presented in this section, it is an approach that recurs to the second order system output 5.27 [53].

$$\frac{\frac{V_{BUS}}{LS} \times (K_{p1} + \frac{\omega_{I1}}{S})}{1 + \frac{V_{BUS}}{LS} \times (K_{p1} + \frac{\omega_{I1}}{S})} = \frac{\omega_n^2}{s^2 + 2 \times \zeta_1 \times s \times \omega_n + \omega_n^2}(1 + s\tau) \tag{5.27}$$

The designer specifications of this kind of system are both ζ_1 and ω_n. And, by varying those parameters we can impose a certain behaviour to the output. Figure 5.8 shows how those variables, independently, affect the closed loop response.

The oscillation growth imposed by the decrease of ζ_1 is due to pole shifting to a place near the edge of the right half-plane of the complex chart, a known source of instability.

By rearranging equation 5.26 to the form of a second order response, 5.28, we can understand the effect of the controller variables in the key variables that impose the system output characteristics. In order to assess the dynamics of the transient and steady state of the output, an analysis to the system poles is sufficient [53], in this case, the denominator of the transfer function.

$$H_{BF} = \frac{1 + \frac{K_{p1}}{\omega_{I1}} \times s}{1 + \frac{K_{p1}}{\omega_{I1}} + S^2 \times \frac{L}{V_{BUS} \times \omega_{I1}}} \tag{5.28}$$

The natural frequency ω_{BF1} can be found in 5.29 and the damping ratio ζ_1 in 5.30. Other variables are used to design the controller, the proportionality gain K_{p1} and the integral gain regulator ω_{I1}.

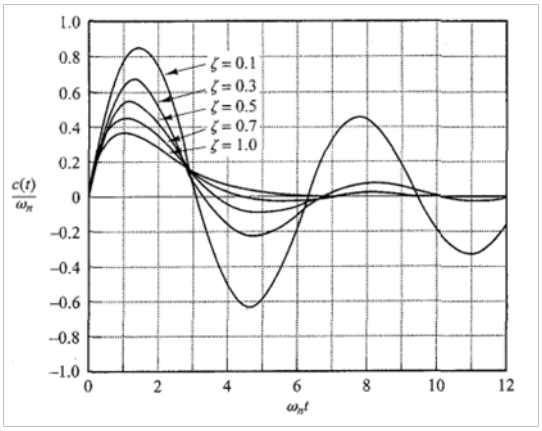

Figure 5.8: Variations of both ζ_1 and ω_n in a response to a unitary impulse

$$\omega_{BF1} = \sqrt{\frac{V_{BUS}}{L} \times \omega_{I1}} \tag{5.29}$$

$$\zeta_1 = \frac{K_{p1} \times \sqrt{\frac{V_{BUS}}{L}}}{2 \times \sqrt{\omega_{I1}}} \tag{5.30}$$

With these expressions we are now able to calculate the PI controller constants. As stated in [5] the current-loop dynamic time response should be tuned to about ten to five times the switching periods, as stated in [69], the switching frequency of the converter is 25 kHz, Bus voltage is 600V and the inductor is about 1.35mH in order to maintain a current ripple of 3A. With these values we can arrive at the constants parameterizing the PI linear controller. The next equations, 5.31 and 5.32 show those calculations.

$$\omega_{I1} = (\omega_{BF1})^2 \times \frac{L}{V_{BUS}} = (2\pi \times 2.5k)^2 \times \frac{1.35m}{600} = 555.1 rads^{-1} \tag{5.31}$$

$$K_{p1} = 2 \times \zeta_1 \times \omega_{BF1} \times \frac{L}{V_{BUS}} = 2 \times 1 \times 2\pi \times 2.5k \times \frac{1.35m}{600} = 0.07068 \tag{5.32}$$

5.2.4.4 Current Control Considerations

Due to some aspects inherent to the concept of the converter, there are issues that, if not accounted, can introduce instability to the system.

1. Anti-Windup Strategies

   The intrinsic saturation behaviour of a duty-cycle (0<d<1) imposes a non-linearity that brings up a windup of the integrative part of the controller. Anti-windup strategies maintain the closed-loop system in a linear domain. In [70] some strategies for anti-windup are presented. Avoiding saturation is always a way to approach the issue, but other architectures

are discussed. Back-calculation is a good way to maintain linearity in the transient period and will be the strategy approached. The next figure, 5.9 represents that same strategy when applied to the converter presented.

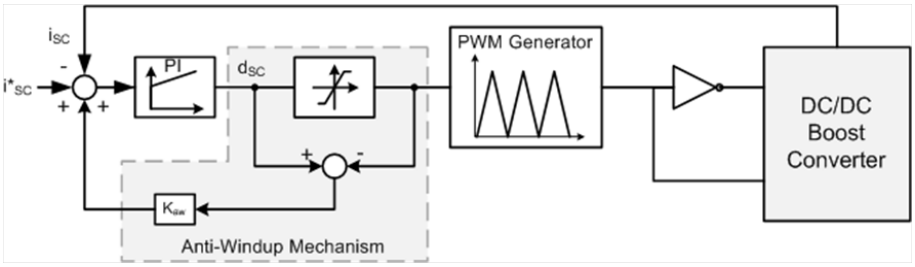

Figure 5.9: Current Control with anti-windup

In [70] is presented a rule of thumb to define the anti-windup gain, it states that the anti-windup gain should be equal to $\frac{w_{I1}}{K_{p1}}$.

2. Reference Current Low-Pass Filter

   To prevent high current overshoot, a low-pass filter can be used to compensate the zero appearing in the closed-loop transfer function of the current control system 5.28. For this filter to be effective, it must have a time constant of τ_1.

   Applying the values of equations 5.31 and 5.32 we can obtain the value for the time constant for the compensator filter, shown in 5.33.

$$\tau_1 = \frac{K_{p1}}{\omega_{I1}} = \frac{0.07068}{555.1} = 12.7ms \tag{5.33}$$

5.2.4.5 Current Control Simulations

In order to understand if the low-frequency transfer function obtained is a good approximation of the real system, MatLab Simulink was used, with the SimPowerSystem toolbox, to generate a simulation, with the same conditions described in this document. This approach allows us to make both a comparative analysis and a system dynamics analysis.

The block diagram shown in the next figure, 5.10, has some points that are noteworthy.

In the MatLab diagram in figure 5.10, the most important aspects to report are, the need to edit the PWM generator block, imposing a saturation of the duty-cycle to values between 0 and 1 by altering the triangular carrier, the standard PWM block has its saturation between -1 and 1. A high capacitance was imposed to the SC bank in order to enforce a low variation in V_{sc}, as that is one of the assumptions made in the subsection 5.2.4.1. To simulate the current absorbed by the powertrain of the electric vehicle a low resistor was inserted in parallel with the DC bus.

The anti-windup method is applied directly in the PI controller block, with the values proposed in the thumb-rule mentioned above. The variable values and linear controller parameters were gathered in an .m. Since the controlled semiconductor of the half-bridge is the bottom one, the

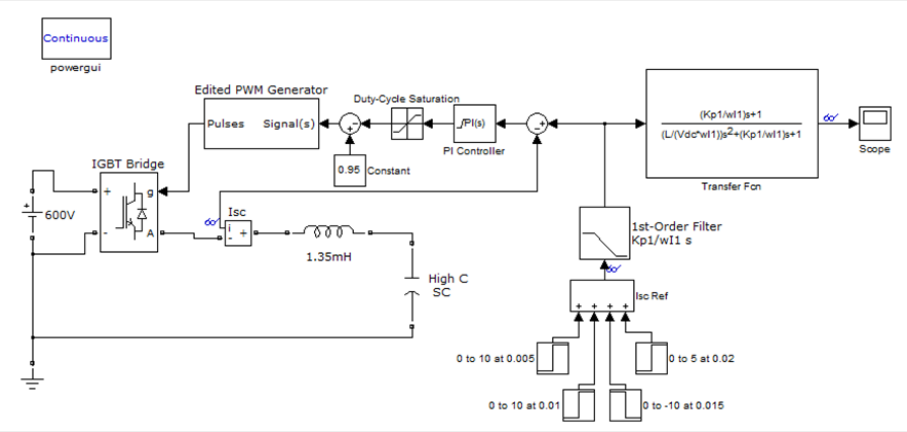

Figure 5.10: Current Control Diagram

high saturation value was subtracted to the duty-cycle signal, this way one can control the bottom semiconductor.

5.2.4.6 Simulation Results

1. Preliminary Results

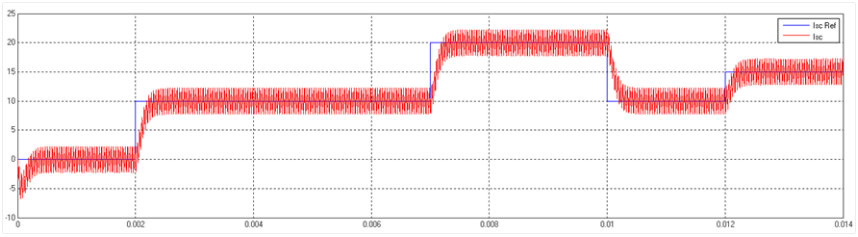

Figure 5.11: Current Control Diagram

Some comments can be made to the dynamics of I_{sc}, the most visible is the current ripple, limited by the inductance in series with the supercapacitor. The initial negative current is due to the SC capacitor charge.

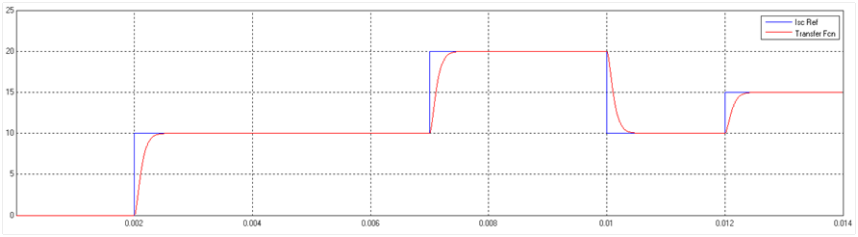

Figure 5.12: Current Control Diagram

Assuming that figure 5.12 represents the low-frequency response of the signal in figure 5.11 without much error. One can assume that the transfer function can be used to validate some parameters imposed to the current control. One of those parameters is the settling time. Using the notion of settling time (5%) and the zoomed MatLab chart for an accurate measure, the settling time result was of 0.2803ms, as we can observe in the next equation 5.34. The theoretical settling time is stated in equation 5.35.

$$t_{ss}(5\%) = t_{19.5V}(95\%) - t_{10.5V}(5\%) = 7.000m - 7.302m = 0.302ms \tag{5.34}$$

$$t_{st}(5\%) = \frac{2\zeta^2 + 3}{\omega_n \times \zeta} = 0.318ms \tag{5.35}$$

An error of about 5% is show by the calculations made, allowing to state that the requirements established at the beginning were attended. Moreover, the theoretical settling time is an approximation, as described in [15].

The transfer function response rejects the high frequency component of the supercapacitor current. Both Matlab simulations using SimPowerSystem and transfer function follow the current reference without overshoots.

2. Simulation starting with V_{BUS} null and with a current reference of 15 Ampere (VEIL Configuration [69, 67])

   In the first test an assessment was done to characterize the performance of the control strategy when the voltage in the bus capacitor is null (see figure 5.13).

   The simulation shows that, during the transient state, the capacitor charges absorbing a very high amount of current during a short period of time. This happens because, during the capacitor charging procedure, the PI controller tries to reduce the current peak reducing the duty cycle to 0. This behaviour imposes a direct connection between power source and bus capacitor with only the inductor between them, therefore the DC bus will get charged, but during that time period there is no current control.

   A conclusion can be attained with this information: in practice a soft start mechanism is needed, pre-charging the bus capacitor. In the next simulations an initial voltage will be introduced in the DC bus capacitor parameters, hence this behaviour will not be observed.

3. Simulations for the VEIL EV [69, 67]

   The boost gain implemented in the previous tests had the output voltage double the value of input voltage, thus not much stress was imposed to the converter. In VEIL, the SC have a voltage around 48V in the worst case scenario, thus an input to output gain of about 12.5 appear. That voltage value was applied to the SC initial voltage in the next simulations.

   In figure 5.14, some overshoot start to appear due to duty-cycle saturation visible in figure 5.15. Those overshoots are limited by the effect of the back-calculation anti-windup method.

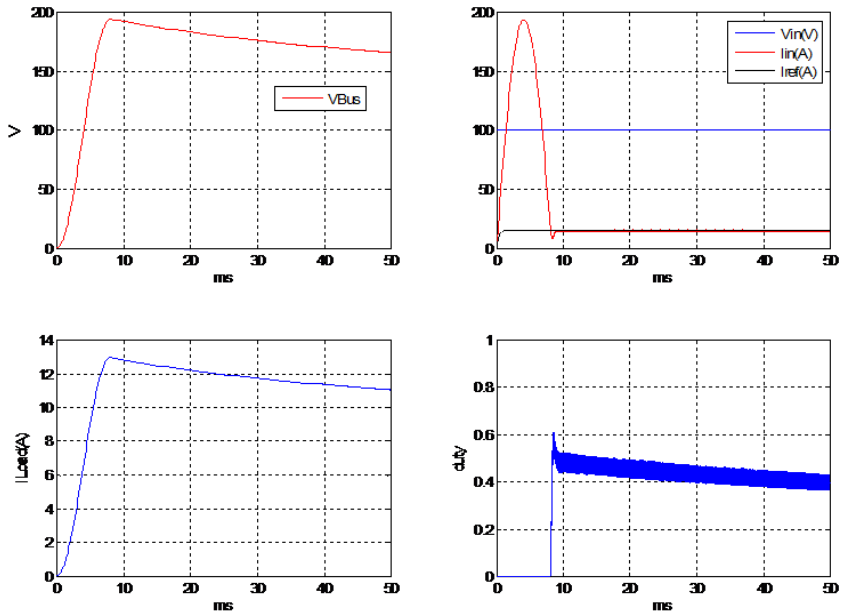

Figure 5.13: Simulation Results with null voltage in the Bus Capacitor

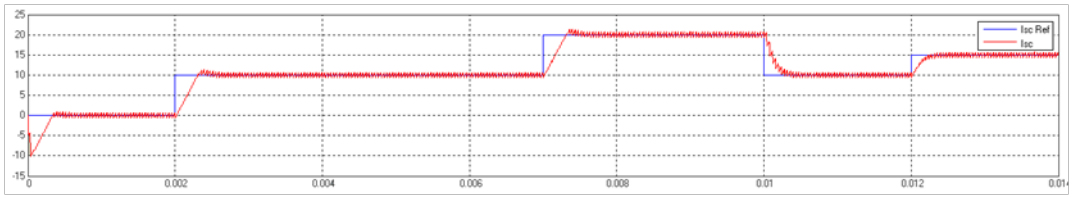

Figure 5.14: VEIL Simulation Results with the Anti-windup Method

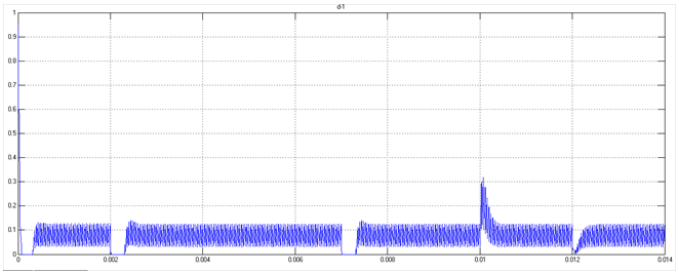

Figure 5.15: Duty-Cycle Saturation

The overshoot difference can be observed comparing figure 5.14 with figure 5.16, where no anti-windup mechanism was used.

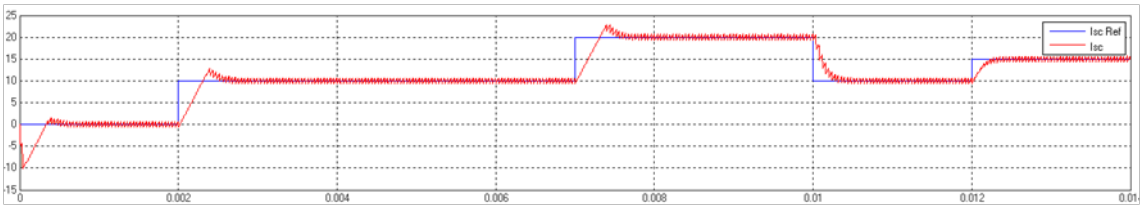

Figure 5.16: VEIL Simulation Results without the Anti-windup method

4. Simulations with negative current (Charging the SC)

   To have the SC bank charging, the inductor current has to be negative, to achieve those current values in the simulation the inductor current reference needs to be changed. In figure 5.17 is possible to observe the power converter dynamic while acting as a buck.

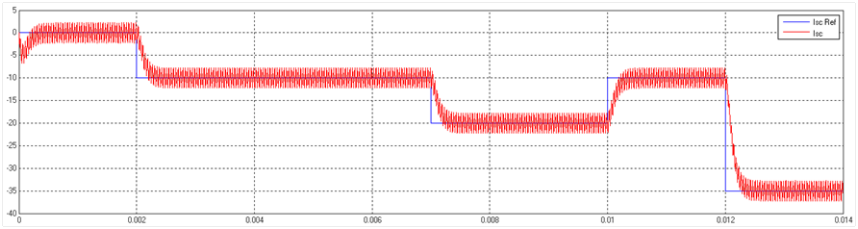

Figure 5.17: Simulation Results with Negative Current

Figure 5.17 demonstrate a behaviour similar to the one appearing to the same converter, only working as a boost. Hence all the conclusions made to the boost operation zone are true when the converter acts as a buck.

5.2.5 DC Bus Voltage Control (Outer Loop)

This control loop is needed mainly to support the assumption made in subsection 5.2.4.1. This strategy ensures the rejection of oscillations in the DC Bus voltage as long as the imbricated loops assume a frequency decoupling, even with overcurrent in the SC/Battery Bank or perturbations injected by the load coupled to the DC Bus. Even though, some assumptions must be done in order to design the controller used to set the system to function as required. The first assumption is that the inner control loop acts as required with a steady DC Bus voltage. The second assumption is due to the need of indirectly control the DC Bus voltage. In order to control that DC Bus voltage we need to control I_{SC}, hence we need to control I_{SC}, so a decoupling method is desired.

5.2.5.1 Voltage Closed-Loop Transfer Function

The equation governing the current responsible to charge the bus capacitor, thus controlling bus voltage is the one shown in 5.36 in a frequency domain.

$$V_{BUS}(s) = \frac{i'_{SC}}{C^s_{BUS}} - \frac{i_{Load}}{C^s_{BUS}} \tag{5.36}$$

If the load current is considered a perturbation, figure 5.18 illustrates the block diagram used to attain the transfer function of the voltage control-loop (equation 5.37) making it possible to use, once again, equation 5.23. This happens with C(s) and P(s) as shown in equations 5.38 and 5.39.

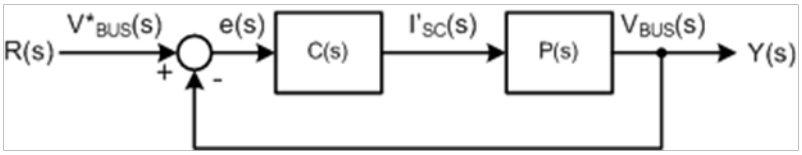

Figure 5.18: Voltage Closed-Loop Block Diagram

$$H_{BF2} = \frac{1 + \frac{K_{p2}}{\omega_{I2}} \times s}{1 + s \times \frac{K_{p2}}{\omega_{I2}} + s^2 \times \frac{C_{BUS}}{\omega_{I2}}} \tag{5.37}$$

$$C(s) = K_{p1} + s \times \omega_{I1} \tag{5.38}$$

$$P(s) = \frac{1}{C^s_{BUS}} \tag{5.39}$$

5.2.5.2 PI Controller Constants

To obtain the constants needed to implement the voltage controller, a second-order transfer function can be used as a support to deduce them, following the same logic as in the current-loop calculation. The possibility of a pole analysis to understand the dynamics of a second-order system is valid, thus to calculate the C(s) design parameters the equation 5.40 is an effective one.

$$1 + s \times \frac{K_{p2}}{\omega_{I2}} + s^2 + 2 \times \zeta_1 \times s \times \omega_n + \omega_n^2 \tag{5.40}$$

The damping ratio ζ_2 and the natural frequency $\omega_{BF2}(\omega_n)$ are used to deduce the controller gains K_{p2} and ω_{I2} gain constants. The next equations, 5.41 and 5.42, state those dependencies and calculated values.

$$\omega_{I2} = C_{BUS} \times \omega^2_{BF2} = 500m \times 2\pi \times 250 = 785.398 rads^{-1} \tag{5.41}$$

$$K_{p2} = 2 \times \zeta_2 \times C_{BUS} \times \omega_{BF2} = 4\pi \times 500m \times 250 = 1570.79 \tag{5.42}$$

Once again the damping coefficient ζ_2 is imposed to a unitary value, to achieve a critical damping response. The period inherent to the natural frequency of the outer loop allows the inner loop to settle, bringing the possibility to treat i_{SC} as constant.

5.2.5.3 Voltage Loop Considerations - the Decoupling Method

In figure 5.19, the control method implemented for the voltage control is presented.

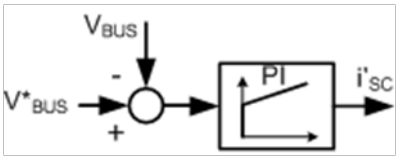

Figure 5.19: Voltage Control Method Implemented

With this method the output is i_{SC}, this is not a directly controlled variable, so a decoupling method is needed in order to the voltage control method have an output compatible with the reference needed for the current control-loop, i_{SC}.

The decoupling method, as proposed in [5] is based on the premise that the semiconductors do not have any kind of energy losses and the inductor is a small storage device when compared to the C_{BUS}. Then and only then we can assume with some certainty that all the energy produced in the SC/Battery Bank arrives at the DC Bus.

Since both V_{BUS} and V_{SC} are measurable variables, the decoupling method explained in figure 5.20, taking advantage of the knowledge given by equation 5.43, is possible to implement.

$$v_{SC} \times i_{SC} = V_{BUS} \times i'_{SC} \Leftrightarrow i_{SC} = \frac{V_{BUS} \times i'_{SC}}{v_{SC}} \tag{5.43}$$

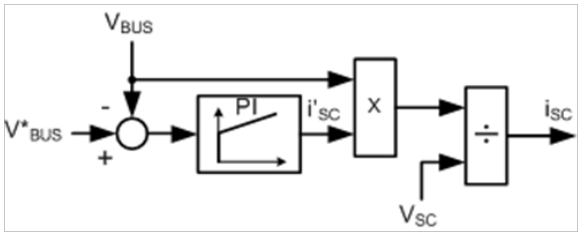

Figure 5.20: Decoupling Method

Now a both voltage and current control topology can be merged in a control topology that controls both the DC bus voltage and the bi-directional current flowing to and from the primary power source. The topology is shown in figure 5.21.

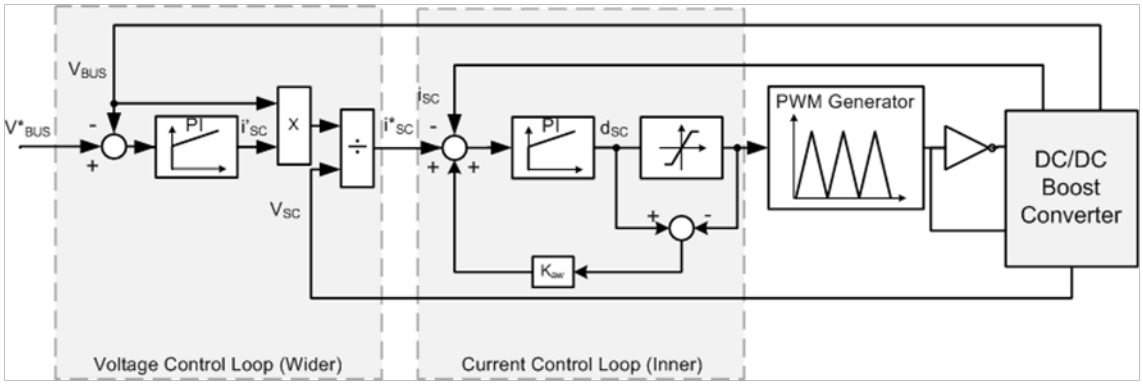

Figure 5.21: Voltage and Current Control Topology

5.2.6 Voltage + Current Control Simulations

In this part of the master thesis, simulation results will be presented. The control strategy applied to the chosen PEC, system the system discussed in this subsection, will be simulated and discussed.

This simulation is intended to validate the operation of current and voltage control loops simultaneously. It is assumed that the single load of the system is an ideal current source with variable value. The performance of the system during the startup phase and before the load current steps, including regenerative braking, will be assessed. The results are shown in figure [figura com os resultados dos loops de corrente + tens.

During the initial phase (0 40 ms), the controller increases dictates a smooth voltage elevation, from the pre-charged value of 100V to the intended reference voltage, 300V. It can be seen that during this period, PI controller saturates the current in 100A (maximum permissible current value). It is also verified that the current loop responds satisfactorily, i.e. the measured current follows the reference quickly and accurately.

The next relevant period to be analyzed is from 20ms to 80ms, during that time period there is a disturbance in the load current 20A (equivalent to a step of 6kW). This step reduces the bus voltage slightly, causing the wider loop PI controller (voltage control) to impose an increased current reference to in the inductor, allowing the elimination of the disturbance in less than 10ms.

At 80ms a negative current is imposed to the load, the system will regenerate energy. This event causes the bus voltage to increase. Again, the PI responds quite well by rapidly inverting the current in the inductor, making allowing the SC to absorb the regenerated energy and maintain the voltage.

In short, these simulations allow a conclusion to be taken. The cascade control of voltage and current proposed, based on linear controllers (PIs), is a sufficient mean to robustly regulate the DC bus voltage.

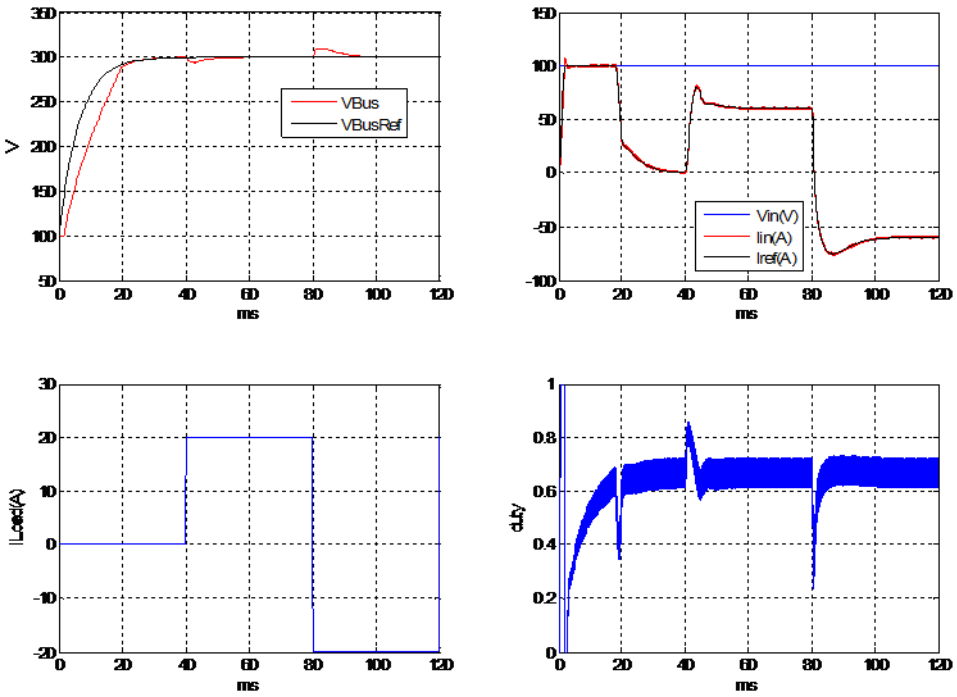

Figure 5.22: Simulation Results from Voltage + Current Control

Chapter 6

Conclusions and Future Work

This chapter will summarize the conclusions gathered throughout the master thesis, acknowledging that, even if the objectives were achieved, much future work can be done in the embracing theme approached.

6.1 Gathered Conclusions

Throughout the master thesis many topics were approached and conclusions could be attained to each one of them.

1. The first chapter, 1, shows the general framework of the electric vehicle both in Portugal and around the world. It is clear that the electric vehicle can play an important role in the solution of many environmental and socio-economic problems faced by countries around the world

2. Based on those premises, a literature review concerning the existent portable energy sources was elaborated regarding both single and hybrid technology systems. A relevant conclusion was presented: hybrid technologies are almost certainly the future of electric vehicle power supply. Lithium based batteries merged with SC were pinpointed in the second chapter (2) as the most promising solution due to their energy/power properties.

3. The second chapter also brought the idea of modelling power sources and, later in the third chapter, 3 the results of the models approached were obtained. With the test bench setup designed it was possible to retain two major conclusions: (1) a battery model based on a surface is mainly constrained by the fitting procedures used. However, if enough samples are measured at a good variety of operations points (a very time-consuming activity) and a fitting procedure which can approximate the measures done is determined (even if it takes long to calculate), then and only then, this method of modeling a battery can be considered good. (2) the main difficulty to create a good electrical model of a battery is to acquire the,

sometimes subtle, voltage variations when a sudden current is demanded. If those voltage points are attained, then a fairly accurate model can be obtained. To achieve those results a reliable test setup is mandatory.

4. The fourth chapter reported that accurate SoC estimations are a difficult task to be obtained on-line, but some methods perform well. The estimation procedure with more consistent results is the "coulomb-counting" method, that can be combined with the "open circuit voltage" in order to have a more reliable method, as happened with the battery hybridization. One of the major drawbacks of the "coulomb-counting" method relies on the fact that it needs an accurate initial state estimation to have a good performance and the "open circuit voltage" method can attain that value.

5. Finally a power electronics topology was chosen and simulated. The chosen topology has very good assessments considering it's performance characteristics and has good controllability with a linear cascaded control. The analysis done can be transposed to systems with the same half-bridge boost as well as the same control topology that use different DC power sources, providing that the frequency response is lower than in SC.

Above all the conclusions is the acknowledgement that the general architecture purposed in 1.5 and shown in figure 1.18 was validated.

6.2 Future Work

Althougth all the objectives were achieved, much work can be continued inside the vast thematic approached in this master thesis.

1. EMCS detailed studies should be prepared. This area is vast, but little studies are public about fully electric hybrid energy management.

2. The results obtained for the discharge procedures gave chance to know that the kind of methods used perform well and can be extrapolated to charging procedures. Hence, those tests should be conducted because both the battery model and the SoC estimation procedures are not complete until the charging region is of the battery is understood.

3. One of the possible steps to be taken after, could be the real-life testing of the simulations done in the subsection **??**. To persecute this objective a hardware topology would have to be designed and acquired.

4. The methods used to attain the battery models can and should be used to obtain different models for other power sources technologies, helping in an analytical rather than qualitative and empirical approach to characterize hybrid solutions.

   Much work is still to be done to achieve the great goal of obtaining a fully electric, fully functional, energy efficient and all purpose electric vehicle that we fully understand.

Bibliography

[1] Sergey Ablameyko. *Neural networks for instrumentation, measurement and related industrial applications*. NATO science series Series III, Computer and systems sciences,. IOS ; Ohmsha, Amsterdam ; Washington, DC Tokyo, 2003. NATO Advanced Study Institute on Neural Networks for Instrumentation, Measurement, and Related Industrial Applications (2001 : Crema, Italy) edited by Sergey Ablameyko ... [et al.]. NIMIA'2001 ill. ; 25 cm. "Nato Advanced Study Institute on Neural Networks for Instrumentation, Measurement, and Related Industrial Applications - NIMIA'2001, held in Crema, Italy, from 9-20 October 2001"–P. v. Includes bibliographical references and indexes. NATO science series. v. 185.

[2] Internation Energy Agency. Technology roadmap electric and plug-in hybrid electric vehicles, 2009.

[3] International Energy Agency. Co2 emissions from fuel combustion highlights, 2010.

[4] Jonn Axsen, Andrew F. Burke, and Kenneth S. Kurani. Batteries for plug-in hybrid electric vehicles (phevs): Goals and the state of technology circa 2008. Technical report, Institute of Transportation Studies, University of California, Davis, 2008.

[5] T. Azib, O. Bethoux, G. Remy, C. Marchand, and E. Berthelot. An innovative control strategy of a single converter for hybrid fuel cell/supercapacitor power source. *Industrial Electronics, IEEE Transactions on*, 57(12):4024–4031, 2010.

[6] D. M. Bellur and M. K. Kazimierczuk. Dc-dc converters for electric vehicle applications. In *Electrical Insulation Conference and Electrical Manufacturing Expo, 2007*, pages 286–293.

[7] Precision BK. Bk precision 8500 series dc electronic loads, 2 September 2009 2009.

[8] Andrew Burke, Marshall Miller, and Nathan Parker. Ultracapacitor technology: Present and future performance and applications. *World Summit on Advanced Capacitors*, 2004.

[9] Aurélio Joaquim de Castro Campilho. *Instrumentação electrónica Métodos e técnicas de medição*. Colecção Manual. Faculdade de Engenharia da Universidade do Porto, Porto, 2000. por.

[10] Steven G. Chalk and James F. Miller. Key challenges and recent progress in batteries, fuel cells, and hydrogen storage for clean energy systems. *Journal of Power Sources*, 159(1):73–80, 2006.

[11] C. C. Chan. The state of the art of electric, hybrid, and fuel cell vehicles. *Proceedings of the IEEE*, 95(4):704–718, 2007.

[12] K. T. Chau and Y. S. Wong. Hybridization of energy sources in electric vehicles. *Energy Conversion and Management*, 42(9):1059–1069, 2001.

[13] J. Chiasson and B. Vairamohan. Estimating the state of charge of a battery. *Control Systems Technology, IEEE Transactions on*, 13(3):465–470, 2005.

[14] T. W. Ching. Review of soft-switching technologies for high-frequency switched-mode power conversion. *International Journal of Electrical Engineering Education*, 46(1):104–119, 2009.

[15] S. H. Choung and A. Kwasinski. Multiple-input dc-dc converter topologies comparison. *Industrial Electronics, 2008. IECON 2008. 34th Annual Conference of IEEE*, pages 2359–2364, 2008.

[16] F. Codeca, S. M. Savaresi, and G. Rizzoni. On battery state of charge estimation: A new mixed algorithm. In *Control Applications, 2008. CCA 2008. IEEE International Conference on*, pages 102–107.

[17] M. Coleman, W. G. Hurley, and Lee Chin Kwan. An improved battery characterization method using a two-pulse load test. *Energy Conversion, IEEE Transactions on*, 23(2):708–713, 2008.

[18] European Parliament and Council. Directiva 2009/28/ce do parlamento europeu e do concelho, 2009.

[19] H. Demuth and M. Beale. *Neural Network Toolbox For Use with MATLAB - User's Guide*. The MathWorks, 2004.

[20] A. M. Dhirde, N. V. Dale, H. Salehfar, M. D. Mann, and T. H. Han. Equivalent electric circuit modeling and performance analysis of a pem fuel cell stack using impedance spectroscopy. *Energy Conversion, IEEE Transactions on*, 25(3):778–786.

[21] Robert W. Erickson and Dragan Maksimovic. *Fundamentals of power electronics*, volume 2nd ed. Kluwer Academic Publishers, Norwell, MA, 2001. eng.

[22] M. A. Fetcenko, S. R. Ovshinsky, B. Reichman, K. Young, C. Fierro, J. Koch, A. Zallen, W. Mays, and T. Ouchi. Recent advances in nimh battery technology. *Journal of Power Sources*, 165(2):544–551, 2007.

[23] Fluke. Pm2811-pm2812-pm2813 pm2831-pm2832 users manual, 1997.

[24] Batteries GP. Battery pack specification, 2010.

[25] M. T. Hagan and M. B. Menhaj. Training feedforward networks with the marquardt algorithm. *Neural Networks, IEEE Transactions on*, 5(6):989–993, 1994.

[26] Zhang Hanlei and Chow Mo-Yuen. Comprehensive dynamic battery modeling for phev applications. In *Power and Energy Society General Meeting, 2010 IEEE*, pages 1–6.

[27] Schweiger Hans-Georg, Obeidi Ossama, Komesker Oliver, Raschke André, Schiemann Michael, Zehner Christian, Gehnen Markus, Keller Michael, and Birke Peter. Comparison of several methods for determining the internal resistance of lithium ion cells, 2010. DOAJ-Articles [http://www.doaj.org/oai.article] (Sweden) ER.

[28] Miguel Luis Delgado Heleno. *Reliability Impact on Power Systems Considering High Penetration of Electric Vehicles*. PhD thesis, 2010.

[29] F. Huet. A review of impedance measurements for determination of the state-of-charge or state-of-health of secondary batteries. *Journal of Power Sources*, 70(1):59–69, 1998.

[30] National Instruments. Ni 6024e multifunction daq - datasheet, 2010.

[31] V. Isastia and S. Meo. Overview on automotive energy storage systems. *International Review of Electrical Engineering*, 4(6):1122–1144, 2009.

[32] W. Jacobi. *Lithium Batteries*. CRC Press, 2003. doi:10.1201/9780203911853.ch18.

[33] N. Jalil, N. A. Kheir, and M. Salman. A rule-based energy management strategy for a series hybrid vehicle. In *American Control Conference, 1997. Proceedings of the 1997*, volume 1, pages 689–693 vol.1.

[34] Jyh-Shing Roger Jang, Chuen-Tsai Sun, and Eiji Mizutani. *Neuro-fuzzy and soft computing a computational approach to learning and machine intelligence*. Prentice Hall, Upper Saddle River,NJ, 1997. eng.

[35] A. Khaligh and Z. Li. Battery, ultracapacitor, fuel cell, and hybrid energy storage systems for electric, hybrid electric, fuel cell, and plug-in hybrid electric vehicles: State of the art. *Vehicular Technology, IEEE Transactions on*, 59(6):2806–2814, 2010.

[36] R. Langari and Won Jong-Seob. Integrated drive cycle analysis for fuzzy logic based energy management in hybrid vehicles. In *Fuzzy Systems, 2003. FUZZ '03. The 12th IEEE International Conference on*, volume 1, pages 290–295 vol.1.

[37] Américo Vicente Teixeira Leite. *Estimação de estados, parâmetros e velocidade do motor de indução trifásico com metodologias de identificação em tempo real*. FEUP, Porto:, 2004. Dissertação apresentada para obtenção do grau de Doutor em Engenharia Electrotécnica e de Computadores, na Faculdade de Engenharia da Universidade do Porto, sob a orientação dos Profs. Doutores Diamantino Freitas e Rui Araújo Américo Vicente Teixeira Leite.

[38] LEM. Lem hy 5p datasheet, 1998.

[39] D. Linden and T. B. Reddy. Handbook of batteries (3rd edition), 2002.

[40] Du Lingling. Study on supercapacitor equivalent circuit model for power electronics applications. In *Power Electronics and Intelligent Transportation System (PEITS), 2009 2nd International Conference on*, volume 2, pages 51–54.

[41] Eric Loveday. Nissan pegs leaf range between 47 and 138 miles individual results may vary, January, 27 2010.

[42] S. M. Lukic, Cao Jian, R. C. Bansal, F. Rodriguez, and A. Emadi. Energy storage systems for automotive applications. *Industrial Electronics, IEEE Transactions on*, 55(6):2258–2267, 2008.

[43] Walter Anatole Marques. 'importacoes' e 'exportacoes' portuguesas de produtos energeticos. 2009.

[44] Phil Kaminsky Iklaq Sidhum Burghardt Tenderich Matt Draper, Ernesto Rodriguez. Economic impact of electric vehicle adoption in the united states. 2008.

[45] Chen Min and G. A. Rincon-Mora. Accurate electrical battery model capable of predicting runtime and i-v performance. *Energy Conversion, IEEE Transactions on*, 21(2):504–511, 2006.

[46] Tom M. Mitchell. *Machine learning*. Computer Science Series. McGraw-Hill Companies, New York [etc], 1997. eng.

[47] C. S. Moo, K. S. Ng, Y. P. Chen, and Y. C. Hsieh. State-of-charge estimation with open-circuit-voltage for lead-acid batteries. In *Power Conversion Conference - Nagoya, 2007. PCC '07*, pages 758–762.

[48] J. Moreno, M. E. Ortuzar, and J. W. Dixon. Energy-management system for a hybrid electric vehicle, using ultracapacitors and neural networks. *Industrial Electronics, IEEE Transactions on*, 53(2):614–623, 2006.

[49] Rede Electrica Nacional. Dados tecnicos electricidade valores provisorios 2009. Technical report, Rede Electrica Nacional, February 2010 2010.

[50] Rede Electrica Nacional. Resultados consolidados 9 meses 2010. Financial brief, November, 3 2010 2010.

[51] Adam Lorimer Boaz Ur Ikhlaq Sidhu Phil Kaminsky Burghardt Tenderich Nicholas DeForest, Jamie Funk. Impact of widespread electric vehicle adoption on the electric utility business - threats and opportunities. 2009.

[52] Nissan. Nissan leaf is world's first mass-marketed 100 Technical report, Nissan, June 11, 2010 2010.

[53] Katsuhiko Ogata. *Modern control engineering*, volume 3rd ed. Prentice Hall International, New Jersey, 1997. eng.

[54] Gaurang Panchal, Amit Ganatra, Y P Kosta, and Devyani Pancha. Behaviour analysis of multilayer perceptrons with multiple hidden neurons and hidden layers. *International Journal of Computer Theory and Engineering*, Vol.3(no.2):pp.332–337, 2011.

[55] phev@ucdavis.edu. Plug-in hybrid electric vehicle research center, 2011.

[56] Sabine Piller, Marion Perrin, and Andreas Jossen. Methods for state-of-charge determination and their applications. *Journal of Power Sources*, 96(1):113–120, 2001.

[57] V. Prajapati, H. Hess, E. J. William, V. Gupta, M. Huff, M. Manic, F. Rufus, A. Thakker, and J. Govar. A literature review of state of-charge estimation techniques applicable to lithium poly-carbon monoflouride (li/cfx) battery. In *Power Electronics (IICPE), 2010 India International Conference on*, pages 1–8.

[58] Shalini Rodrigues, N. Munichandraiah, and A. K. Shukla. A review of state-of-charge indication of batteries by means of a.c. impedance measurements. *Journal of Power Sources*, 87(1-2):12–20, 2000.

[59] L. Rosario and P. C. K. Luk. Applying management methodology to electric vehicles with multiple energy storage systems. In *Machine Learning and Cybernetics, 2007 International Conference on*, volume 7, pages 4223–4230.

[60] K. J. Runtz and M. D. Lyster. Fuel cell equivalent circuit models for passive mode testing and dynamic mode design. In *Electrical and Computer Engineering, 2005. Canadian Conference on*, pages 794–797.

[61] Md Salam and Toshikuni Noguchi. Impact of human activities on carbon dioxide (co2) emissions: A statistical analysis. *The Environmentalist*, 25(1):19–30, 2005.

[62] B. Schweighofer, K. M. Raab, and G. Brasseur. Modeling of high power automotive batteries by the use of an automated test system. *Instrumentation and Measurement, IEEE Transactions on*, 52(4):1087–1091, 2003.

[63] G. Steinmauer and L. del Re. Optimal control of dual power sources. In *Control Applications, 2001. (CCA '01). Proceedings of the 2001 IEEE International Conference on*, pages 422–427.

[64] TeslaMotors. Tesla roadster features and specs, 2011.

[65] O. Tremblay, L. A. Dessaint, and A. I. Dekkiche. A generic battery model for the dynamic simulation of hybrid electric vehicles. In *Vehicle Power and Propulsion Conference, 2007. VPPC 2007. IEEE*, pages 284–289.

[66] Nguyen Trong Duy, Tseng King Jet, Zhang Shao, and Nguyen Hoan Thong. On the modeling and control of a novel flywheel energy storage system. In *Industrial Electronics (ISIE), 2010 IEEE International Symposium on*, pages 1395–1401.

[67] J. P. Trovao, P. G. Pereirinha, F. J. T. E. Ferreira, and H. M. Jorge. Study of inductor effects in a bidirectional dc-dc converter for electrical vehicle. In *Electrical Machines (ICEM), 2010 XIX International Conference on*, pages 1–6.

[68] J. P. Trovao, P. G. Pereirinha, and H. M. Jorge. Analysis of operation modes for a neighborhood electric vehicle with power sources hybridization. In *Vehicle Power and Propulsion Conference (VPPC), 2010 IEEE*, pages 1–6.

[69] J. P. Trovao, P. G. Pereirinha, and H. M. Jorge. Analysis of operation modes for a neighborhood electric vehicle with power sources hybridization. In *Vehicle Power and Propulsion Conference (VPPC), 2010 IEEE*, pages 1–6.

[70] Antonio Visioli. *Practical PID control*. Advances in industrial control. Springer, London, 2006. 2006932289 GBA667067 013522923 Antonio Visioli. ill. ; 24 cm. Includes bibliographical references (p. [299]-308) and index.

[71] Junping Wang, Binggang Cao, Quanshi Chen, and Feng Wang. Combined state of charge estimator for electric vehicle battery pack. *Control Engineering Practice*, 15(12):1569–1576, 2007.

[72] B. M. Wilamowski, Chen Yixin, and A. Malinowski. Efficient algorithm for training neural networks with one hidden layer. In *Neural Networks, 1999. IJCNN '99. International Joint Conference on*, volume 3, pages 1725–1728 vol.3.